DEFENSE DOCUMENTATION CENTER

FOR

SCIENTIFIC AND TECHNICAL INFORMATION

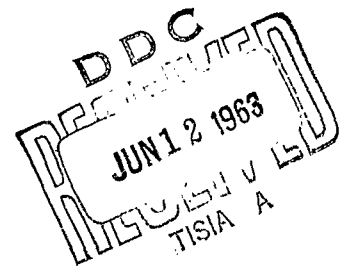CAMERON STATION. ALEXANDRIA. VIRGINIA

63-4-1

R-61-620

STUDY OF CREATURE COMMUNICATIONS

TECHNICAL REPORT NO. ASD-TR-61-620, Part II
June 1963

Electromagnetic Warfare and Communications Laboratory
Aeronautical Systems Division
Air Force Systems Command
United States Air Force
Wright-Patterson Air Force Base, Ohio

Project No. 4335, Task No. 433526

NOTICES

When Government drawings, specifications, or other data are used for
any purpose other than in connection with a definitely related Government
procurement operation, the United States Government thereby incurs no
responsibility nor any obligation whatsoever; and the fact that the Government
may have formulated, furnished, or in any way supplied the said drawings,
specifications, or other data, is not to be regarded by implication or other-
wise as in any manner licensing the holder or any other person or corpora-
tion, or conveying any rights or permission to manufacture, use, or sell
any patented invention that may in any way be related thereto.

Qualified requesters may obtain copies of this report from the Armed
Services Technical Information Agency, (ASTIA), Arlington Hall Station,
Arlington 12, Virginia.

This report has been released to the Office of Technical Services, U.S.
Department of Commerce, Washington 25, D.C., for sale to the general
public.

Copies of this report should not be returned to the Aeronautical Systems
Division unless return is required by security considerations, contractual
obligations, or notice on a specific document.

STUDY OF CREATURE COMMUNICATIONS

ASD-TR-61-620, Part II

FOREWORD

This report was prepared by members of the staff of the Armour Research Foundation of the Illinois Institute of Technology, Chicago, Illinois, under Air Force Contract No. AF 33(657)-8807, Project No. 4335 entitled "Study of Creature Communications". It constitutes the final technical report on the subject program. The work was performed over the period 1 June 1962 through 1 May 1963 under the administration of the Electromagnetic Warfare and Communications Laboratory, Aeronautical Systems Division, with Mr. James Falter, acting as Project Monitor. The program was a continuation of work begun under Air Force Contract No. AF 33(616)-7724.

The research described herein represents the interdisciplinary effort of specialists in many fields and includes Messrs. S. H. Cameron, F. R. Hand, E. J. Hawrylewicz, G. T. Jacobi, H. B. Karplus, M. E. King, D. Owen, and E. F. Uretz.

ABSTRACT

The work reported has as its goal the development of new communication components, techniques and systems from the analysis and/or use of biological phenomena. Research was performed in three major areas selected during a first year program.

    **A photoconductive sensor which performs a contrast detecting function was designed and the microelectronic fabrication techniques necessary for its construction were developed. The work culminated in an operational sensor cell.

    **Since networks of threshold operators serve as a rough model of neural structure and are amenable to mathematical analysis, the design of minimal networks of such threshold operators was investigated. Although no general synthesis algorithm was discovered, rules for the synthesis of special classes of Boolean function, notably symmetric functions, were formulated.

    **Utilizing materials extracted from photosynthetic bacteria, organic sensors which exhibited both photoconductive and photovoltaic response to illumination were constructed.

A system for the efficient encoding of multi-shade pictures is described. The system uses a modified version of the contrast detecting sensor cell to transform a gray scale photograph to a two level (black-white) form without loss of pertinent pictorial detail in most cases. The transformed picture requires a channel with only one-fifth the bandwidth needed for direct transmission of the original picture. Finally, the maximum additional bandwidth saving which can be attained by efficiently encoding the transformed picture while considering intersymbol influence to a given depth is determined.

ASD-TR-61-620, Part II

TABLE OF CONTENTS

ASD-TR-61-620, Part II

LIST OF ILLUSTRATIONS

LIST OF TABLES

SECTION I.

INTRODUCTION

This Technical Report was prepared to inform Aeronautical Systems Division on the work performed under Contract AF 33(657)-8607, dated 9 April 1962. The report is prepared in accordance with the requirements of Item III of the contract.

The program is a continuation of activity begun under Contract AF 33(616)-7724, and the reader is referred to ASD Technical Report 61-620[*] dated December 1961 for a complete description of the first year's work.

The overall objective of these programs was to develop new communication components, techniques, and systems from analysis of biological phenomena. An interdisciplinary team of biologists, biochemists, physicists, and engineers was used to perform this analysis.

During the early months of the second year program, work was concentrated in three major areas judged to offer maximum payoff probability. These areas are summarized below.

1. Property Sensor Synthesis

  Sensing elements and retinas which respond to specific optical configurations of the environment were developed, and the microelectronic techniques necessary for the synthesis of such sensor cells were investigated. Using these techniques operational property sensing cells were constructed.

---

[*]This was not designated Part I.

ASD-TR-61-620, Part II

2. Threshold Operator Networks

Networks of threshold operators were used as a rough model of neural structure, and mathematical analysis was applied to such networks in an effort to obtain minimal structures for the computation of given functions of the input to the network.

3. Bio-Transducers

Materials extracted from photosynthetic bacteria were used to make sensor cells which exhibited a small but definite sensitivity to light. Sensors which gave both a photoconductive and a photovoltaic response were constructed.

Section II of this report describes the research in each of these areas in detail.

In addition to these major activities, a mechanism of a correlation theory of hearing was developed and described in a paper given at the 1963 Bionics Symposium. Using the concept of property sensitive photoconductive sensors, a numerical character reader was developed. This reader was described in a second paper given at the 1963 Bionics Symposium.

Section III describes a system used for the efficient coding of Air Force continuous tone pictures. A modified version of the contrast detecting sensor cell is used to transform pictorial data to a two-level (black-white) picture without the loss of any pertinent pictorial data for most pictures of interest. Groups of adjacent pictorial elements are considered to be characters and the frequency of occurrence of characters of each size was determined for several sets of data. This allowed an estimate to be made of the maximum bandwidth saving which can be obtained by efficient encoding of the pictorial data into blocks of a given size.

SECTION II.

MAJOR AREA RESEARCH

A.   SENSOR FABRICATION

The design of property sensitive photoconductive sensor cells was suggested during the first year's program by the operation of the frog's eye.[1] Photoconductive sensors were designed to duplicate some of the property sensing functions performed in this animal's eye. The reader is referred to the final report of the first year's program[2] for a complete description of these sensors. One of the sensors, a contrast detecting sensor, is shown in Figure 1. This sensor can be usefully employed in a pictorial data coding system, and therefore, the fabrication work was concentrated on the synthesis of this cell. The reader should refer to Section III B for a description of the operation of the sensor in the system. The following paragraphs of this section deal primarily with the procedures and analysis which led to the successful synthesis of such a cell.

All materials are vacuum deposited in a bell jar exhausted by a 6" CVC oil diffusion pump trapped with a liquid nitrogen baffle. The ultimate pressure of this system is on the order of 2×10^{-6} torr. The system is equipped with suitable Pirani, discharge, and ionization gauges for the measurement of pressures at various points of the system.

The materials to be deposited are contained in a cylindrical crucible 1/2" diameter and 1/2" deep. A lip at the top of the crucible permits suspending it in a furnace where it is radiantly heated. A single furnace can serve to heat each of the materials used. The furnace construction is shown in Figure 2. Tantalum foil 0.003 inch thick is spot-welded to form a cylinder 5/8" diameter with a flat electrode disc at the top. Two concentric tantalum cylinders act as heat radiation shields around the furnace. Alternating current is supplied to the central cylinder by a pair of water-cooled copper electrodes.

Radiant heating of the crucible gives superior control over the temperature of the source in the case of metal evaporation. When direct resistance heating of the crucible is used, the shunting effect of the metal evaporant causes excessively large heating currents and as the melt depletes

3

$\boxtimes$ — C_dS

$\square$ — In

$\blacksquare$ — S_iO

$\diagdown\diagdown$ — C_u
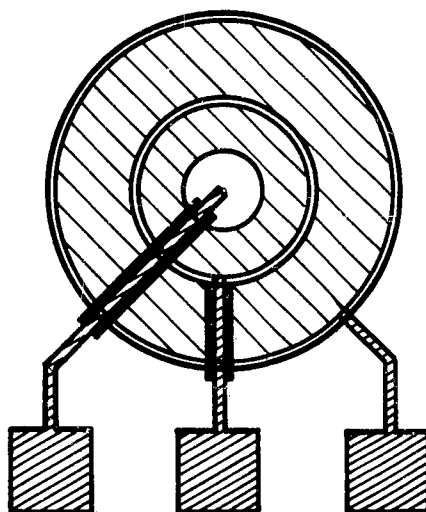
FIG. I   DETAIL OF CONTRAST DETECTOR EXPERIMENTAL CELL
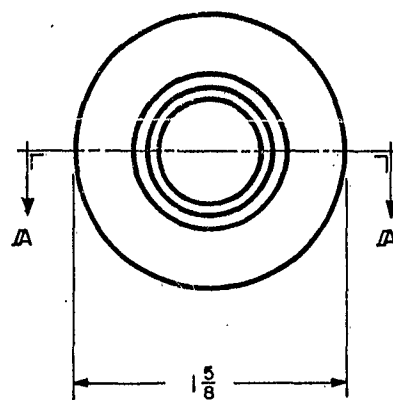
BOTTOM   VIEW
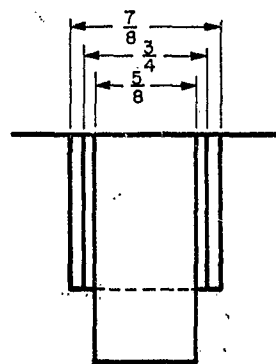
SECTION _A_-_A_

FIG. 2   EVAPORATION   FURNACE   DETAIL

due to evaporation, this shunting decreases, causing a corresponding change in the power dissipation. The result is that the temperature of the source increases. The evaporation rate of the metal is proportional to temperature so that it is imperative to control the temperature if one requires a constant evaporation rate.

The silicon monoxide is obtained in pellets of 1/2" diameter from Kemet Corporation and the pellets are suspended in the furnace on a tantalum wire so that their sides are heated by direct radiation. The temperature of the furnace is maintained at 1350°C during this evaporation since it has been found that the stress in the resultant SiO film is a minimum at this source temperature.[3] The substrate is at room temperature during the evaporation.

At the outset of the program the cadmium sulfide was evaporated in much the same manner as the silicon monoxide. Reagent grade CdS powder was compacted into 1/2" pellets and suspended in the furnace which was heated to 1050°C. High rates of deposition were obtained with this method but the purity of the films was low. Ultra-high purity cadmium sulfide was obtained from Eagle-Picher Corporation in the form of small crystallites which cannot be compacted into pellets. Consequently, a flat spiral coil of 0.020 inch tantalum wire was placed above a crucible containing the CdS so that the top surface of the CdS was heated by radiation. The temperature of the filament was 1050°C so that excessive dissociation of CdS did not occur. The substrate temperature was at first maintained at 300°C during the evaporation of CdS in order to reduce the contamination of the films by free cadmium. This was later reduced to 150°C as it was found that the sticking properties of the CdS molecules were adversely affected at the higher temperature and this led to non-uniformities in the thin film.

The substrates used during the program were always pyrex glass slides one inch square. They are thoroughly cleaned by first scrubbing in a detergent solution, immersing in a bath of chromic acid, rinsing in distilled water and, finally, alcohol drying in a vapor degreaser containing isopropyl alcohol. The substrate is then mounted in a holder in the vacuum system. The holder is an aluminum block 3" x 5" x 1/2" which is threaded with coils of tantalum wire with which the block can be heated during the evaporation.

The temperature is controlled by a Leeds and Northrup Electromax controller using an iron-constantan thermocouple as the sensing element.

Masks made of thin copper foil (.005 inch) are used to form the device patterns and are placed on top of the substrate on a special groove in the substrate holder. Four masks are used during the course of the cell fabrication, as illustrated in Figure 3. Mask A forms the photoconductive area. Mask B is used twice in order to deposit a complete set of rings of indium. Silicon monoxide is deposited through mask C, and the copper connector lines through mask D.

When it is necessary to control the deposition rate, an ionization gauge is placed in the vapor stream to measure the density of the evaporant. The evaporation rate is proportional to the indication on the gauge. A shutter, placed between the substrate and the source, is used to control the time of evaporation. In this way the resultant thickness of the films can be predicted quite accurately. The film thicknesses are measured using a Michelson-type interferometer.

1. Cadmium Sulfide Preparation

The major problem encountered during the synthesis of the cell was in the preparation of highly sensitive cadmium sulfide films. After noting that the first few films were only slightly sensitive to light excitation, the conductivity of the films was measured and found to be approximately 10^{-3} (ohm-cm)$^{-1}$ a value which was several orders of magnitude larger than that found in sensitive bulk cadmium sulfide, indicating that defects in the film, such as free cadmium atoms, vacancies, etc., were giving rise to excess electrons in the conduction band of the cadmium sulfide. These excess electrons overshadowed the excited photoelectrons and thus the photosensitivity of the films was minimal.

To eliminate these excess electrons, atoms of an acceptor material, i.e., one of the Group I elements such as copper or silver, can be incorporated into the cadmium sulfide lattice. Copper atoms have one less valence electron than cadmium and on substitution for cadmium create a hole in the lattice which has a large capture cross section for electrons. Then the excess electrons are captured by the copper sites and are removed from the conduction

7
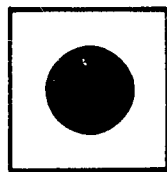
MASK A
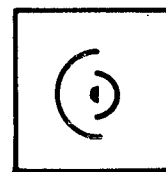
MASK B
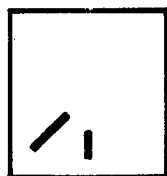
MASK C
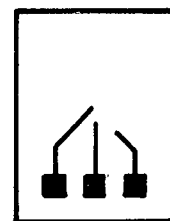
MASK D

FIG. 3   EDGE DETECTOR CELL MASKS

process. The conductivity of the cadmium sulfide is thus reduced and the photosensitivity is increased. This is illustrated by the graph of Figure 4. This plot shows the log of resistivity, both dark and light, versus copper concentration. Notice that the dark resistivity rises sharply at an earlier concentration of copper than does the light resisitivity. The light resistivity increases when the number of copper atoms get large enough because they begin to trap the photo-excited electrons. There is a particular concentration of copper for which the photosensitivity is a maximum. The experiment described in the next paragraph was performed to determine this best copper concentration.

The experiment was initiated by depositing strips of cadmium sulfide 0.75 inch long and 0.094 inch wide on a pyrex substrate. The thickness of the deposits averaged 6600 Å. The resistivity of the films at room temperature averaged about 1.2×10^3 ohm-cm. If one estimates the mobility of electrons in a thin film of cadmium sulfide at 10 cm^2/volt-second, then the number of free electrons (assuming majority carrier conductivity) is

$$n_e = \frac{\sigma}{e \mu_e} = \frac{1}{\rho \, e \, \mu_e}$$

$$= \frac{1}{1.2 \times 10^3 \times 1.6 \times 10^{-19} \times 10} = 5.2 \times 10^{14}/\text{cm}^3,$$

where

n_e = number of electrons,

σ = bulk conductivity of film,

ρ = bulk resistivity of film,

e = electronic charge,

and μ_e = electron mobility.

These are electrons already free in the conduction band of the film. This does not take into account all of the trapping centers in the energy gap which are occupied by electrons. A measurement of the slope of the plot of log dark conductivity versus inverse temperature yields the imperfection ionization energy in the following way. The number of free electrons is given by the expression:
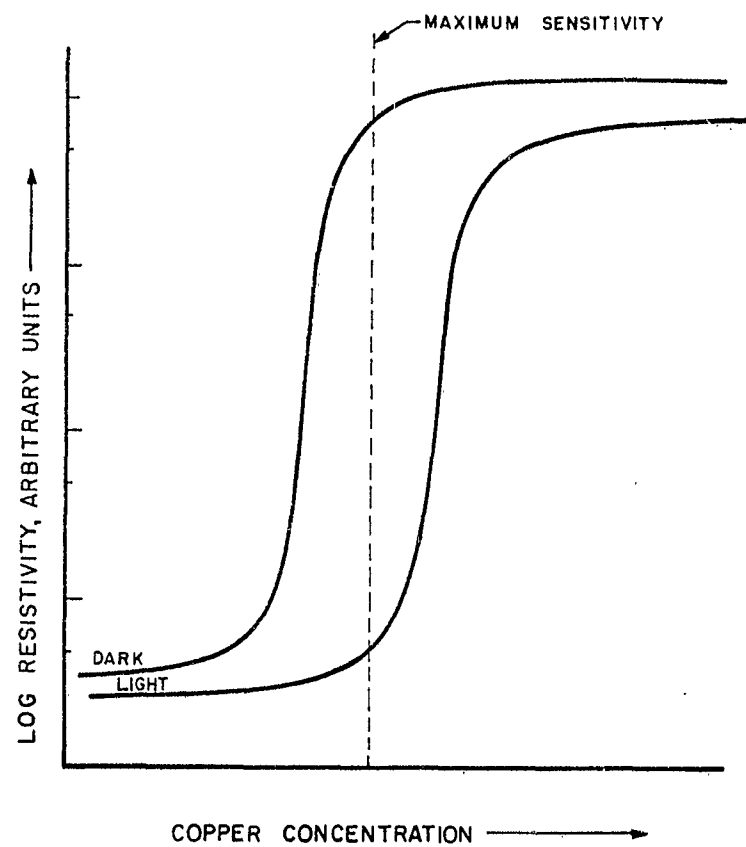
FIG. 4   LOG RESISTIVITY vs. COPPER CONCENTRATION
SHOWING REGION OF MAXIMUM SENSITIVITY

$$n_e = n_o \exp \left[- \Delta E / kT \right]$$

where

ΔE = the ionization energy,

n_o = constant,

k = Boltzmann's constant,

and   T = temperature.

Then
$$\sigma = e \mu_e n_o \exp \left[-\Delta E / kT \right] .$$

Taking the log of both sides

$$\log \sigma = \log (e \mu_e n_o) - (\Delta E / kT) \log e.$$

Taking the ratio of conductivities at two different temperatures gives

$$\log \sigma_1 - \log \sigma_2 = \frac{-\Delta E}{k} \left[\frac{1}{T_1} - \frac{1}{T_2} \right] \log e$$

since μ_e remains effectively constant for the two temperatures.

Selecting data from the curve of Figure 5 and inserting these numbers into the above equation, the ionization energy is found to be

$$\Delta E = - \log \frac{1}{2} \frac{k}{\left[\frac{1}{T_1} - \frac{1}{T_2} \right] \log e} = .31 \text{ electron-volts}$$

This energy is very close to the conduction band as the energy gap for cadmium sulfide is 2.4 electron-volts.

There are undoubtedly many other levels in the gap occupied by electrons. In order to compensate for these electrons more than 5×10^{14} copper atoms must be added to the CdS to compensate for the free electrons calculated from the conductivity at room temperature. In our experiments a 100 Å layer of copper was deposited onto the substrate prior to depositing a 10,000 Å layer of cadmium sulfide. This amounts to a concentration of copper of about 4 atomic per cent.
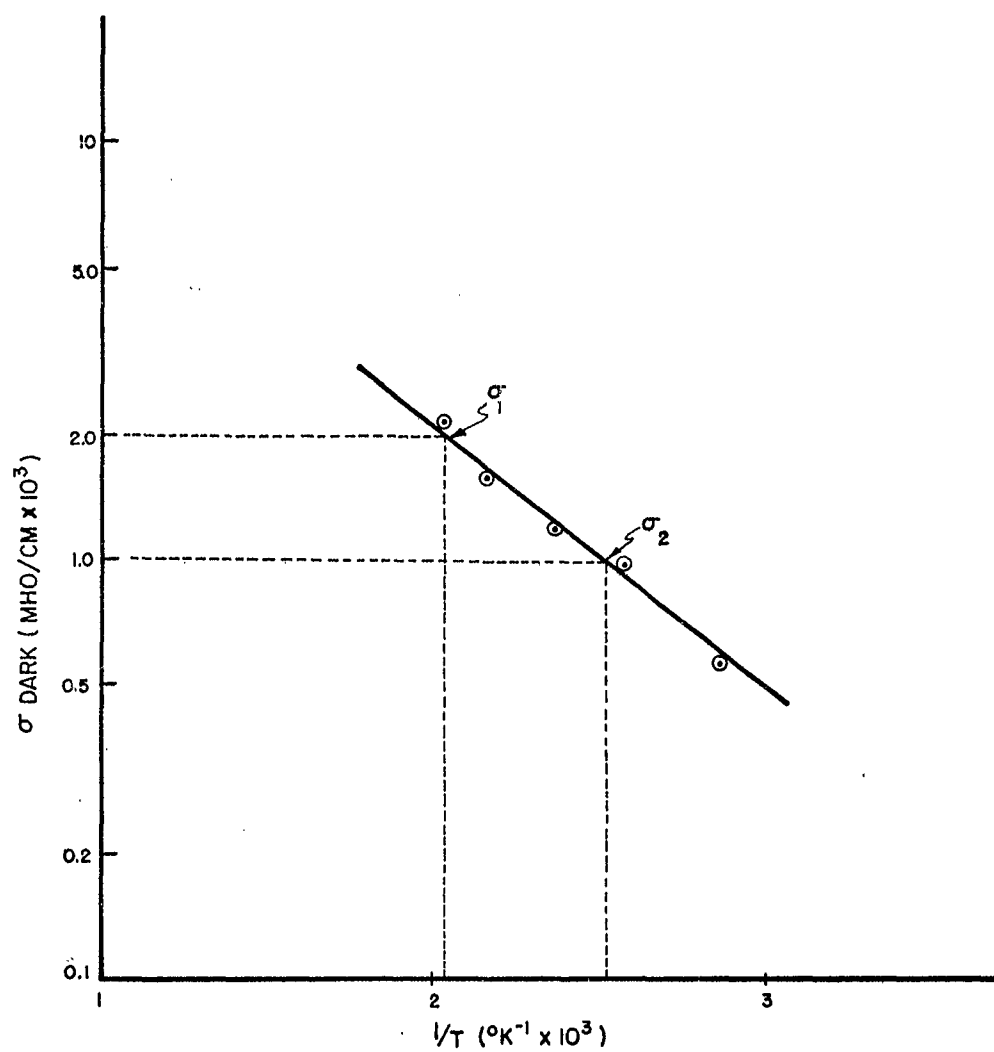
FIG.5   DARK   CONDUCTIVITY vs. INVERSE TEMPERATURE

12

The first attempts at incorporating copper into the cell were made by heating the copper-cadmium sulfide films, while still on the substrate holder, to 500° C. Repeatedly, as the temperature rose above 450° C, a reaction occurred between the aluminum of the holder and the cadmium sulfide, causing dissociation of the cadmium sulfide and the growth of small, barnacle-like deposits of cadmium on the holder and a resultant contamination of the film. After several failures in attempts to correct this problem, the procedure was modified by performing the diffusion in air in a combustion tube furnace. The specimen was placed in a pyrex tube and inserted into the furnace whose temperature was 550° C. A 15 minute diffusion was sufficient to distribute the copper throughout the cadmium sulfide.

The first film in which the diffusion was successful had the configuration shown in Figure 6. This configuration was adopted in order to measure the resistance of the cadmium sulfide which, for this sample, should be several orders of magnitude higher than for uncompensated material. Indeed, after the specimen had reached a stable value of dark resistance, the resistivity had increased to a value greater than 10^6 ohm-cm. This value is three orders of magnitude greater than for the uncompensated cadmium sulfide and indicates a corresponding decrease in the number of free electrons.

At the same time, the material became highly sensitive to photo-excitation. Where the uncompensated cadmium sulfide had shown reduction by a factor of about 3 in resistance on exposure to bright fluorescent light, the compensated film changed from a resistance greater than 10 megohms in the dark to about 7000 ohms under bright illumination, or a ratio of more than 1000. (All resistance measurements were made using a wheatstone bridge whose maximum measurable resistance was 10 megohms.)

The dark resistivity of the cell exhibited an unstable nature initially. At first measurement, the cell resistance was approximately 25,000 ohms, but at each subsequent measurement the resistance increased until after two days it had reached the limit of the bridge. A plausible explanation for this is that a highly conducting surface layer was formed on the cadmium sulfide during the diffusion by a reaction with air. After cooling, this surface layer formed a low impedance path between the electrodes. A different reaction,

13
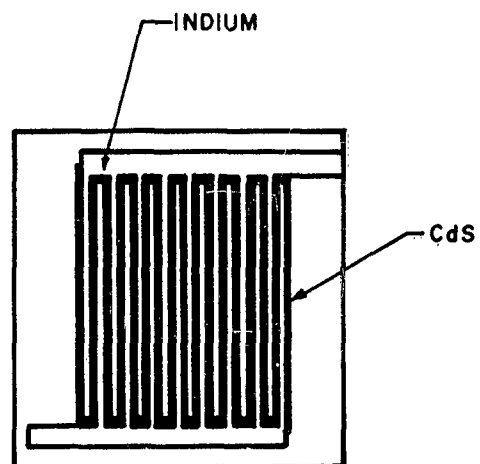
FIG.6   CELL FOR CONDUCTIVITY EXPERIMENT

14

occurring at room temperature, tended to destroy this surface layer, causing the cell conductivity to approach the bulk value. The nature of the reactions occurring are not known, but this aging phenomena has been observed by other workers.[4]

After the successful production of highly sensitive cadmium sulfide, a retinal cell with the configuration shown in Figure 1 was synthesized using the same technique for compensation of the excess electrons. The cell displayed high photosensitivity although, again, its dark resistance could not be measured.

The cell was mounted in a test apparatus constructed for analysis of sensor performance and was examined for response speed and uniformity of resistance. The apparatus consists of a light source focused onto the cell while being chopped by a wheel containing one square hole. The response was measured by observing the photocurrent pulse on an oscilloscope as the wheel was rotated. The rise time of the photocurrent was approximately 100 milliseconds while the decay took about one-half second.

By introducing copper into the cadmium sulfide lattice, free electrons and electrons which were held for a short time in the traps near the upper edge of the energy gap were captured. These traps become empty and available for trapping of photo-excited electrons. The photo electrons can wander into a trapping site, be thermally excited back into the conduction band, and wander again into a trapping site, doing this several times before finally combining with a hole in the valence band. Thus, the effective lifetime of the photo electrons is extended, causing a corresponding increase in the decay time. Therefore, one must pay the price of slower response if he is to achieve high sensitivity with thin films.

Recently, because of a contamination, the diffusion of the copper into cadmium sulfide has resulted in a pebbly structure in the film which produces a non-uniform photo response in the completed cell. A cadmium sulfide film deposited onto a clean glass substrate and subjected to the same steps occurring in diffusion showed no effects of contamination. Our first suspicion was that the diffusion was too fast; and that the copper film formed into globules when exposed to high temperature because of its extreme thinness. However, a slower diffusion did not improve the film.

15

About the same time as the contamination appeared in the films, the copper slug used in depositing the copper film became visibly coated with a glossy surface film. The crucible, slug and the surface contamination were spectroscopically analyzed and gave indications of having a relatively high concentration of silicon. This could be originating from the silicon monoxide residue in the furnace or from a "cracking" of silicone diffusion pump oil which is always present in the vacuum system. It is believed that a new crucible, uncontaminated with silicon, will yield pure films similar to those obtained initially.

B.   THRESHOLD OPERATOR NETWORKS

The threshold operator is an element which computes a function variously referred to in the literature as a threshold function, linearly separable function, realizable function, consistent function, or setting function. It was selected for study and use during this program for several reasons: It is a well defined structure for which a number of descriptive notations exist; it approximates present notions of the behavior of neural elements; several hardware implementations of the threshold operator exist; and it can be a very useful component in an artificial information processing system.

The threshold operator is defined in Figure 7, along with the diagrammatic conventions to be employed in describing networks of such operators.

$$-\infty < a_i < +\infty$$

$$-\infty < \theta_j < +\infty$$

$$x_i = 0 \text{ or } 1 \text{ for each } i$$

$$y_j = 1 \text{ if } \sum_i a_i x_i > \theta_j$$

$$y_j = 0 \text{ if } \sum_i a_i x_i \leq \theta_j$$
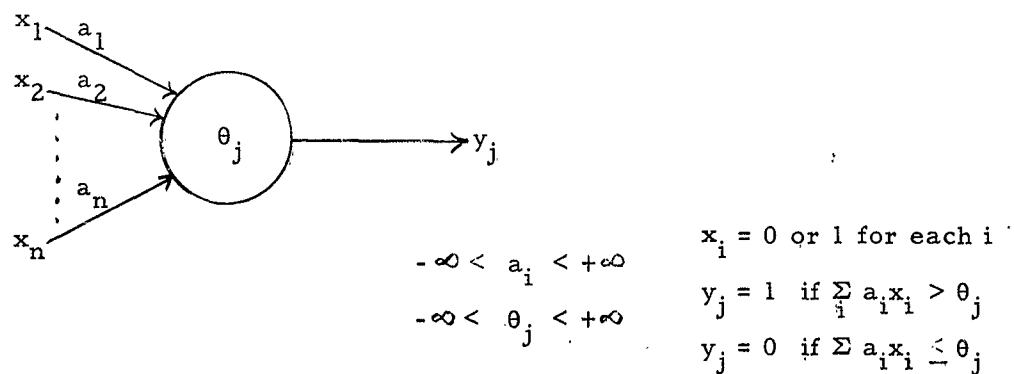
FIG. 7   THRESHOLD OPERATOR

16

1.   Synthesis Problem

This study addressed itself to the development of algorithms useful in the synthesis of the simplest (minimal) network of threshold operators to perform a given Boolean function calculation. The computation of a given Boolean function can be thought of as performing a recognition function on a set of binary input variables; and hence the satisfactory solution of this problem would be of appreciable aid in the selection of networks to be used in the encoding of the block characters described in Section III.

The general synthesis problem has long resisted satisfactory solution; and in an effort to simplify the task, the analysis was restricted to symmetrical Boolean functions. As the name implies, a symmetrical Boolean function is one in which the input variables can be interchanged without affecting the output value. The problem which was attacked can be described as follows:

Given an arbitrary symmetric Boolean function of
n variables, what is the minimum number of
threshold operators which will realize this function
and what are the weights and connections associated
with these threshold operators?

The function under consideration will be denoted by

$$f(x) = (x^0, x^1, x^2, x^3, x^4, \ldots x^n)$$

where the x^i's have the values of 0 or 1 depending on whether the function is to have an output of 0 or 1 when i of the input variables have the value of 1.

An illustration should help to clarify this notation. Consider a symmetric function of six variables which takes on the value 1 when either exactly two or exactly four of the input variables are 1 and which otherwise has a value of 0. This is denoted as

$$f(x) = (0, 0, 1, 0, 1, 0, 0) .$$

In the discussion that follows, the form illustrated in Figure 8 will be assumed for the combination of threshold devices needed to compute a given symmetric function. Each circle represents a threshold operator with threshold θ_j.

17
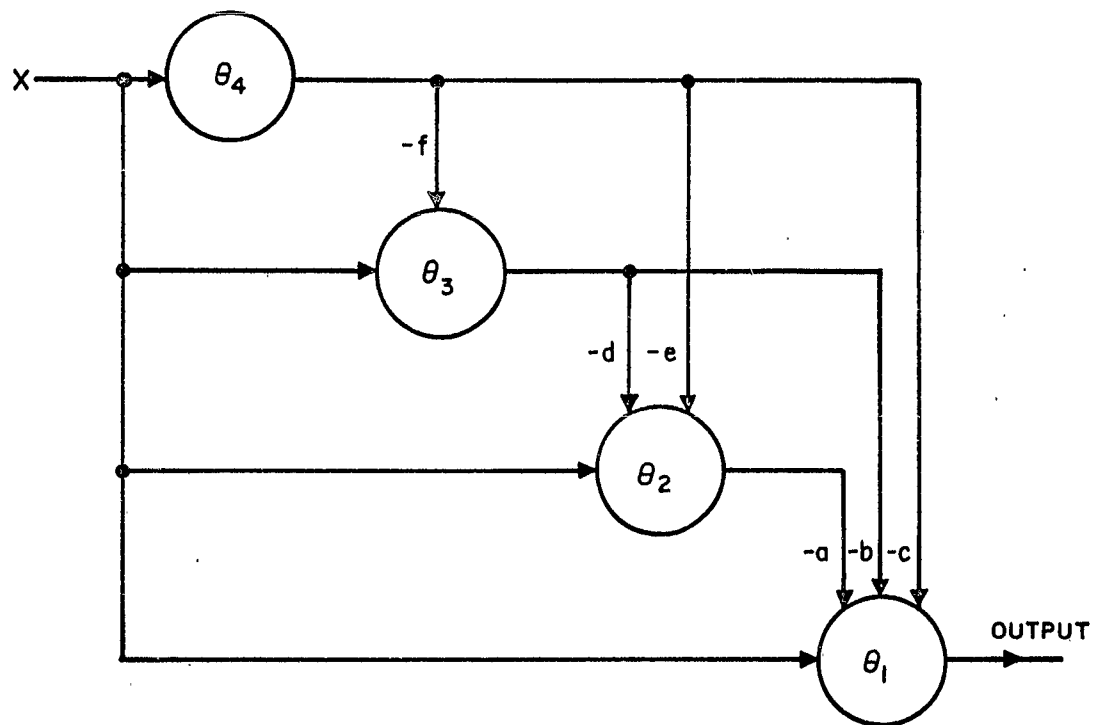
FIG. 8   THRESHOLD NETWORKS FOR COMPUTING
SYMMETRICAL FUNCTIONS

In the diagram of Figure 8 there is only one input to each operator. This input actually represents all of the input variables. However, since symmetric functions are being computed, the weights associated with each input are equal, and in fact, can be normalized to be unity. Thus x is considered to be a variable taking on a numerical value equal to the number of input variables which are equal to 1.

Now consider a stair step function, Q, of the input variables. Define a symmetrical Boolean function from Q by using the rule: If Q is greater than x then the function is to have the value of 0; if Q is less than x then the function is to have the value of 1.

Figure 9 illustrates a typical symmetric function, $f(x) = (1, 0, 0, 1, 0, 1)$ and its associated Q function. Note that Q completely describes $f(x)$ and conversely, $f(x)$ completely determines Q. Then if a simple way of synthesizing Q can be found, the synthesis of $f(x)$ will be completed. By referring to Figure 8, it can be seen that Q has the value of the weighted sum of the outputs from the other threshold devices going to the final operator. In fact by adjusting the weights of the leads associated with these outputs and adjusting the thresholds of operators, the shape of the Q function can be controlled. Figure 10 is a graph of a general Q function for four threshold operators. On the graph the reader will find the portion of the Q function which is controlled by the various parameters of the operators of Figure 8. Note that for a six step Q function there is not complete freedom as to where the steps will occur. In fact, the last step is fixed to within one unit in either direction. Of course, the magnitude of the Q function steps is also fixed accordingly.

It was hoped that once the decomposition of the Q function into appropriate steps was accomplished, the positions of the steps could be adjusted to generate the desired function. If this were so, then the numbers which specify the magnitude of the steps would serve to identify a large class of Q functions. The Q functions could then be used to synthesize any function which had the same magnitude steps associated with it.

However, the example of Figure 11 illustrates a set of three operators which will generate the steps 4, 6, 10, 13, 17, 19, 23 and yet these operators together with the output operator will not generate the function

19
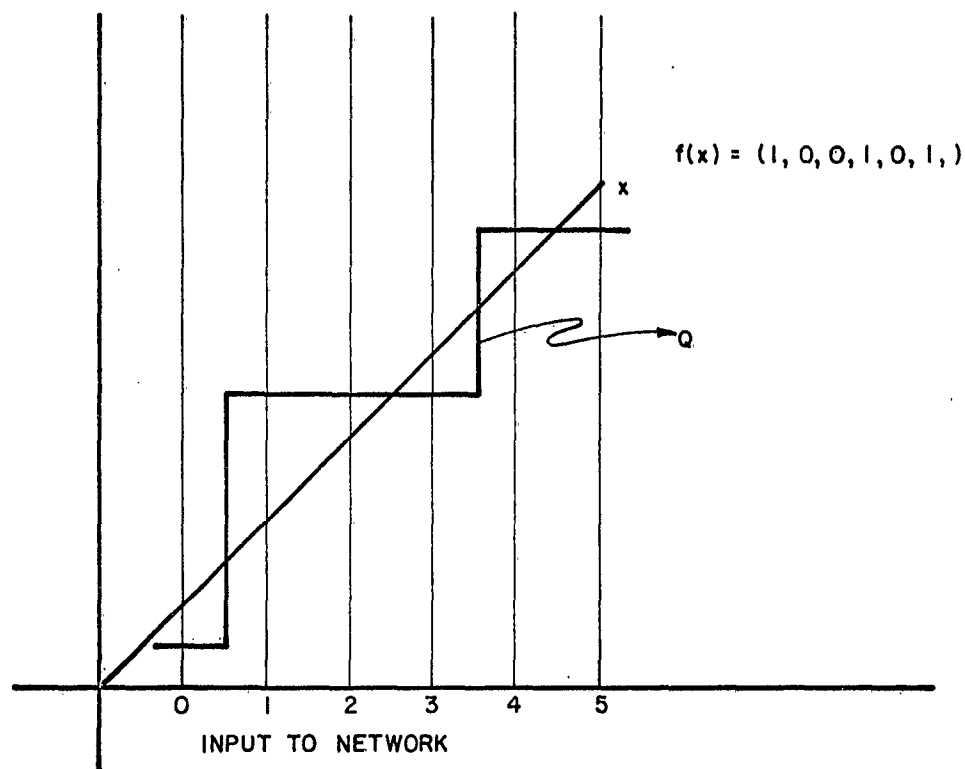
$f(x) = (1, 0, 0, 1, 0, 1,)$

FIG. 9   ILLUSTRATION OF A Q FUNCTION
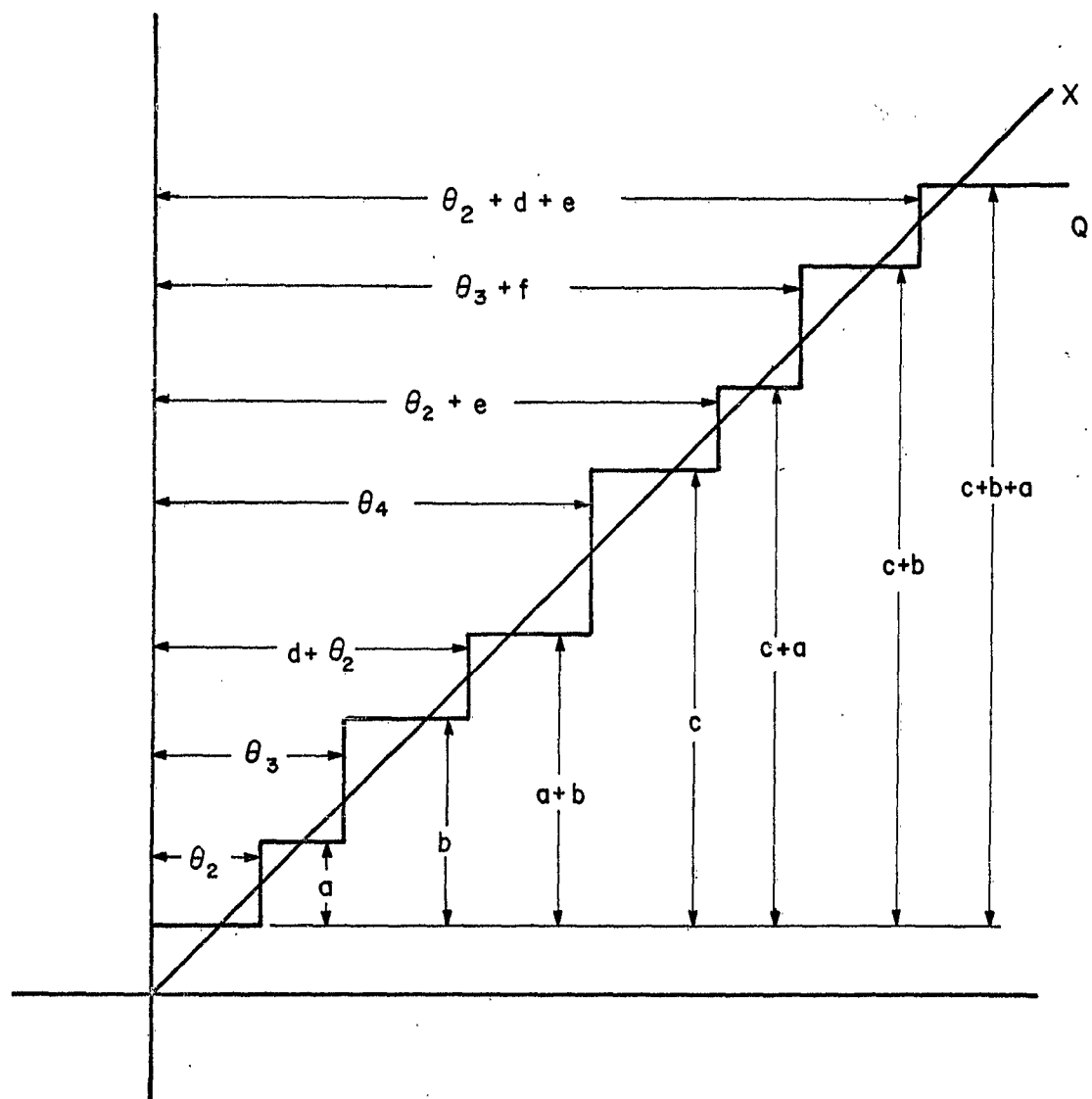
FIG.10   Q-FUNCTION ASSOCIATED WITH NETWORK
OF FIGURE

21
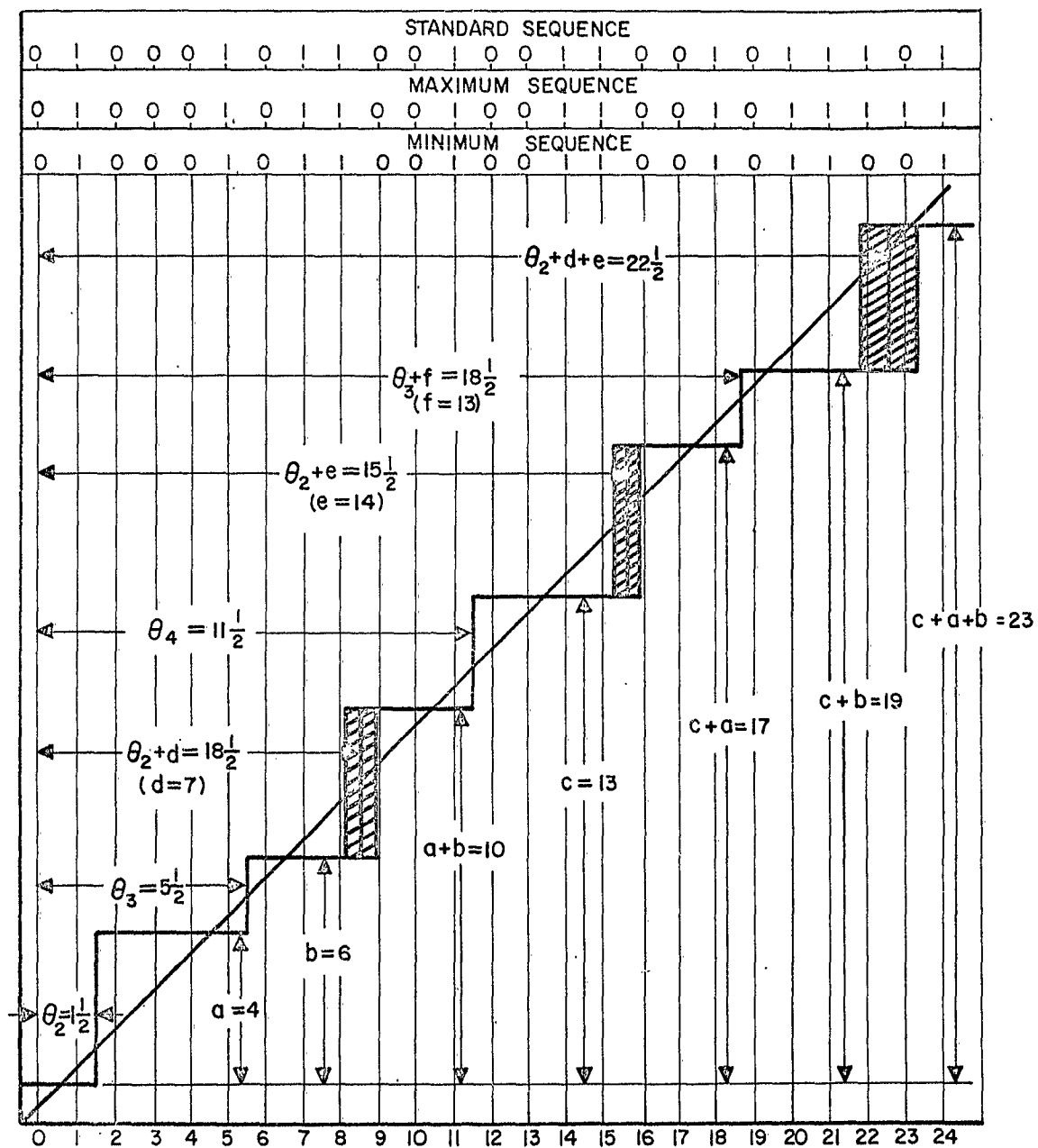
FIG. II   Q-FUNCTION WITH STEPS
AT 4, 6, 10, 13, 17, 19, AND 22

22

$f(x) = (0100010110010011001010001)$, although this function has precisely the above steps. Shown above the graph are the sequences which this set of operators will form by adjusting the last step to its extreme values. This adjustment is denoted by the shaded portion of the graph and is accomplished by slightly changing the appropriate threshold and weights.

Therefore, although the Q function is a useful artifice for studying the synthesis of symmetric Boolean functions, it does not realize an algebraic solution of the synthesis problem.

2. Threshold Operator Capability

It was noted earlier in this report that many hardware implementations of a threshold operator exist. In some of these implementations there is no basic difference between the threshold input and all other inputs. For example, a threshold operator of dimension n may be constructed of a magnetic core with n + 1 windings, one of which corresponds to the threshold and the other n to weights. Any of the n + 1 windings may be chosen to be the threshold winding in a given application.

It is instructive and useful in a hardware sense to examine the set of external wiring changes which can be performed on such a threshold operator.

First consider the changes that can be made without altering the number of turns in each winding on the core. These changes are:

      (1) reversal of sense of a winding

      (2) relabeling of the input and/or threshold windings

      (3) not connecting a winding, and

      (4) connecting together two or more windings in an appropriate manner. *

Depending on the pulsing system used, that is, whe' .er a current, no current (1, 0) system or a positive current, negative current (+1, -1) system is used to represent the input variables, different threshold functions result. . Table I is a list of the permissible wiring changes for a threshold operator with initial threshold θ and initial weights w_i for the input windings.

---

*Series connection for a current source, parallel connection for a voltage source.

Table 1

PERMISSIBLE WIRING CHANGES

Wiring Changes of Threshold Operator	Description of Changes	Alg. Interpretation in (1, 0) System	Alg. Interpretation in (+1, -1) System	Comments About Algebraic Interpretations
θ, w_1, w_2, w_3	Initial threshold operator	$f(x_1, x_2, x_3)$	$g(x_1, x_2, x_3)$	Initial functions corresponding to the threshold operator given
$\theta, -w_1, w_2, w_3$	Reversing leads of No. 1 winding	No algebraic interpretation	$g(\overline{x}_1, x_2, x_3)$	Complementation of x_1 variable in (+1, -1) system
$\theta, 0, w_2, w_3$	No connecting No. 1 winding	$f(0, x_2, x_3)$	No algebraic interpretation	Setting x_1 variable equal to 0 in (1, 0) system
$-\theta, -w_1, -w_2, -w_3$	Reversing leads of all input windings and threshold winding	$\overline{f}(x_1, x_2, x_3)$	$\overline{g}(x_1, x_2, x_3)$	Complementation of function
$\theta, 0, w_1, +w_2, w_3$	Connecting input winding No. 1 to input winding No. 2 while preserving sense of each	$f(x_2, x_2, x_3)$	$g(x_2, x_2, x_3)$	Setting x_1 equal to x_2 in both systems
$\theta, -w_1, 0, w_2, w_3$	Reversing sense of No. 1 winding and then connecting it to the threshold winding	$f(1, x_2, x_3)$	$g(1, x_2, x_3)$	Setting x_1 variable equal to 1 in both systems
$\theta, +w_1, 0, w_2$	Connecting input winding to No. 1 to threshold winding with sense of each preserved	No algebraic interpretation	$g(0, x_2, x_3)$	Setting x_1 variable equal to 0 in the (+1, -1) system
$0, w_1, w_2, w_3, \theta$	Interpreting threshold winding as another input	No algebraic interpretation	$\overline{\theta} g(x_1, x_2, x_3) + \theta\, \overline{g}(\overline{x}_1, x_2, x_3)$	
$0, w_1, w_2, w_3, -\theta$	Interpreting threshold as input winding sense reversed	No algebraic interpretation	$\theta g(x_1, x_2, x_3) + \overline{\theta}\, \overline{g}(\overline{x}_1, x_2, x_3)$	

All of these weights will be assumed to be integers. Also, it is assumed that the threshold is not strictly equaled for any combination of input variables. That this offers no restriction of generality has been shown by Kazerman, In the (1, 0) system the initial function is denoted $f(x_1, x_2, x_3)$ while in the (+1, -1) system the initial function is denoted $g(x_1, x_2, x_3)$.

By observing Table I, we see that all of the algebraic operations complementing a variable, complementing the function, relabeling the variables, or setting a variable equal to a Boolean constant, can be interpreted as an appropriate wiring change if we use the (+1, -1) system. If we use (1, 0) system then all except the first of the algebraic operations can be interpreted as appropriate wiring changes. Because all the algebraic operations can be so interpreted in the (+1, -1) system, our discussion will be restricted to this system.

A notion of equivalence of threshold functions will not be defined. Two definitions are given--one based on algebraic operations, the other on wiring changes. Two functions f and g will be said to be F_A^n equivalent if there exists a 50-50 threshold function[*] F_A^n of n Boolean variables such that both f and g can be derived from F_A^n under one or more of the algebraic operations mentioned previously. Alternately two threshold functions f and g will be said to be F_w^n equivalent if there exists a 50-50 threshold function of n Boolean variables such that both f and g can be derived from F_w^n under one or more of the wiring changes mentioned previously. Note that in the (+1, -1) system F_w^n includes F_A^n for a given pair of functions f and g since all algebraic operations can be interpreted as wiring changes. The question then arises of whether there exists a "simpler" function which includes f and g under wiring changes than the function which includes them under algebraic changes. This question has been partly answered if two functions are compared only on the basis of the number of windings they possess. The following theorem illustrates this.

---

[*]A Boolean function is said to be a 50-50 function if it is true for exactly 1/2 of min terms, i.e., points in the n - dimensional space.

THEOREM

Given two 50-50 threshold operators f and g with n and m positive integral weights respectively in the $(+1, -1)$ system, which are F_w^q equivalent and which are not $F_w^{q'}$ equivalent for any $F_w^{q'}$ such that $q' < q$; then there exists a 50-50 threshold operator F_A^r such that f and g are F_A^r equivalent where r = at most $q + 1$.

PROOF

Let $\quad w_1, \ldots, w_n \qquad$ be the weights of operator f

$\qquad v_1, \ldots, v_m \qquad$ be the weights of operator g

$\qquad p_1, \ldots, p_q \qquad$ be the weights of operator F_w^q

Define the following sets:

$\qquad S \quad = \quad \{ p_1, \ldots, p_q \}$

$\qquad S_a \quad = \quad \{ p_{a_1}, \ldots p_{a_r} \}$, weights set = 0 when realizing f.

$\qquad S_b \quad = \quad \{ p_{b_1}, \ldots p_{b_s} \}$, weights set = 0 when realizing g.

$\qquad S' = S - (S_a \cup S_b) = \{ p_{c_1}, \ldots, p_{c_t} \} \quad$ weights not set = 0 when realizing f or g.

Note that $S_a \cap S_b = \phi$ (null set) since any weight set = 0 when realizing both f and g would not be needed and hence q would not be minimum as required.

Consider the following cases:

$\quad$ I $\qquad - S_a = \phi$ and $S_b = \phi$.

$\quad$ II $\qquad - S_a = \phi$ and S_b consists of one element.

$\quad$ III $\qquad - S_a$ consists of one element and $S_b = \phi$.

$\quad$ IV $\quad - S_a$ consists of one element and S_b consists of one element.

$\quad$ V $\qquad - S_a$ consists of two or more elements and S_b consists of one element.

$\quad$ VI $\qquad - S_a$ consists of one element and S_b consists of two or more elements.

$\quad$ VII $\quad - S_a$ consists of two or more elements and S_b consists of two or more elements.

26

In following the proof of the various cases, remember that all wiring changes are algebraic with the single exception of setting a weight equal to 0 (e. g. disconnecting a winding). When windings are described as connected opposing or aiding, it is meant that they are connected together serially on the core threshold device used. Although the input variable to be connected to the new winding combinations are not indicated, this input variable should be apparent from the construction.

CASE I

Take

$F_A^r = F_w^q$ with $r = q$ and theorem is trivially satisfied.

CASE II

Let

F_A^r have weights $p_{c_1}, \ldots, p_{c_t}, \dfrac{p_{b_1}}{2}, \dfrac{p_{b_1}}{2}$, where p_{b_1} is the element of S_b.

By connecting the last two windings to oppose, f can be algebraically realized. Whereas when these two windings aid each other, g can be algebraically derived.

Counting weights, we find $r = q + 1$.

CASE III

Essentially the same as Case II.

CASE IV

Assume

$p_{a_1} > p_{b_1}$ where $p_{a_1} \in S_a$, $p_{b_1} \in S_b$.

Let

F_A^r have weights $p_{c_1}, \ldots, p_{c_t}, \dfrac{p_{a_1} - p_{b_1}}{2}, \dfrac{p_{a_1} + p_{b_1}}{2}$.

Then

f and g are F_A^r equivalent (again seen by alternately connecting the last two windings opposing and aiding).

Counting weights, we find $r = q$.

Let

$F_A{}^r$ have weights $p_{c_1}, \ldots, p_{c_t}, p_{a_2}, \ldots, p_{a_n},$

$$\frac{\sum\limits_{j=2}^{n} (p_{a_j}) + p_{a_1} + p_{b_1}}{2}, \qquad \frac{\sum\limits_{j=2}^{n} (p_{a_j}) - p_{a_1} + p_{b_1}}{2}$$

To derive f algebraically, connect the last two windings opposing, and to derive g algebraically, connect $p_{a_2}, \ldots, p_{a_n}$ aiding each other while opposing the last two windings.

Again counting weights, we find $r = q$.

CASE VI

Essentially the same as Case V.

CASE VII.

Let

$F_A{}^r$ have weights $p_{c_1}, \ldots, p_{c_t}, p_{a_2}, \ldots, p_{a_r}, p_{b_2}, \ldots, p_{b_s}, \psi_1, \psi_2$

where

$$\psi_1 = \frac{\sum\limits_{i=2}^{r} p_{a_i} + \sum\limits_{j=2}^{s} p_{b_j} + p_{a_1} + p_{b_1}}{2}$$

$$\psi_2 = \frac{\sum\limits_{i=2}^{r} p_{a_i} - \sum\limits_{j=2}^{s} p_{b_j} - p_{a_1} + p_{b_1}}{2}$$

By connecting ψ_2 to oppose ψ_1 and to aid $p_{b_2}, \ldots, p_{b_s}$, f can be algebraically derived.

Similarly, by connecting ψ_2 to aid ψ_1 and to oppose $p_{a_1}, \ldots, p_{a_n}$, g can be algebraically derived.

Therefore, again counting weights, we find $r = q$.

Although the algebraic operator contains at most one more winding than the operator derived using wiring changes, it usually consisted of more total turns. Table 2 tabulates the total number of turns for each of the cases cited in the proof of the theorem for each of the operators. Also the excess is computed.

28

Table 2

COMPARISON OF ALGEBRAIC AND WINDING OPERATORS

Case	Total Number of Turns Algebraic Operator	Total Number of Turns Winding Operator	Excess Turns Algebraic Operator Minus Turns Winding	Excess Windings
I	Σ_3	Σ_3	0	0
II	$\Sigma_3 + p_{b_1}$	$\Sigma_3 + p_{b_1}$	0	1
III	$\Sigma_3 + p_{a_1}$	$\Sigma_3 + p_{a_1}$	0	1
IV	$\Sigma_3 + p_{a_1}$	$\Sigma_3 + p_{a_1} + p_{b_1}$	p_{b_1}	0
V	$\Sigma_3 + 2\Sigma_1 + p_{b_1} - 2p_{a_1}$	$\Sigma_3 + \Sigma_1 + p_{b_1}$	$\Sigma_1 - 2p_{a_1}$	0
VI	$\Sigma_3 + 2\Sigma_2 + p_{a_1} - 2p_{b_1}$	$\Sigma_3 + \Sigma_2 + p_{a_1}$	$\Sigma_2 - 2p_{b_1}$	0
VII	$\Sigma_3 + 2\Sigma_1 + \Sigma_2 - 2p_{a_1}$	$\Sigma_3 + \Sigma_2 + \Sigma_1$	$\Sigma_1 - 2p_{a_1}$	0

where

$$\Sigma_1 = \sum_{i=1}^{r} p_{a_i} \qquad \Sigma_2 = \sum_{j=1}^{s} p_{b_j} \qquad \Sigma_3 = \sum_{k=1}^{t} p_{c_k}$$

It is assumed all p's are positive, $s \geq 2$, $r \geq 2$, $\psi_1 > 0$, $\psi_2 > 0$, $p_{a_1} > p_{b_1}$

The values derived are obviously dependent upon the fact that ψ_1 and ψ_2 are integers. $F_w^{\,n}$ will be called minimum if it is true that a minimal number of windings, n, are used and the sum of the number of turns on all windings is minimal for F_w of dimension n. For $F_w^{\,n}$ minimum, it can be shown that ψ_1 and ψ_2 are indeed integers.

From Table 2 we see that there exists an algebraic operator which is (in terms of the number of windings) nearly as good as the wiring operator which will realize a group of functions. In fact, it was found for the case of 1, 2, 3, 4, and 5 Boolean variables that the algebraic operator was exactly the same as the wiring operator which would realize all the threshold functions formed from these variables. The algebraic operators were not formed by applying the method used in the proof of the theorem, but were discovered on a trial and error basis and then compared to the wiring operator which would do the same job.

3. Invariance Relations in Threshold Networks

The purpose of the study reported in this section has been an attempt to formulate a theory of threshold networks, i. e., formal abstractions of neural networks, in which it is possible to find invariance relations over sets of alternate networks capable of "equivalent" behavior or computation. The fact that such "equivalent" networks exist, and that they seem to imply some sort of trade-off among variables loosely defined as speed, complexity, and accuracy, is discussed in the first year's Creature Communications final report, and will not be repeated here. We will however, before proceeding to the results obtained, make at least one observation not contained in the previous report. We must require that the theory make some sort of physical "sense" in terms of the elements of the networks themselves. Note that we might define an invariance relation in terms of the networks themselves by simply stating that all networks that compute the same function are equivalent and have the same formal measure. However, such a definition is clearly a tautology unless we discover how to reflect the network "measure" back to the components themselves and find rearrangements of the components yielding sensible networks.

The initial attempts to find such a measure took the point of view that a useful measure would have to hold over all functions and that we could therefore obtain useful information about the properties of such a measure by the study of a very special case. The networks we shall first examine are those which evaluate the "disjunction" of a set of Boolean variables. If we define $f(t, n)$ to be the Boolean function of n arguments that is true if t or more of its arguments are true, then the disjunction of n arguments is of course the function $f(1, n)$. This is an interesting function in that it is itself a threshold function so that a network computing the function $f(1, n)$ might consist of a single element (threshold operator), or it might be decomposed into a large number of elements. Figure 12 illustrates two obviously "equivalent" nets each of which computes the function $f(1, n)$.

We now attempt to associate a cost, $C(i, j)$ with each of the elements in such a way that the cost of each network is the sum of the cost of the parts, and the utility is given by the rate at which calculations can be made. Since the net of Figure 12B apparently operated at one-half the rate of the net of Figure 12A (i. e., the time required is assumed to be the time required for two elements to switch in time sequence) we obtain the following relation.

$$C(1, n) = \frac{1}{2} [C(1, m) + C(1, n - m + 1)] . \tag{2-1}$$

However if we consider the case of $n = 3$, and $m = 2$, we find

$$C(1, 3) = \frac{1}{2} [C(1, 2) + C(1, 2)] = C(1, 2) \tag{2-2}$$

This suggests that the cost of an element computing $f(1, 3)$ is the same as the cost of one computing $f(1, 2)$ which makes no sense at all. We now note that if with respect to Figure 12B, we arrange to present the variables x_{m+1} through x_n to the input of the second operator one unit of time later than the time at which variables x_1 through x_m appear, that although there is a greater time delay in the computation of $f(1, n)$ by the net of Figure 12B, the actual rate at which computation may take place is the same in both nets so that we modify (2-1) to read,

$$C(1, n) = C(1, m) + C(1, n - m + 1) . \tag{2-3}$$

A. One Operator Realization
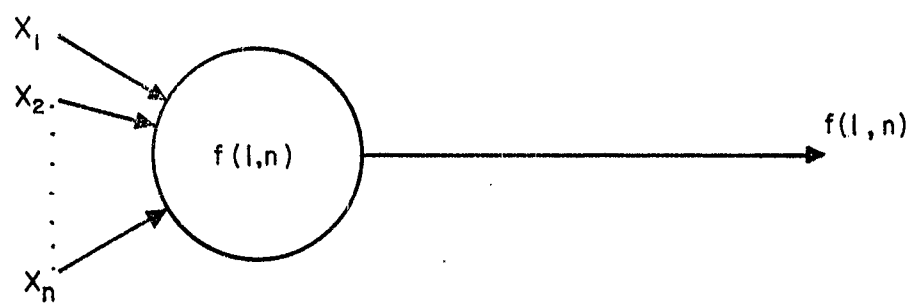
B. Two Operator Realization

FIG. 12   TWO REALIZATIONS OF DISJUNCTION OF n VARIABLES

Equation (2-3) may be solved by recessive techniques to obtain the following results. $C(1,1)$ is equal to zero. This, of course, makes sense since $f(1,1)$ is nothing but a _connection_ with which we have associated no cost. Further we obtained $C(1,n) = (n-1) C(1,2)$ for $n \neq 1$. This leads to the following results. If we take $C(1,2) = 1$, the cost of an element for computing $f(1,n)$ is simply $(n-1)$ and further the sum of the costs of the elements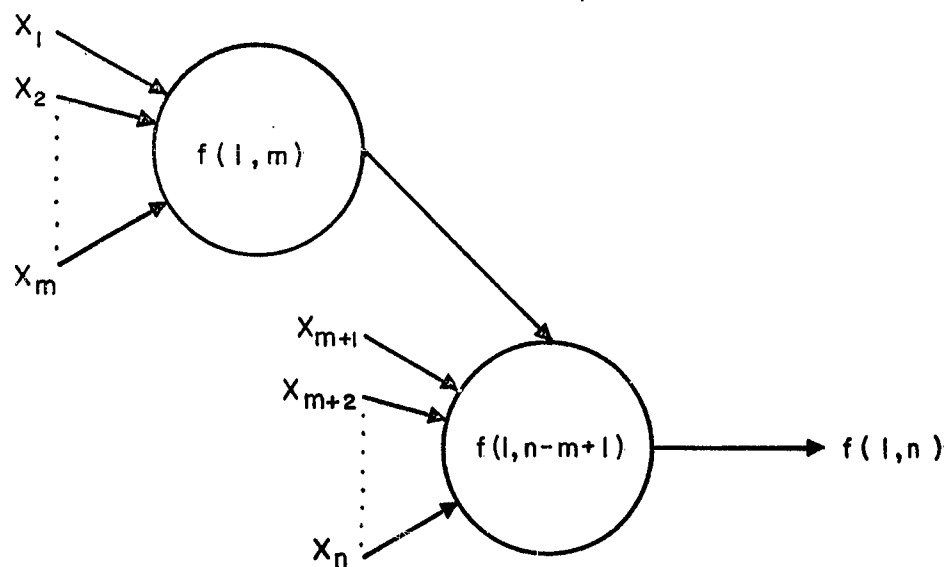 of any effective network computing the function $f(1,n)$ will be equal to $(n-1)$. This is illustrated in Figure 13 in which several nets are illustrated each of which computes the function $f(1,8)$. Thus we have a measure relative to the threshold elements that compute functions of the form $f(1,n)$ which has the desired conservation properties relative to the set of networks which compute functions of this same form. It is in fact the only measure which has the desired conservation property. We next attempt to generalize the measure to more general functions. We note that the previously discussed measure might be interpreted as the minimum number of 2-input operators required to construct a network realization of a given function. With this interpretation we note that conjunction behaves in exactly an analogous manner so that if $C(1,2) = C(2,2) = 1$, we have $C(1,n) = C(n,n)$. In fact, we may conclude that $C(1,n) = C(n+1-i, n)$ for $i \leq n$. The physical interpretation of this observation is that if we have a minimal net for the computation of $f(t,n)$, we may obtain a minimal net for the computation of $f(n+1-t, n)$ by simply complementing all input variables and complementing the network output as well. The proof that the resulting net is also minimal may proceed by contradiction; if not minimal, the minimal net for the computation of $f(n+1-t, n)$ could be transformed as above into a still smaller net for the computation of $f(t,n)$, negating the hypothesis that the original net for the computation of $f(t,n)$ was minimal.

We next attempt to obtain an expression for $C(t,n)$. A series of trial designs led to the values tabulated in Table 3 in matrix form. Although no general proof of minimality for these networks has been obtained, several of the designs have been established as minimal by exhaustive enumeration of the alternative nets, so that we may place a high degree of confidence in the resultant values. The structure of Table 3 is immediately apparent (the first differences are one in the first row, three in the second row, five in the third row, etc.). From this we may reasonably infer the equation,

33
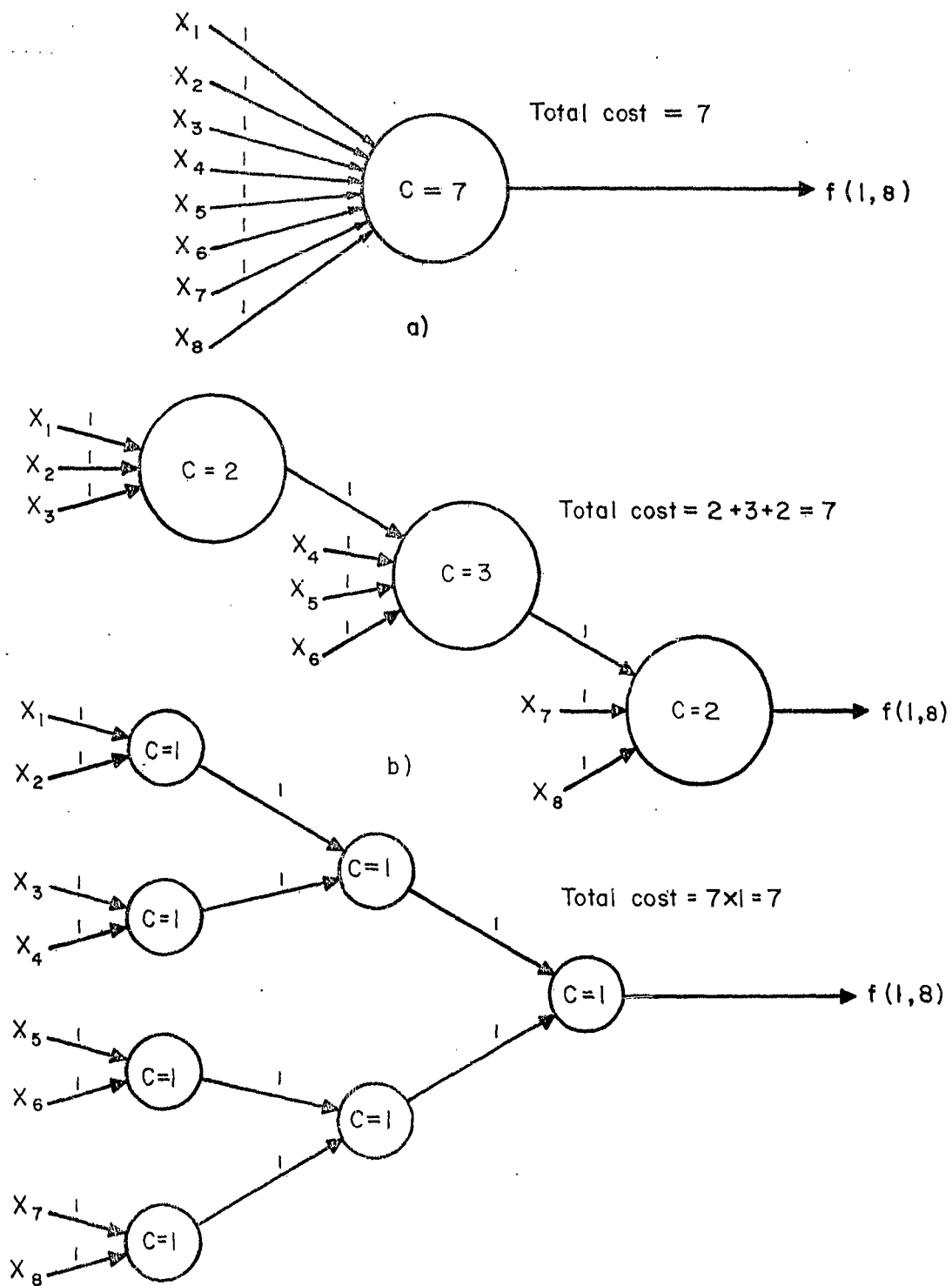
FIG.13 REPRESENTATIVE NETS FOR THE
EVALUATION OF f(1,8)

Table 3

MATRIX OF VALUES FOR C(t, n)

n \ t	1	2	3	4	5	6	7	8	9	10	11
1	0	1	2	3	4	5	6	7	8	9	10
2	0	1	4	7	10	13	16	19	22	25	--
3	0	0	2	7	12	17	22	27	--	--	--
4	0	0	0	3	10	17	--	--	--	--	--
5	0	0	0	0	4	13	22	--	--	--	--
6	0	0	0	0	0	5	16	27	--	--	--

$$C(t, n) = (t-1) + (2t-1)(n-1) \qquad (2-4)$$

While several attempts to prove the validity of (2-4) have been made, only certain special cases have been successfully established, e. g. , $C(1, n)$, $C(n, n)$, $C(2, n)$, and $C(n - 1, n)$.

However, if we assume that equation (2-4) is a valid equation an interesting comparison is possible. Let us assume that the cost of an element for computing $f(1, 2)$, i. e. $C(1, 2)$, is unity and find the cost of a network composed of such elements designed to evaluate the function $f(t, n)$ where we assume $n = kt$. We obtain,

$$C(t, kt) = (t-1) + (2t-1)(kt-t) \qquad (2-5)$$

or for reasonably large t

$$C(t, kt) = 2(k-1) t^2 \qquad (2-6)$$

Let us compare this solution with the single element computing the same function in which we assume nominal weights associated with each input variable of unity, input variables having the values of $+1$ or -1, and a threshold value, $\theta = n+1 - 2t$, so that the function $f(t, n)$ will be obtained. We further assume that each of the weights and the threshold value θ is to some extent inaccurately established, and in fact may take on any value between $w/(1+a)$ and $w(1+a)$, i. e. a may be thought of as related to the percentage variation we expect in the values of the actual weights. We next ask what the value of a must be in order to insure that in the worse possible case the value of the output of the operator will be correct. The worst case occurs when only $t-1$ of the variables are true, i. e. take on the value $+1$, and the weights associated with these have the maximum value $1+a$, the weights associated with the remaining $n - t+1$ variables having the value false, have decreased to $1/(1 + a)$, and the threshold value has increased to $(n+1 - 2t)(1 + a)$. In order that the output be proper, e. g. false, we must have that

$$(t-1)(1+a) - (n-t+1)/(1+a) + (n+1 - 2t)(1+a) \leq 0. \qquad (2-7)$$

36

From this we obtain $(1+a)^2 \leq 1 + 1/\text{n-t}$, and for large n and t, a series approximation gives

$$1 + a \leq 1 + \frac{1}{2(\text{n-t})} \tag{2-8}$$

or with the assumption that n = kt.

$$a \leq \frac{1}{2(k-1)t} . \tag{2-9}$$

If we next assume that the cost of a weight implementation, e.g. a resistor, varies inversely as the required accuracy, and note that for an operator computing the function f(t, kt), that kt such weights are required, the cost of a single operator network will be proportional to $1/a$ times the number of inputs, or, taking a to be maximum

$$C^* (t, n) = \frac{kt}{a} = 2 k (k-1) t^2. \tag{2-10}$$

Note that with respect to these assumptions, and except for the difference in the multiplicative factor, the equations (2-6) and (2-10) exhibit the desired invariance at the two extremes of network design. We may also note the conditions under which the alternate approaches become more or less favorable. If the cost of a weight component increases at a rate less than inversely as the required accuracy, the single operator solution is to be sought, while if the converse holds the distributed network is to be preferred. Which of these two conditions holds depends of course on the technology under consideration as well as the actual values of t and n.

Attempts to extend these results to more general classes of functions have been frustrated by mathematical difficulties so far. It is conjectured however that this development, or something very closely related to it, will lead ultimately to a useful, well defined conservation law of network structure. It is also very probably true that the "worst case" accuracy analysis considered herein will have to be replaced with a probabilistic formulation in which information theoretic techniques can be applied.

C.   BIOTRANSDUCERS

Efforts to develop a biotransducer were based on the discovery of photoconductivity in chloroplasts and chloroplast pigments by Arnold and Maclay.[5] The biological material utilized in these experiments is normally concerned with absorption of light energy and the production of oxygen and chemical energy. Photoconduction is generally associated with regions of high spectral absorption. Because of the infrared absorption bands of bacteriochlorophyll in photosynthetic bacteria, this material was selected as the starting material for use in the development of biotransducers.

Three strains of the organism Rhodospirillum rubrum were used in this study. Initially a culture No. 11170 was obtained from the American Type Culture Collection in Washington, D. C. The culture, however, proved to be contaminated and a new strain No. 9791 was obtained. Meanwhile, a pure culture was isolated from the original strain and Dr. A. W. Frenkel of the University of Minnesota donated a culture from his strain No. SCI-DA5.

The organisms were grown under continuous illumination in a medium consisting of 0.2% yeast extract and 0.2% agar. Anaerobic conditions were maintained by bubbling a mixture of 5% CO_2 in nitrogen through the culture medium. At the end of the growth period, the cells were harvested by centrifugation and washed twice with deionized water. Bacteriochlorophyll (BCHL) was obtained by grinding the cells with activated alumina and then extracting with a mixture of 7 parts acetone and 2 parts methanol. The cellular debris was removed by centrifugation and the supernatant liquid lyophillized to remove the solvent. Films of BCHL were deposited on conductive glass by applying of aqueous solutions and allowing the solvent to evaporate.

Bacterial chromatophores were also obtained by grinding the cells with alumina. The mixture was, however, extracted with 0.1 molar phosphate buffer at pH 7.5 and centrifuged to remove the alumina and cellular debris. The supernatant liquid was placed in the ultracentrifuge for one hour at 105,000 g and the red precipitate of the chromatophores collected. This material was spread in films on conductive glass, allowed to dry and the electrical properties observed.

The current measuring components consisted initially of a modified Aminco-Keirs spectrophosphorimeter, a Keithley 610-A electrometer, and an Electro-Instruments X-Y recorder. The spectrophosphorimeter utilizes a xenon light source for excitation, monochromators for emission and excitation, and produces a voltage output proportional to the wavelength setting of the monochromators. The sample compartment was modified such that light from the excitation monochromator illuminated the experimental cell and external leads were provided for current measurement.

The Keithley 610 A is an ultra-high impedance voltmeter with maximum input resistance greater than 10^{14} ohms. Current is measured by determining the voltage drop across a resistor shunted across the input or by applying negative feedback across the shunt resistor, thereby making the input drop negligible and improving the speed of response on the low current ranges. An output of 1 milliampere at 10 volts for full-scale deflection is provided for driving a pen recorder. In most of the latter experiments, a 1 milliampere Esterline-Angus recorder was used for recording the current changes and the sample was illuminated by a 300 watt G. E. reflector-spot lamp.

Sandwich and surface type cells were used in making the measurements. The configuration of the cells and a block diagram of the measuring circuit is shown in Figure 14. When using the sandwich type cell the BCHL or chromatophores were spread over an area of approximately 1 cm^2 on the conductive surface of a glass slide which served as one electrode. Printed-circuit board, on which the configuration had been photoetched, was used as the other electrode. In some cases another piece of conductive glass was used as the second electrode.

The surface type cells were made on printed circuit board on which the electrode configuration was photoetched. The alternate copper electrodes were 1/64 inch wide and the interelectrode distance was 1/32 inch. The total electrode area was 0.8 square inch. In one instance, chromatophores were spread on a regular glass slide and indium electrodes were evaporated on to the surface. Thin films of copper were evaporated over the ends of the indium electrodes such that the configuration was the same as on

CONFIGURATION OF BACK
ELECTRODE OF SANDWICH
COIL.

CONFIGURATION OF SURFACE
ELECTRODE

COATING ON SLIDE

FILM OF CHROMATOPHORES

BACK ELECTRODE

METER-KEITHLEY 610A ELECTROMETER

hλ (LIGHT)

RECORDER

METER

FIG. 14   MEASURING CIRCUIT AND ELECTRODE CONFIGURATION
           OF PHOTOCONDUCTIVITY CELLS

the printed circuit board. Gold wire was soldered to the copper strips to provde external leads.

The absorption spectra of BCHL solution and a suspension of chromatophores are shown in Figure 15. The curves are not for equivalent concentrations, however the absorption peaks at 890 and 840 mμ which are characteristic for the presence of BCHL in the intact organism are quite predominate in the curve for the chromatophore suspension in contrast to that for the organic solution of BCHL.

The first conductivity experiments were performed using films of BCHL in sandwich cells. With applied potentials as high as 180 volts, some of the preparations exhibited dark currents of about 10^{-14} amperes but were completely insensitive to light either from the monochromator at wavelengths from 250 to 800 mμ or to white light from a 300 watt lamp.

Some light sensitivity, although very slight, was obtain when β-carotene was added to the films. These results suggested the possibility that extraction of the bacteria with organic solvents did not remove water soluble constituents that might be necessary for photoconduction. Therefore the chromatophores were used in subsequent experiments.

Chromatophores from the three strains of R. rubrum were used in fabricating photoconductivity cells with essentially the same results for each strain. In the earlier experiments the relative sensitivity of the cells varied considerably, even when prepared from the same batch of chromatophores. This situation changed in the latter experiments when the contact between the electrodes and the films was improved and most cells gave similar results. Initially 180 volts were used as the external potential. With this arrangement dark currents of the order of 10^{-12} amperes were obtained in the sandwich cells with the printed circuit back electrode. The intensity of the monochromatic light was not sufficient to produce a response so the cells were illuminated by the 300 watt lamp at a distance of one foot. A typical cell had a dark current of 2.8×10^{-12} amperes which increased to 8.4×10^{-12} amperes when illuminated for 15 seconds. Use of conductive glass as the second electrode produces a dark current of about 10^{-10} amperes but the change on illumination was of comparable magnitude. The increase
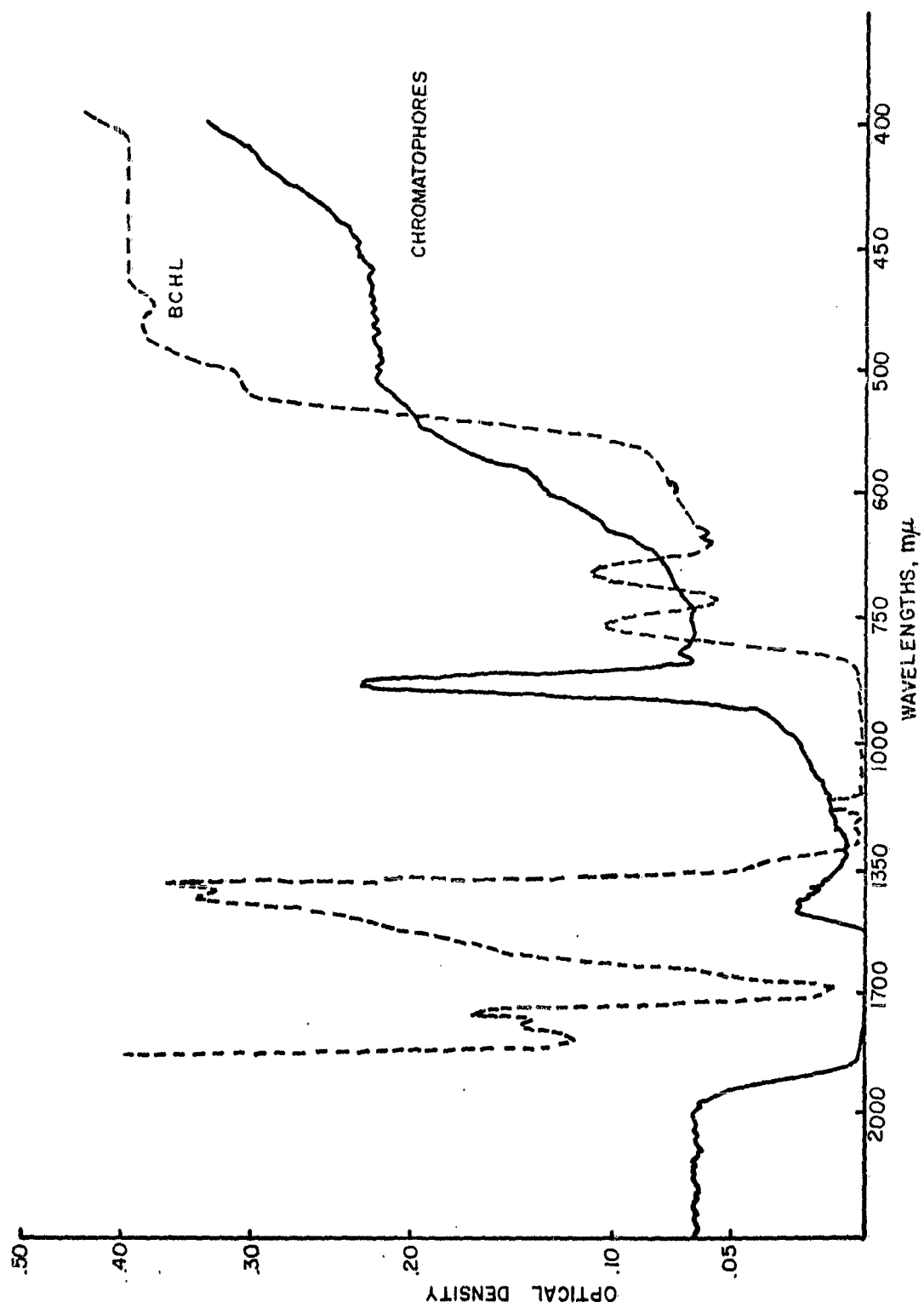
41

FIG.15 ABSORPTION SPECTRA OF BCHL SOLUTION AND CHROMATOPHORE SUSPENSION

in dark current is probably due to the larger surface area of these cells. The current change started when the light exposure began and usually required 3 to 4 minutes to decay to the original value on termination of the exposure.

In addition to photoconductivity, an inherent voltage is exhibited by the cells. This was discovered when the battery was accidently eliminated from the measuring circuit and a current of opposite polarity was observed.

Early attempts to characterize the potential were masked by extraneous 60 cycle pickup. On elimination of ground loops, voltages between 50 and 460 millivolts were obtained with a value of 300 millivolts for most cells.

Chromatophores on the surface type cell with no external battery gave a negative dark current of 1.4×10^{-13} amperes; a 15 second exposure to the 300 watt lamp causes a change to positive 4.6×10^{-13} amperes. The same change in current was obtained when the light was passed through a 10% alcoholic iodine solution which absorbs light below 700 mμ. Similar results were obtained with the surface cell in which indium has been evaporated on to the chromatophore film. A negative dark current of 6.2×10^{-14} amperes is changed to positive 1.1×10^{-13} amperes on exposure to 15 second of white light. The same exposure to iodine filtered light produced a change from negative 6.5×10^{-14} amperes to positive 7.0×10^{-14} amperes.

Although the sensitivity of the preparation does not favorably compare with inorganic materials such as cadmium sulfide and lead sulfide, these results show the feasibility of the use of films of bacterial chromatophores as photosensing material. The spectral sensitivity could not be determined since high intensity monochromatic light was not available, however, sensitivity to wavelengths above 700 mμ was shown. Only photoconduction was used in this study and a complete characterization of the semiconductor properties should be made to determine the possible use of chromatophores as the sensing element of a biotransducer.

SECTION III.

PICTORIAL DATA TRANSMISSION SYSTEM

A.   THE PROBLEM

With the advent of space travel has come a strong requirement for pictorial data compression. The tremendous transmission distances, coupled with the limited transmission power that is available, places a premium on the use of channel capacity and results in very low signal-to-noise ratios.

If all pictures to be transmitted had equal a priori probability, e. g., all input configurations were equally likely, then an optimum code for pictorial information would have each code work of constant length. For example, suppose each resolvable element of a set of pictures is to have dimension r x r, S shades of gray are to be distinguished, all pictures have dimension m x n and have equal a priori probability of occurrence. There exists $S \exp \left[\dfrac{m \times n}{r^2} \right]$ pictures each of which has information

$$\log \left\{ S \exp \left[\frac{m \times n}{r^2} \right] \right\} = \frac{m \times n}{r^2} \ \log S \quad \text{bits.}$$

Then binary sequences of length $\dfrac{m \times n}{r^2} \log S$ would represent an optimum code for these pictures. Therefore, a conventional BCD code would be optimum, or if the S/N ratios of a communication channel allowed M levels of signal to be distinguished, then a sequence of signals of length $\left[\dfrac{m \times n}{r^2} \right] \left[\dfrac{\log S}{\log M} \right]$ each with log M bits of information could be used.

It is evident that in most communication applications all $S \exp \left[\dfrac{m \times n}{r^2} \right]$ pictures do not have equal a priori probability, and, as a matter of fact, most pictures would be described by the engineer as noise. Therefore, if a pictorial code could be developed that took into account the a priori probabilities of occurrence of pictures, a great saving in bandwidth or transmission time could be obtained. Unfortunately, the probability of occurrence of any given picture is not easy to determine, even when the type of material contained in the pictures to be transmitted is known. In fact, so many pictures are possible that the a priori probability of any one picture approaches zero.

In order to develop methods of transmitting pictorial data which reduce time-bandwidth requirements of the communication channel, the great redundancy which is inherent in many pictures to be transmitted is often used. For example, in most pictures the probability that a white element will be followed by a white element is much higher than the probability that a white element will be followed by a black element, i.e., often pictures have large areas with little detail. Many techniques for utilizing such redundancies have been investigated. These use methods such as variable rate line scan, where the scan rate is varied as a function of the detail present in the picture, or multiple line scan systems which perform a similar function. Other coding systems include run length codes, predictive codes, Shannon-Fano codes and Huffman codes. The use of these systems or any other coding or variable scan system has an inherent weakness in that delay lines and/or storage equipment as well as coding hardware are an inherent part of the system and, therefore, increase the overall cost of the communication system. However, since in many Air Force communication applications bandwidth-time limitations are severe, such systems do serve an important function.

The methods listed in the above paragraphs are all examples of information preserving transmission systems. These methods usually offer only a limited saving in bandwidth, or can be used only in conjunction with quite limited types of pictorial data. A second method of compressing pictorial information has recently begun to be investigated.[6, 7] This method actually reduces the entropy of the picture to be transmitted by changing the picture in such a way as to remove unneeded or uninteresting material.

Utilizing techniques and components developed from earlier investigations under this program, both methods of picture compression are being employed. This section describes the results of research thus far attained.

B. ENTROPY REDUCING TRANSFORMATION

The development of photoconductive sensor cells under the Creature Communication program has made feasible the simple implementation of a technique which reduces many toned pictures to a black and white form while preserving several important properties of the original picture.

Although the transformed black-white picture is not identical to the original picture, the coding rule results in a picture which has lost essentially no shape detail and is furthermore characterized by all dark areas being classified as black, and all light areas being classified as white. Thus the transformed pictures should be usable in many standard pictorial data applications, e. g. , recognition of structures or objects.

1.   Advantages of Reduction

The transformation of pictorial data to binary (black or white) data immediately results in a reduced bandwidth requirement, $\overline{B}$, such that

$$\frac{B}{\overline{B}} = \log M \qquad (3-1)$$

where

B = original bandwidth requirement

M = number of shades of gray in the initial pictorial data.

For example, if 32 shades of gray were previously distinguishable in a picture, a channel with one-fifth the bandwidth can transmit the transformed black-white picture in the same amount of time.

When noise is introduced into the transmitting system, a further possible advantage of reducing a picture to black and white prior to transmission may be noted. Since less bits are to be transmitted, many fewer elements will be incorrectly transmitted over the transmission channel.

Again consider a picture with 32 shades of gray. Assume each element is coded in binary form (5 bits), and transmitted over a noisy channel such that the probability of an error in transmitting a bit is $1/6$. This corresponds to a signal-to-noise ratio (S/N) = 1, when N is white Gaussian noise. The probability of an error in the received element is

$$P_E(S_i) = 1 - \left(\frac{5}{6}\right)^5 = 1 - 0.4 = 0.6.$$

The average change in gray caused by a single error is

$$\frac{16 + 8 + 4 + 2 + 1}{5} = 6.2 \text{ levels (out of a maximum 32).}$$

If the black-white picture is transmitted over the same channel, the probability of error in a received element is simply, $P_E = P_B = .16$, but each error results in a complete reversal of the element.

A question as to which of these two transmitted pictures will contain more useful information in various pictorial data applications still remains to be answered. It is evident that error correcting codes can be used in the transmission of the black-white picture, thereby improving its quality while still keeping a favorable bandwidth ratio as compared to that needed for the transmission of the original multilevel picture.

Still another advantage of reducing the picture to black and white prior to transmission is that many of the coding techniques listed earlier become applicable over a much wider range of pictorial material. In its original form even a 2 x 2 block of pictorial data with 32 distinguishable shades of gray contains $(2^5)^4 = 2^{20}$ or over a million possible characters. It is evident that a reasonable coding procedure for this many characters is extremely hard to come by. Contrast this with the case of all black-white data, where only $2^4 = 16$ possible characters occur. As one of the activities under the present program, the efficient encoding of black-white pictures, obtained through reduction of the initial picture in the fashion mentioned previously is being studied. Section III C describes the research performed in this area to date.

2.   Idealized Transformation Rule

The rule which is implemented with the aid of a geometrical photoconductive sensor cell is formulated below.

Referring to Figure 16, where each square represents a resolvable element of a given picture,

$a_{i-1,j-1}$	$a_{i-1,j}$	$a_{i-1,j+1}$
$a_{i,j-1}$	$a_{i,j}$	$a_{i,j+1}$
$a_{i+1,j-1}$	$a_{i-1,j}$	$a_{i+1,j+1}$

Figure 16

3 X 3 BLOCK OF PICTORIAL ELEMENTS

define:

$B(a_{i,j})$ = apparent brightness of $a_{i,j}$

B_{med} = brightness judged half way between black and white

(a)   If $B(a_{i,j}) \geq B_{med}$

     and $B(a_{k,l}) \leq B(a_{i,j})$ for six or more of the eight surrounding elements

     then $a_{i,j}$ is classified as white.

(b)   If $B(a_{i,j}) \geq B_{med}$

     and $B(a_{k,l}) > B(a_{i,j})$ for three or more of the eight surrounding elements

     then $a_{i,j}$ is classified as black.

(c)   If $B(a_{i,j}) < B_{med}$

     and $B(a_{k,l}) \geq B(a_{i,j})$ for six or more of the eight surrounding elements

     then $a_{i,j}$ is classified as black.

(d)   If $B(a_{i,j}) < B_{med}$

     and $B(a_{k,l}) < B(a_{i,j})$ for three or more of the eight surrounding elements

     then $a_{i,j}$ is classified as white.

It would be desirable if the function B corresponded to the threshold of subjective brightness exhibited by the human eye as closely as possible. If more sensitive than this, pictorial information not visible to the human observer would become visible in the transformed picture. In some cases this might be desirable, but when fidelity of visible pictorial information is desired, this is not so. If less sensitive than the human eye to brightness variations, pictorial detail will be lost.

In order to see how the above rule transforms pictorial data, a few simple pictorial patterns have been drawn and transformed by the rule. These are shown in Figures 17, 18, 19, and 20. The reader should observe the following pertinent facts.

1) No borders are lost, therefore all shapes are preserved.

2) All areas darker than a preassigned medium gray have their interiors black.

3) All areas lighter than this preassigned gray have their interiors white.

4) Isolated elements and lines of a single resolution thickness are always preserved.

3. Sensor Cell for Rule Implementation

The initial sensor cell which will be used in the system to reduce the pictorial data from multilevel to black and white is quite similar to the contrast detecting sensor described in ASD Technical Report 61-620.[2] Certain changes particularly in the electrical hook-up and loading of the cell have been made, and Figure 21 illustrates the cell as it will be utilized in the data classification system. As in the case of the original contrast detecting sensor, the radii are chosen so that

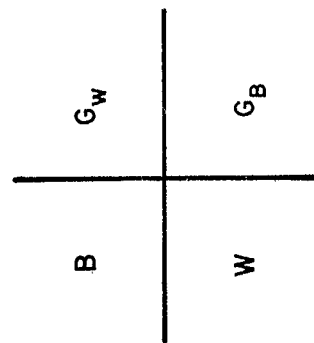$$\frac{R_1}{R_2} = \frac{R_3}{R_4} .$$

= BLACK

= WHITE

B = BLACK
G_B = DARK GRAY $\big\}$ BELOW THRESHOLD

G_W = LIGHT GRAY $\big\}$ ABOVE THRESHOLD
W = WHITE

B G_W

W G_B

Before Transformation

After Transformation
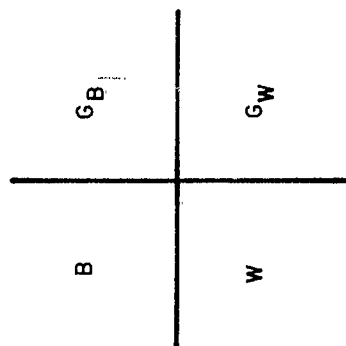
FIG.17   TRANSFORMATION OF RECTANGULAR SHAPES

B = BLACK
G_B = DARK GRAY } BELOW THRESHOLD

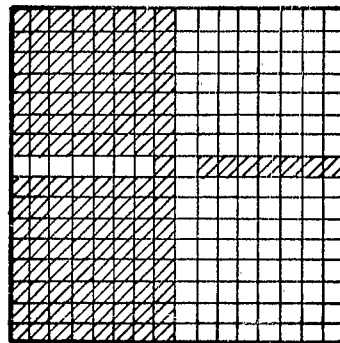G_W = LIGHT GRAY } ABOVE THRESHOLD
W = WHITE

▨ = BLACK

☐ = WHITE

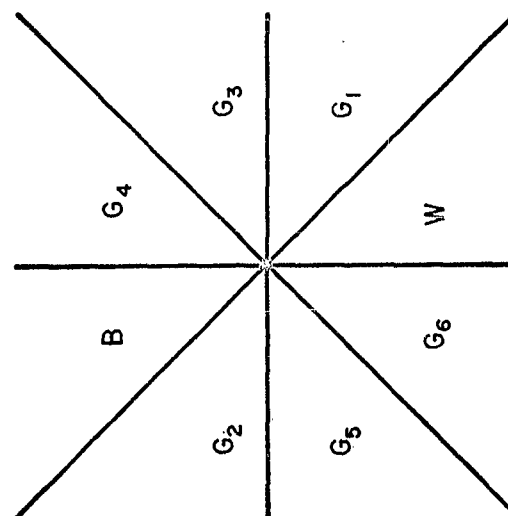G_B G_W

B   W

Before Transformation

After Transformation

FIG.18   TRANSFORMATION OF ADJACENT DARK AND LIGHT AREAS

SYMBOLS LISTED IN ASCENDING ORDER OF BRIGHTNESS

B = BLACK
G_6 = GRAY
G_5 = GRAY   BELOW
G_4 = GRAY   THRESHOLD
G_3 = GRAY
G_2 = GRAY
G_1 = GRAY   ABOVE
W = WHITE   THRESHOLD

◨ = BLACK
□ = WHITE

Before Transformation
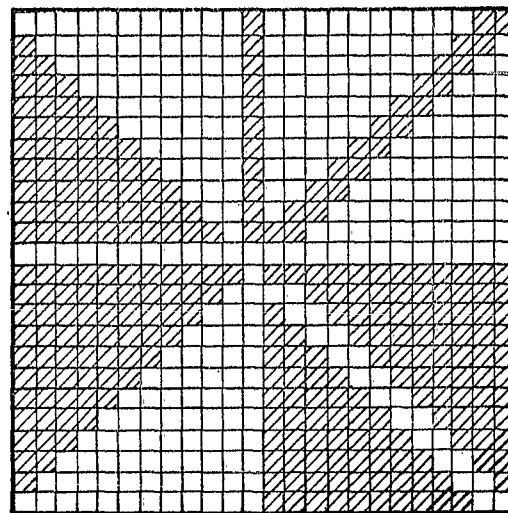
After Transformation

FIG.19   TRANSFORMATION OF OCTAGON SHAPE

BLACK = BLACK

WHITE = WHITE

AFTER TRANSFORMATION

BELOW THRESHOLD

ABOVE THRESHOLD

BLACK = BLACK

DARK GRAY = DARK GRAY

LIGHT GRAY = LIGHT GRAY

WHITE = WHITE

BEFORE TRANSFORMATION

FIG.20 TRANSFORMION OF ARBITRARY SHAPE

54

BEFORE TRANSFORMATION

= BLACK
= DARK GRAY } BELOW THRESHOLD
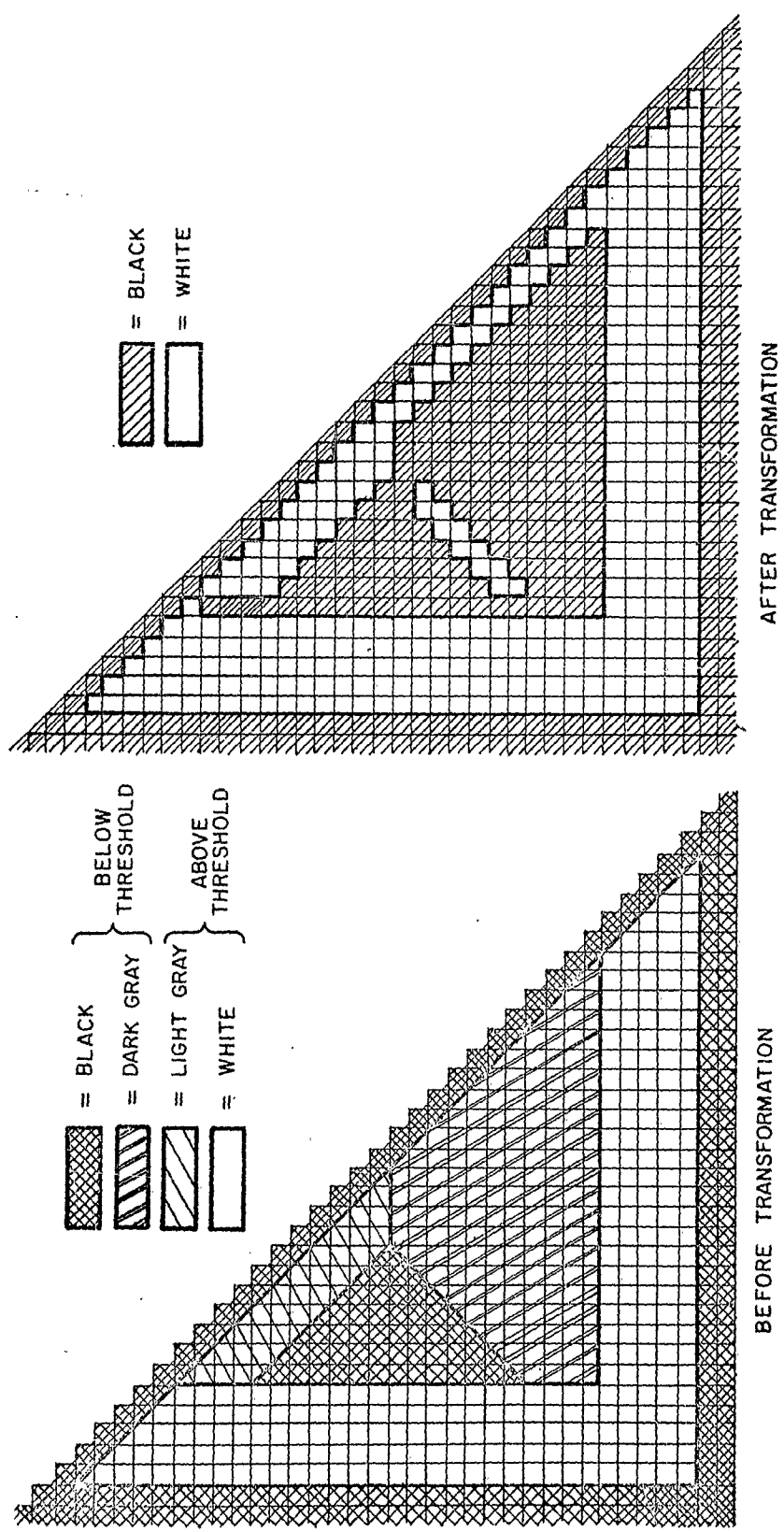= LIGHT GRAY } ABOVE THRESHOLD
= WHITE

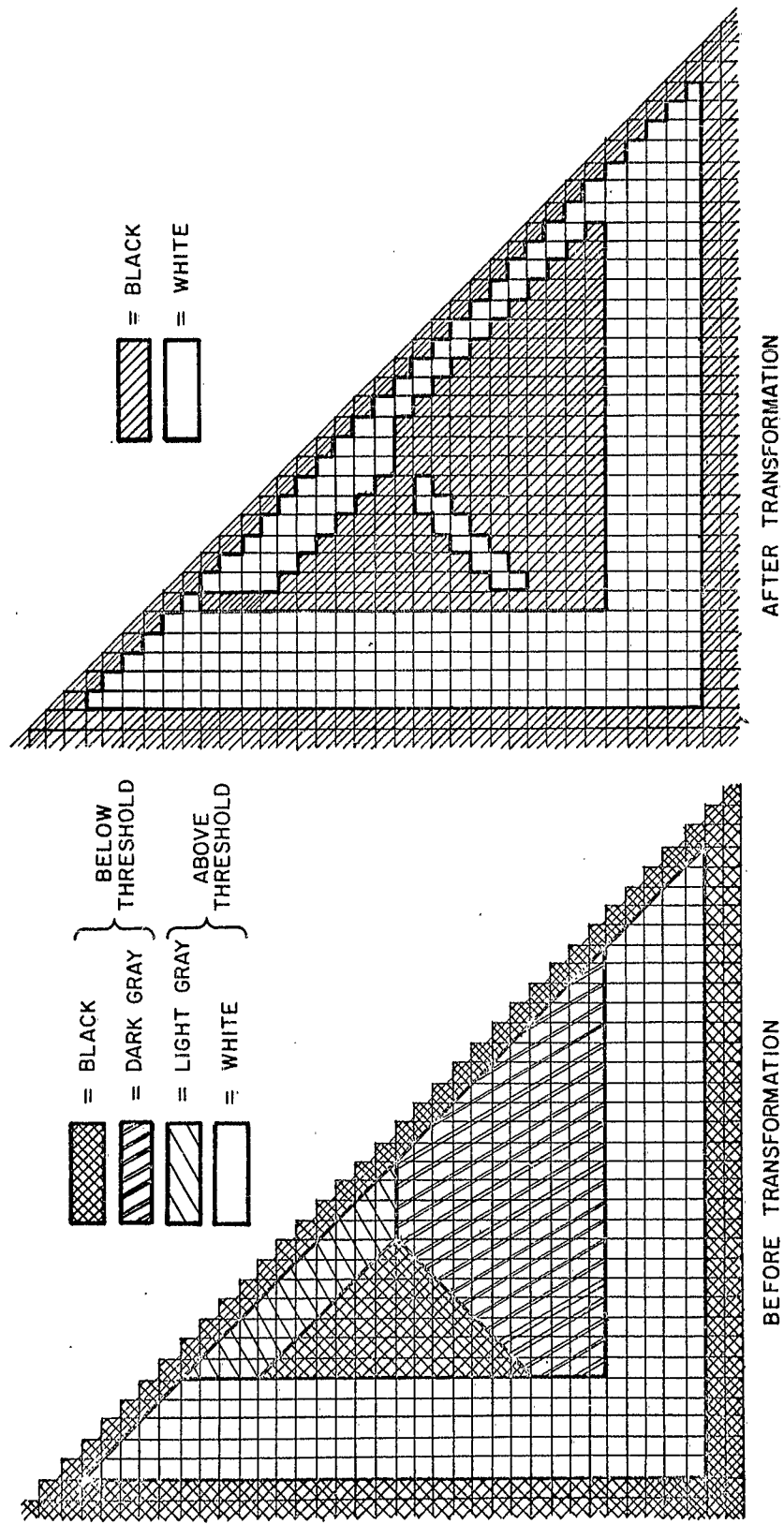AFTER TRANSFORMATION

= BLACK
= WHITE

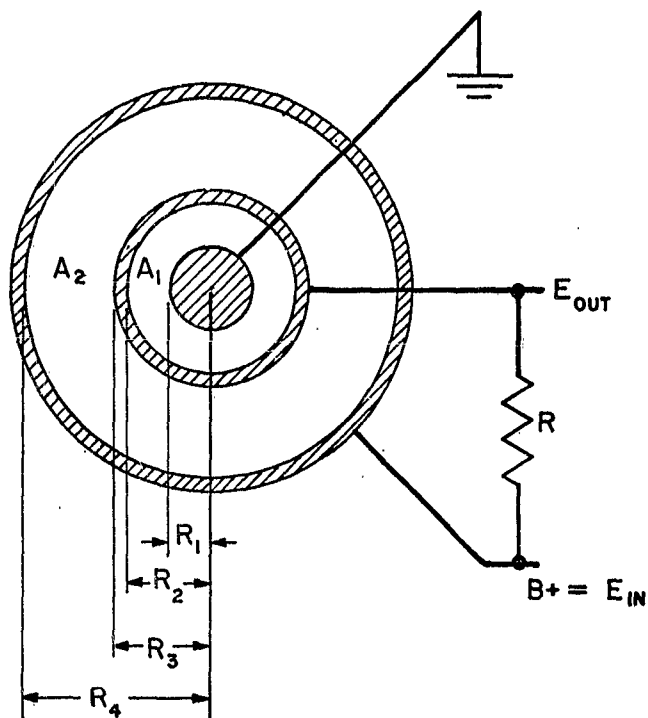FIG.20 TRANSFORMION OF ARBITRARY SHAPE

54

FIG. 21   PICTORIAL   DATA   CONVERTER

Preliminary results with cells synthesized in the ARF Micro-electronics Laboratory indicate that a sensor cell with a light to dark working range such that

$$Z_{A_1} (\text{DARK}) = Z_{A_2} (\text{DARK}) = 10^7 \text{ ohms}$$

and

$$Z_{A_1} (\text{LIGHT}) = Z_{A_2} (\text{LIGHT}) = 10^4 \text{ ohms}$$

is feasible. Furthermore, a linear relationship between illumination level and impedance value over this range is easily attained. The inner area, A_1, is to correspond in size (after optical magnification) to a single resolvable element of the picture.

To determine the threshold value, which corresponds to a subjective brightness half way between black and white, one notes from studies on subjective brightness[8] (as contrasted with subjective threshold where a logarithmic relationship holds) that subjective brightness varies as an exponential function of brightness. Then, the relation

55

$$Z = K_o \, e^{\epsilon B} \hspace{3cm} (3-2)$$

where

K_o = constant

ϵ = constant

B = actual brightness

Z = impedance of cell.

can be used in conjunction with the characteristics described in the above paragraph to obtain:

$$Z_D = 10^7 = K_o \, e^{\epsilon(o)} = K_o$$

or

$$K_o = 10^7 \; .$$

Also

$$Z_L = 10^4 = 10^7 \, e^{\epsilon \, B_{max}}$$

$$1 \, n \, 10^{-3} = \epsilon \, B_{max}$$

or

$$B_{max} = \frac{1}{\epsilon} \left(1 \, n \, 10^{-3} \right).$$

Then

$$\frac{B_{max}}{2} = \frac{1}{2\epsilon} \left(1n \, 10^{-3} \right)$$

and the corresponding impedance

$$Z = 10^7 \, e^{1n \, 10^{-3/2}}$$

$$= 10^7 \, \times \, 10^{-3/2} = 315,000 \text{ ohms}.$$

Therefore <u>under uniform illumination conditions</u>, cell impedances higher than 315,000 ohms should result in a dark classification while cell impedances lower than 315,000 ohms should result in a light classification.

By selecting an appropriate value for R (of Figure 22), a sensor circuit which performs a transformation roughly equivalent to that described in Section III B-2 is obtained. For example, if R is selected to be 3 megohms, the threshold voltage can be computed with the aid of Figure 22 as:

56

$$E_{Threshold} = \frac{E_{in}\,(3.15 \times 10^5)}{\dfrac{3.15 \times 10^5 \times 3 \times 10^6}{3.31 \times 10^6} + 3.15 \times 10^5}$$
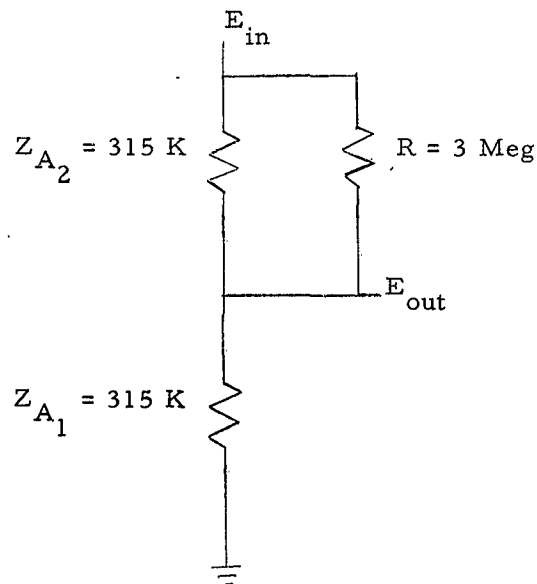
$$= .525\, E_{in}$$

FIG. 22 CONVERTER CIRCUIT AT THRESHOLD

Then by assigning

$$a_{i,j} = 0 \quad \text{if } E > E_{Threshold}$$

$$a_{i,j} = 1 \quad \text{if } E \leq E_{Threshold}$$

Table 4 can be constructed from the equation:

Table 4

THRESHOLD VALUE OF Z_{A_2} AS A FUNCTION

OF CENTER AREA IMPEDANCE

Z_{A_1} Center Area Impedance	For Positive (White Output) $Z_{A_2} \geq$
10 K	10 K (All values)
20 K	18. 1 K or more
50 K	45. 3 K or more
100 K	92. 5 K or more
200 K	193 K or more
315 K	315 K ←———— Threshold
500 K	535 K or more
1, 000 K	1, 300 K or more
2, 000 K	4, 600 K or more
5, 000 K	10, 000 K (no values)
10, 000 K	10, 000 K (no values)

$$Z_{A_2} = \frac{1.42 \times 10^6 \times Z_{A_1}}{1.57 \times 10^6 - .475\, Z_{A_1}} \quad . \tag{3-3}$$

From Table 4, it is easy to see that all uniformly dark areas will be classified as black, while all uniformly light areas will be classified as white. Furthermore, although it is difficult to form a quantitative estimate of the amount and size of area Z_{A_2} which must differ in brightness from the area Z_{A_1} to cause a reversal in classification, it is evident that the transformation rule is being carried out, at least approximately, by the sensor. Since the design of the sensor is easily altered by changing the value of R or moving the threshold slightly, a sensor cell which performs exactly as desired should be easily designed from laboratory tests on sensors as they are synthesized in the Microlaboratory.

C.   CODING RESEARCH

1.   Objective and Method

After pictorial data is converted to a black and white form many coding procedures become practical. Present activity seeks to determine how much gain can be expected if such efficient codes are used. To do this, the entropy associated with typical pictorial data when various size blocks of pictorial elements (referred to as characters in this report) are considered. The entropy places a bound on the maximum gain that can accrue from optimum coding of blocks of pictorial data for a given block size. Four distinct sets of pictorial data were considered. Each set of pictorial data contained approximately 10,000 elements. The photographs from which this data were taken are shown in Figures 23, 24, and 25. Two sets of data were obtained from Figure 23, one set consisting primarily of water, the second set primarily of the ship. The transformation of data was accomplished by a straightforward and tedious visual classification technique. Slides of the photographs were made and projected on a large vertically mounted drawing board with a hollowed out center upon which a transparent plexiglass sheet had been mounted. Cross-hatched paper was placed on the drawing board, a movable straight edge was mounted on the rear of the board, and an
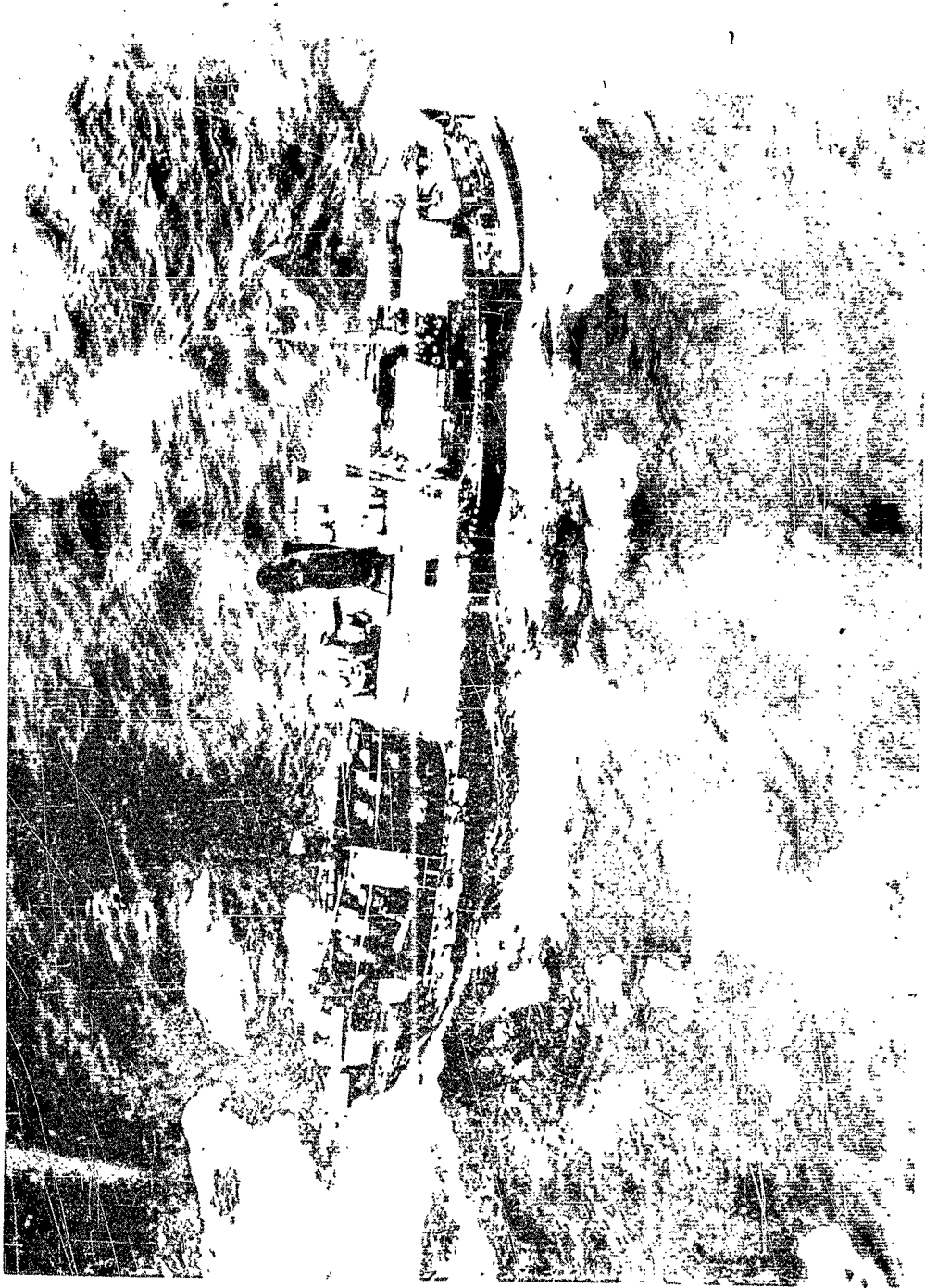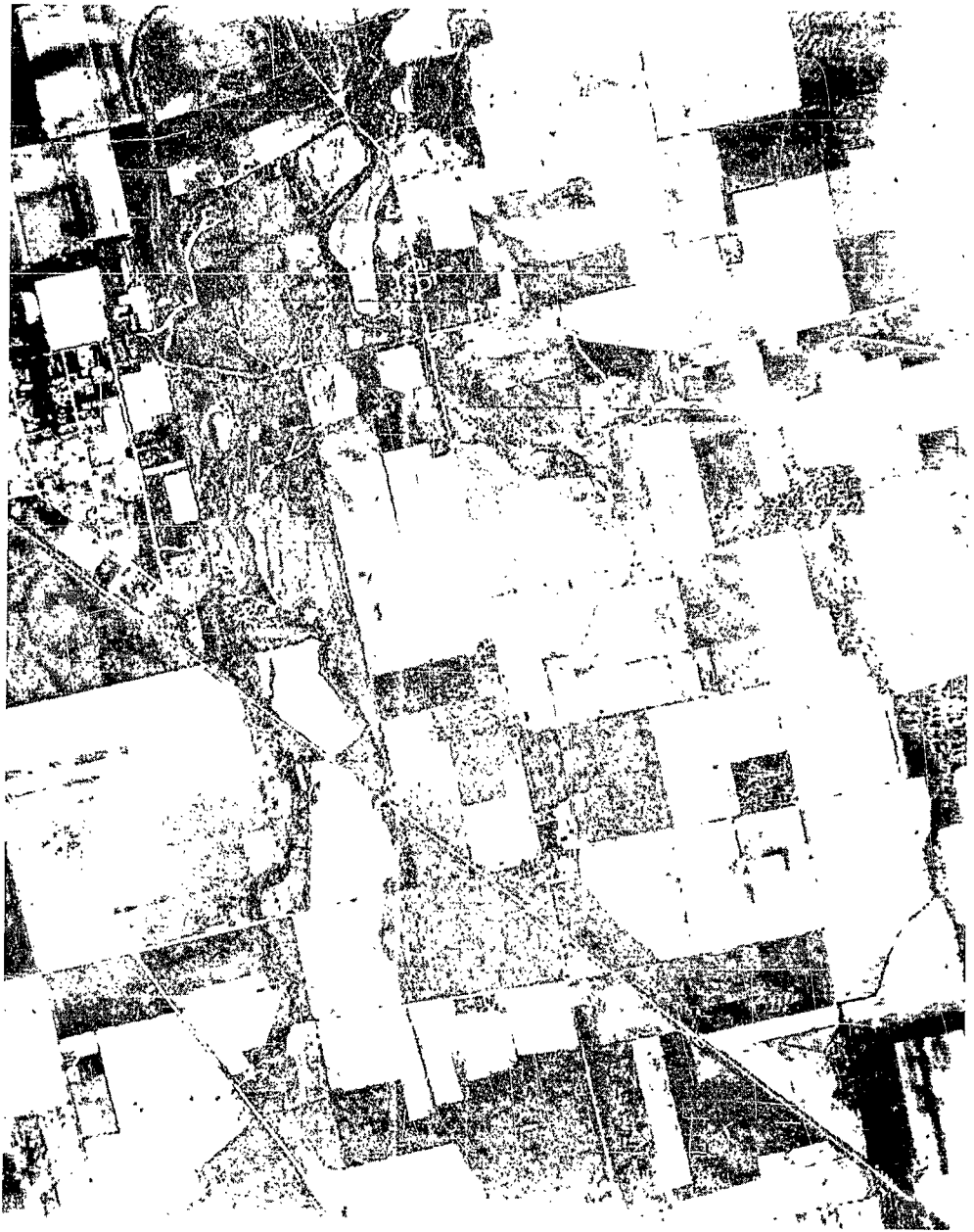
FIG. 23   SHIP

FIG 24 AERIAL VIEW

aperture 3 x 3 elements in size was moved across the projected image (see Figure 26). By spacing the projector at the correct distance, each resolvable element filled exactly one square of the cross-hatched area. Thus, it was possible to stand behind the drawing board and apply the transformation rule on each element in sequence. Since a visual judgment was involved, there is no doubt that a few erroneous classifications were made. However, the over-all data should approximate quite closely the data classification which would be obtained with an automated system. Figure 27 illustrates the appearance of the ship picture after its central portion has been transformed by the above described procedure.

2. Computer Program

The computer program performed the function of breaking the data into block characters, counting the number of block characters of each kind, and placing these in frequency order. A complete tabulation of the actual characters that appear for the given sets of data, plus the associated frequency of occurrence of each character has been obtained with the aid of the Foundation's 7090 computer. Block sizes of 1 x 1, 1 x 2, 2 x 2, 2 x 3, 3 x 3, 4 x 3, 4 x 4, 4 x 5, 6 x 5, and 6 x 6 were synthesized.

Although the actual characters and their associated frequencies are available at Armour Research Foundation, these are not included in this report because of size limitations (except for the 2 x 2 block size). Instead the entropy associated with each of the block sizes has been computed. The entropy/bit is given by the equation

$$E = \frac{1}{n \times m} \sum_{i=1}^{s} - p_i \log_2 p_i \qquad (3-4)$$

where

E = entropy/bit

p_i = probability of occurrence of the ith character

n = number of rows in the block character

m = number of columns in the block character

s = number of distinct characters that occur in the data.

PLEXIGLASS MOUNTED IN DRAWING BOARD

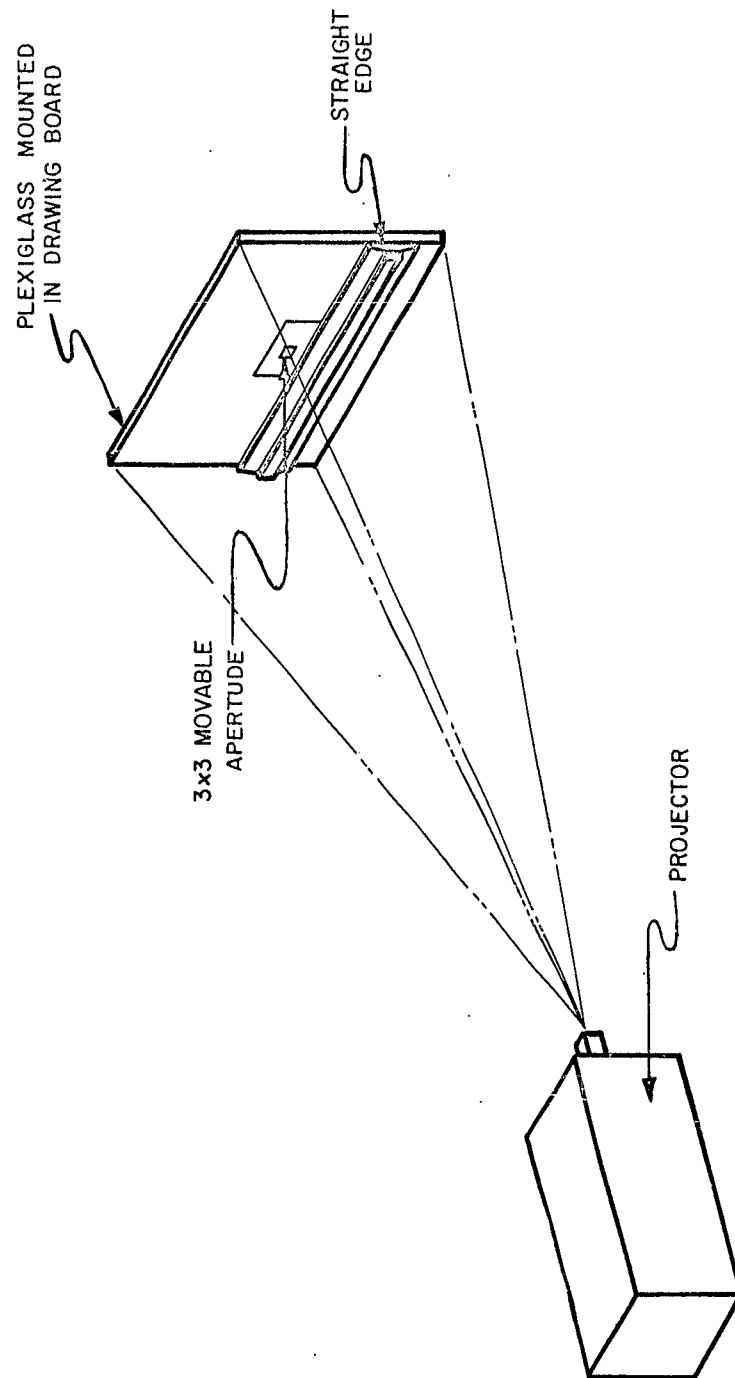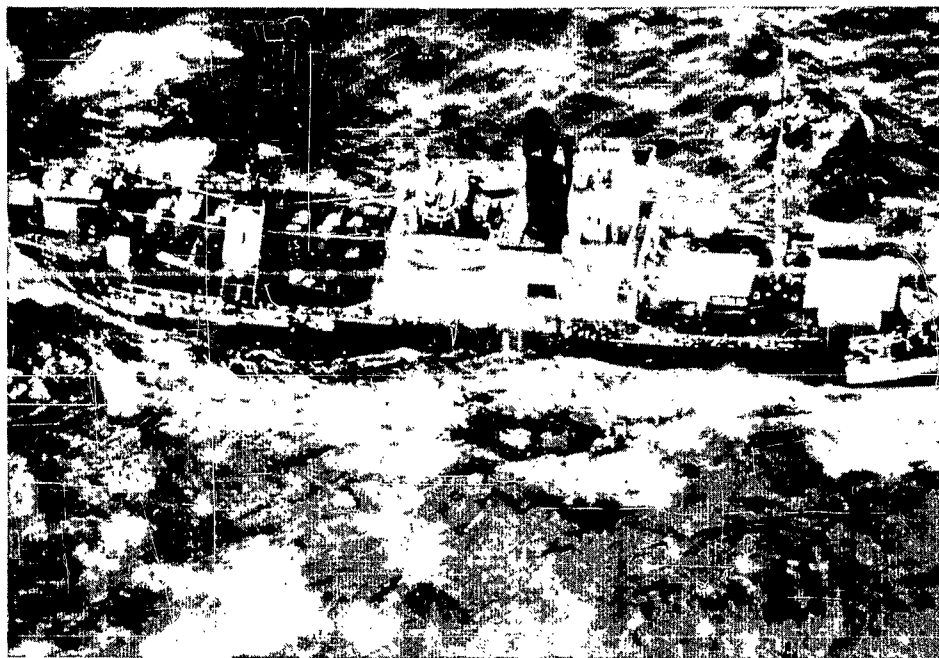STRAIGHT EDGE

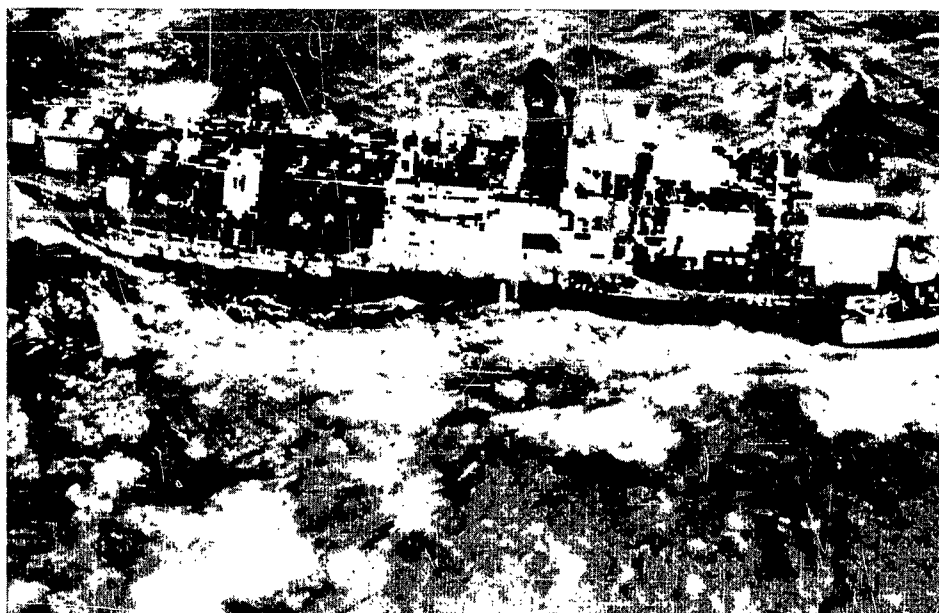3x3 MOVABLE APERTUDE

PROJECTOR

FIG. 26 EXPERIMENTAL APPARATUS FOR CLASSIFYING DATA

A. BEFORE CENTER TRANSFORMED

B. AFTER CENTER TRANSFORMED

FIG. 27   ILLUSTRATION OF TRANSFORMED DATA

65

Figure 28 displays curves of the entropy/bit computed from equation (3-4) as a function of character size for each set of data, and Table 5 illustrates the frequency of occurrence of each 2 x 2 character.

It may be recalled that the entropy/bit of a message code under the assumption of equal a priori occurrence of zeros and ones is

$$E = 0.5 \log_2 2 + 0.5 \log_2 2 = 1.0$$

Therefore, the ratio

$$\frac{1}{E\ (B,\ D)} \qquad\qquad (3-5)$$

where

$$B = \text{block size} = n \times m$$
$$D = \text{given data set},$$

is an expression which determines the reduction in transmitted message length that can be obtained by optimum coding of that set of data in blocks of size B. (Recall that the original reduction to a black and white picture has already reduced the message length by a large factor.)

It is not at all unreasonable to assume that codes very close to the optimum in size can be constructed. For example, consider the 2 x 2 data associated with the ship. The optimum entropy/bit from Figure 28 is 0.651. Figures 29 and 30 list the number of occurrences of each one of the 16 possible characters and indicates the construction techniques for a Huffman code associated with the data, as well as the resulting code. From Figure 30 it may be seen that 8107 symbols would be needed to send the data using the Huffman code. An optimum code would use

$$0.651 \times 12,096 = 7860 \text{ symbols.}$$

Therefore, the Huffman code is only

$$100 \times \frac{8107 - 7860}{7860} = 3.4\%$$

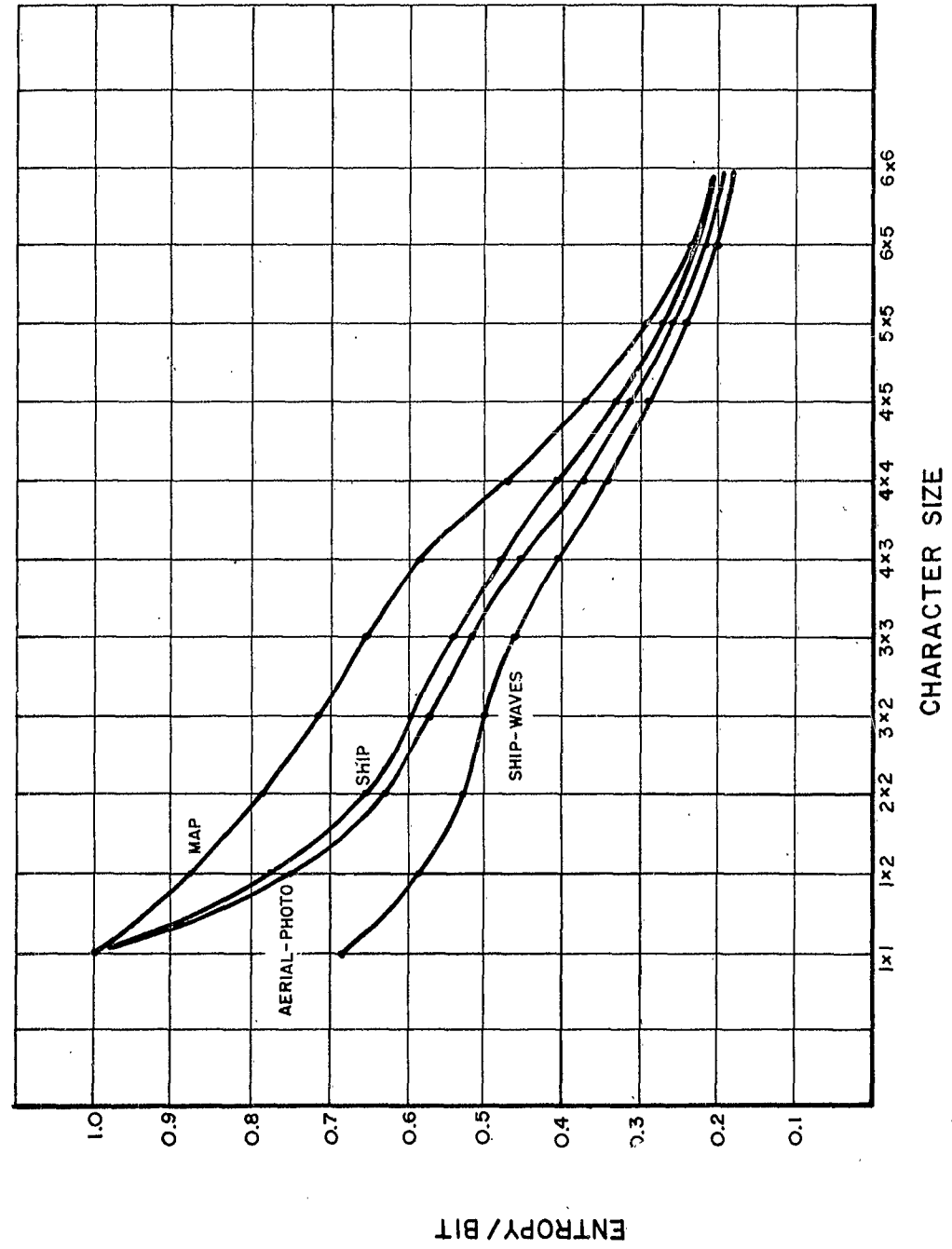longer that the optimum code for this data.

FIG. 28   ENTROPY   ASSOCIATED   WITH   EACH   DATA   SET

67

Table 5

FREQUENCY OF 2 x 2 CHARACTERS

Block Character	Frequency			
	Ship Water 1	Ship 2	Weather Map 4	Aerial View 3
(1 1) (1 1)	.659	.361	210	.294
(0 0) (0 0)	.0607	.360	.338	.331
(1 0) (1 1)	.0370	.028	.0264	.0198
(0 1) (1 1)	.0357	.0205	.0562	.0212
(1 1) (0 0)	.0334	.039	.0271	.046
(1 1) (1 0)	.0321	.0182	.0595	.0198
(1 1) (0 1)	.0304	.0202	.0258	.0179
(0 0) (1 1)	.0251	.041	.0503	.0394
(0 1) (0 1)	.0198	.024	.0304	.0126
(1 0) (1 0)	.0159	.027	.0278	.0155
(1 0) (0 0)	.0123	.0168	.0456	.0189
(0 0) (1 0)	.0115	.0191	.0192	.0192
(0 0) (0 1)	.0106	.0152	.0467	.0208
(0 1) (0 0)	.0083	.0152	0172	.0168
(1 0) (0 1)	.0036	.0016	.0139	.0050
(0 1) (1 0)	.0022	.0013	.0046	.0033

CODE WORD	NUMBER OF OCCURENCES	CONSTRUCTION	NUMBER OF SYMBOLS IN CODE
0 1 1 0	4		8
1 0 0 1	5		8
0 0 0 1	46		7
0 1 0 0	46		6
1 0 0 0	51		6
1 1 1 0	55		6
0 0 1 0	58		6
1 1 0 1	61		6
0 1 1 1	62		6
0 1 0 1	73		6
1 0 1 0	82		5
1 0 1 1	86		5
1 1 0 0	118		5
0 0 1 1	124		5
0 0 0 0	1074		2
1 1 1 1	1079		1

Construction nodes: 9, 55, 110, 97, 207, 375, 119, 871, 237, 135, 1945, 496, 168, 259, 3024

3024 words each of 4 elements = 12,096 elements

FIG.29 CONSTRUCTION OF HUFFMAN CODE

Typical Code	Symbols Sent		
1 1 1 1 1 1 1 1	8 x 4	=	32
1 1 1 1 1 1 1 0	8 x 5	=	40
1 1 1 1 1 1 0	7 x 46	=	322
1 1 1 1 1 0	6 x 46	=	276
1 1 1 1 0 1	6 x 51	=	306
1 1 1 1 0 0	6 x 55	=	330
1 1 1 0 1 1	6 x 58	=	348
1 1 1 0 1 0	6 x 61	=	366
1 1 1 0 0 1	6 x 62	=	372
1 1 1 0 0 0	6 x 73	=	438
1 1 0 1 1	5 x 82	=	410
1 1 0 1 0	5 x 86	=	430
1 1 0 0 1	5 x 118	=	590
1 1 0 0 0	5 x 124	=	620
1 0	2 x 1074	=	2148
0	1 x 1079	=	1079
			8107 symbols

FIG. 3 HUFFMAN CODE

In a similar manner, for any given set of data and given character size, a nearly optimum code can be constructed. However, we are seeking to accomplish a more difficult task. A single code is being sought which will do a good job of conserving on bandwidth when used with most, if not all, military pictorial data of a type of interest in communication applications. Observing the entropy curves of Figure 28, the false conclusion should not be made that using a very large character size is the best way to encode. For example, if this type of reasoning is carried to an extreme, the entire picture could be considered as the character size, and a different code word used for each distinct picture that occurs in the data. Obviously, this procedure is not valid, for no matter how many pictures are examined the probability that any unknown (or new) picture will be the same as any of the previous pictures is vanishingly small, and, in fact, the code is worthless.

That this effect has already come into play in even the small character sizes considered in this section can be demonstrated by noting the percentage of non-overlap between two sets of data. Table 6, for example, lists the percentage of non-overlap between the aerial photograph data, and the boat data as a function of character size.

It is easy to see that for sizes greater than 3 x 3 a code constructed from one set of data would be unsatisfactory for transmitting the second set of data.

To determine the best character size for encoding a variety of diverse data, all data gathered was tabulated according to character size and frequency of occurrence. All characters that occur more than once in the data were assumed to be encoded in optimum fashion. Then, the ratio of the number of characters which occurred only once to the total number of characters considered was used to estimate the number of characters which would have to be sent uncoded for each block size. This estimate seems reasonable since any character which occurs only once appeared in only one data subset and would not have a code word if the data were new.

Finally the message length for each of the four data subsets was computed for each character size. The curves of Figures 31, 32, 33, and 34 indicate the results in length per transmitted element. These curves

71

Table 6

NON-OVERLAP OF AERIAL PHOTOGRAPH

AND

BOAT DATA

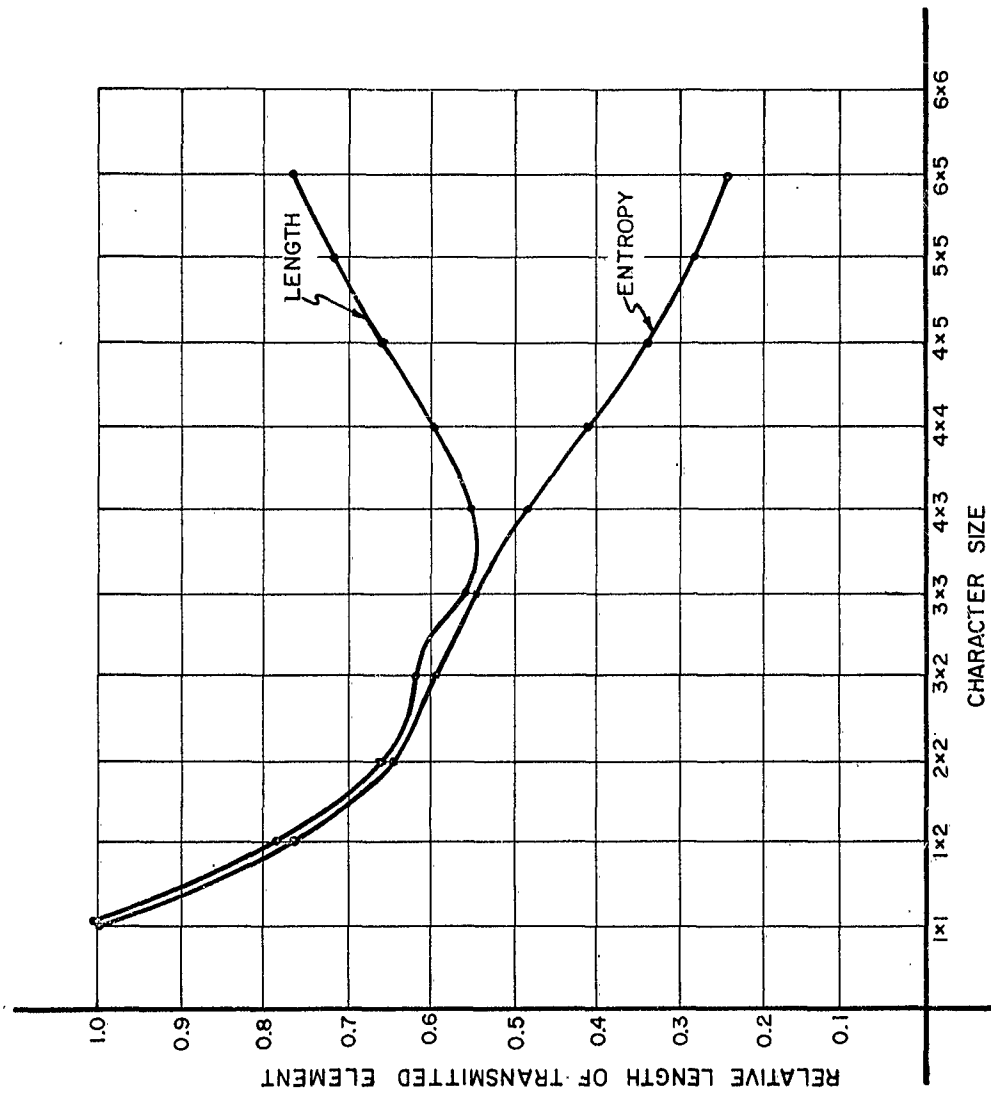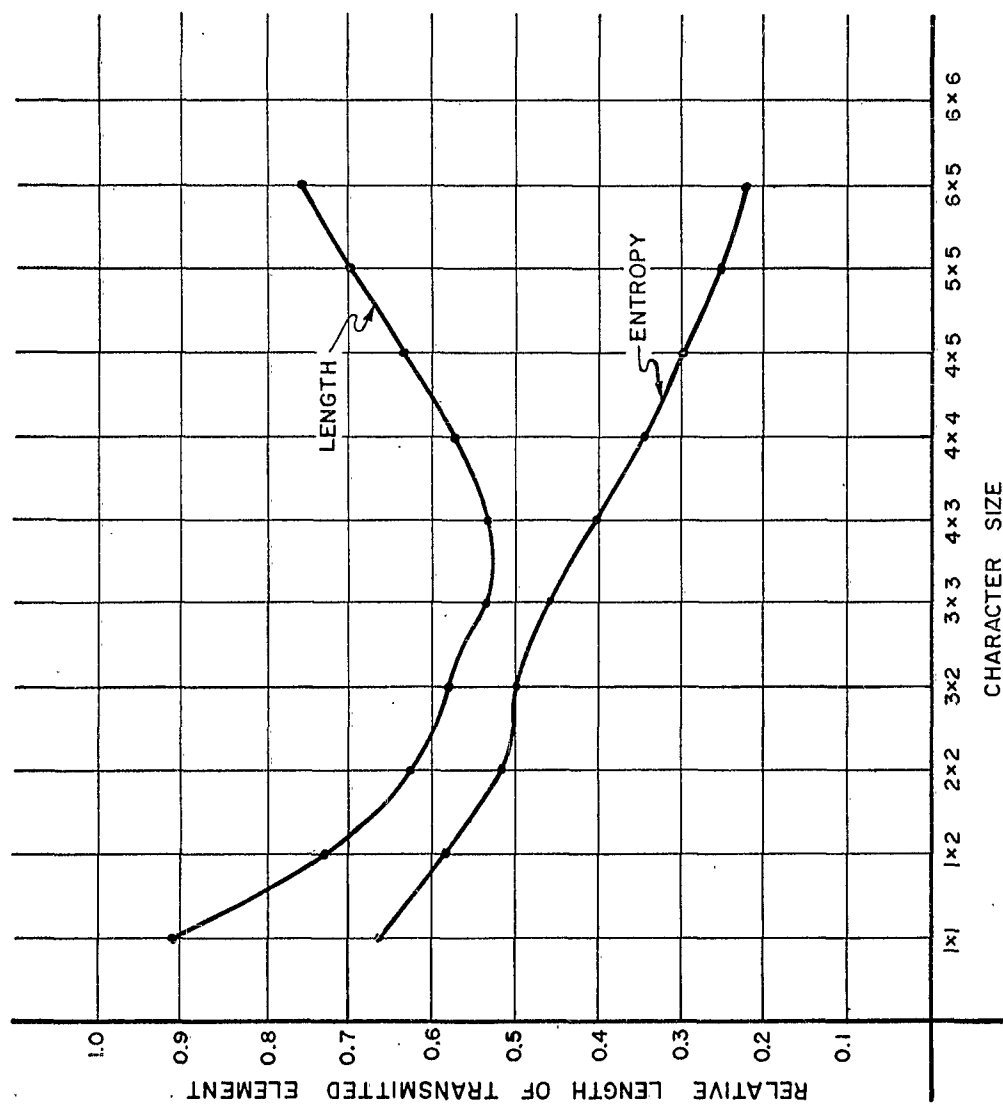| Character Size	% Non-Overlap
1 x 1	0
1 x 2	0
2 x 2	0
3 x 2	0. 2
3 x 3	4. 2
4 x 3	15. 4
4 x 4	34. 8
4 x 5	49. 2
6 x 5	67. 0
6 x 6	74. 0

FIG.31 CODE LENGTH/ELEMENT FOR SHIP DATA

FIG. 32 CODE LENGTH/ELEMENT FOR WATER ABOVE SHIP

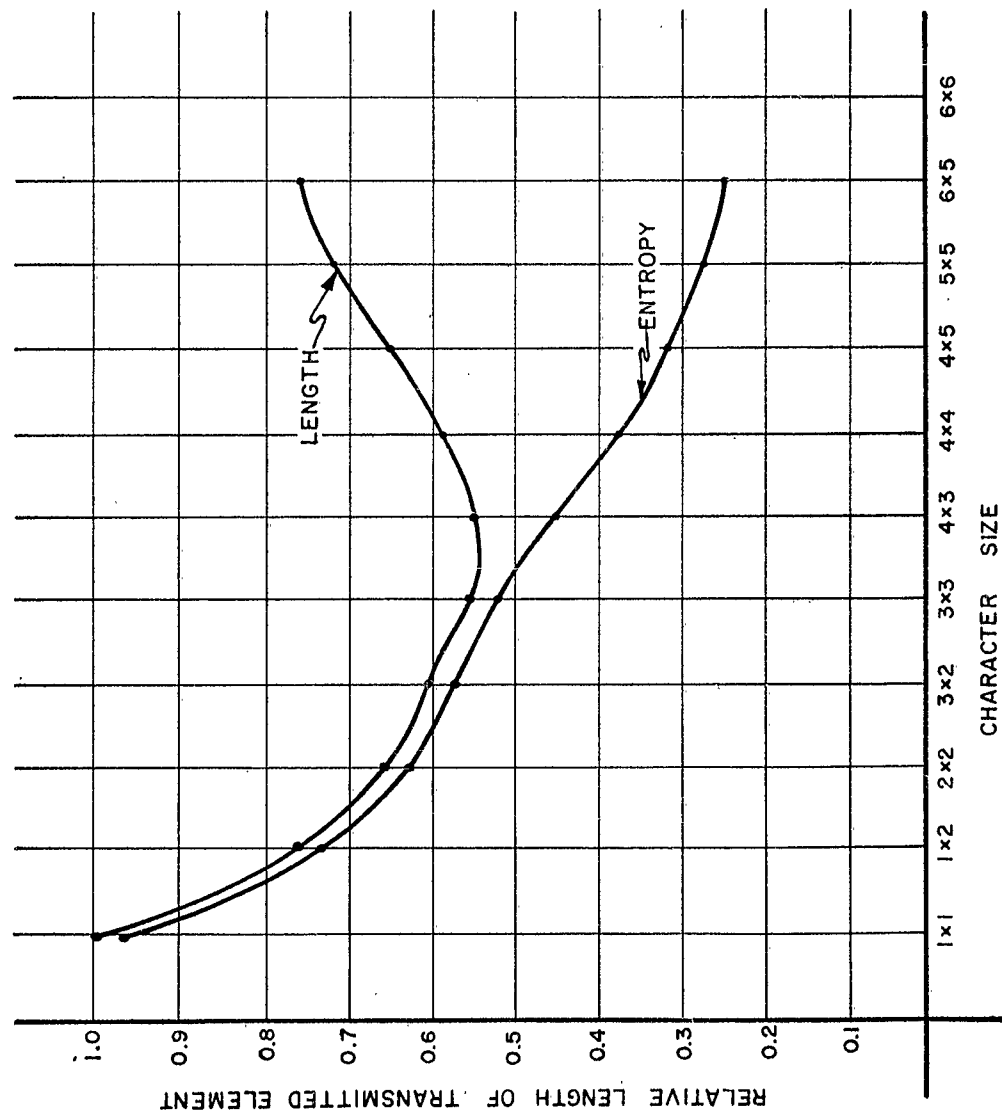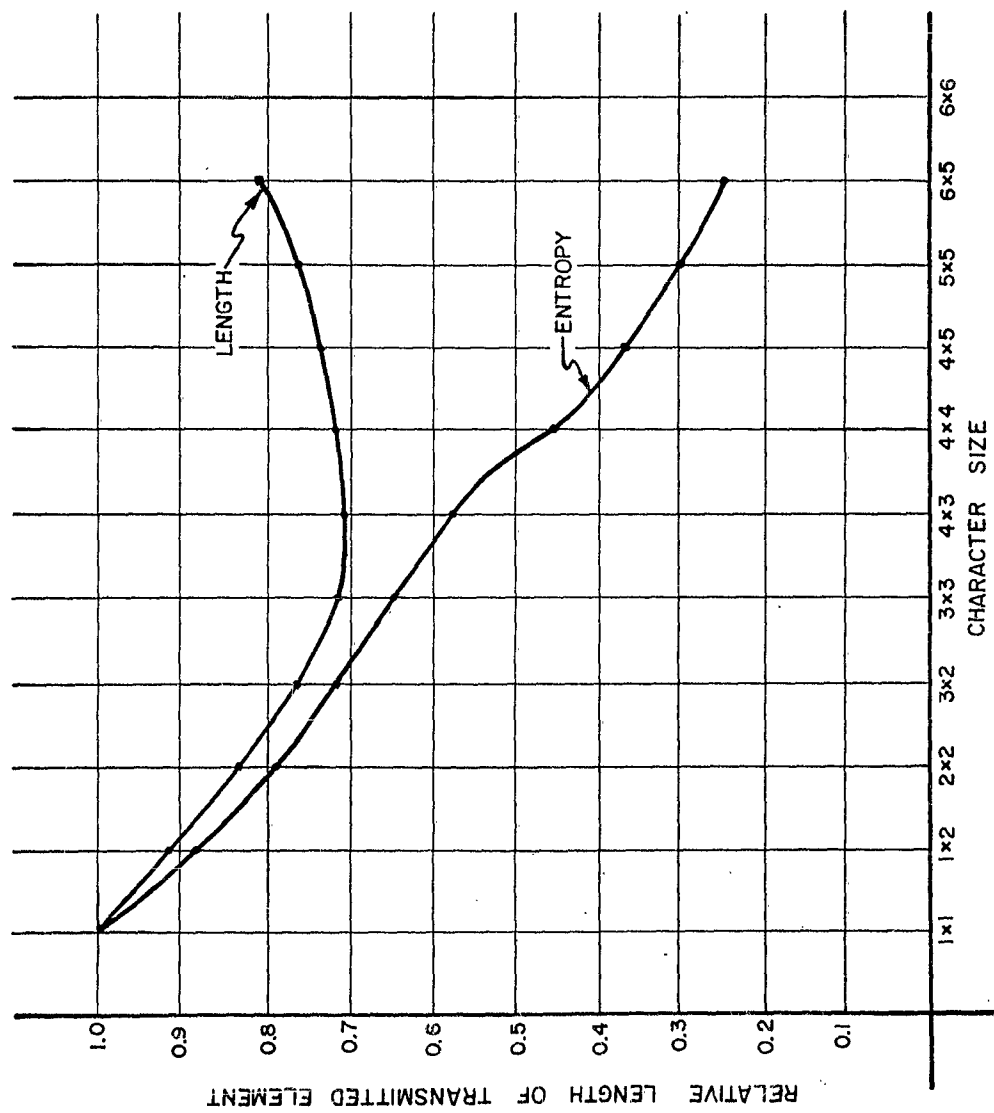74

FIG.33   CODE LENGTH/ELEMENT FOR AERIAL VIEW

75

FIG. 34 CODE LENGTH/ ELEMENT FOR WEATHER MAP

76

indicate that a 3 x 3 to 3 x 4 character size allows a maximum reduction in message length. Table 7 lists the number of coded characters for each block size. Notice that the total number of coded characters is relatively small in all cases. By considering larger data sets and/or more data sets, the number of coded characters would be increased and a further decrease in message length effected.

Table 7

CODE SIZE

Character Size	Number of Code Characters	Number of Total Characters Tabulated
1 x 1	2	39, 312
1 x 2	4	19, 656
2 x 2	16	9, 828
3 x 2	62	6, 552
3 x 3	217	4, 368
4 x 3	277	3, 276
4 x 4	210	2, 457
4 x 5	132	1, 911
6 x 5	54	1, 274

SECTION IV.

CONCLUSIONS

The work performed under this program in each of the basic research areas led to interesting and potentially useful results. In the area of biotransducers, although the sensitivity of sensors synthesized from the bacteriochlorophyll is at present small, a response is definitely present, and the need for sensitive and selective optical transducers could well be aided by additional research on these sensors.

The research in threshold logic resulted in some useful approaches to the problem of synthesizing minimal networks to compute specified Boolean functions. The method developed for effecting tradeoffs between network complexity and accuracy for symmetrical Boolean functions is of use in obtaining economical circuit designs.

However, we feel that the most exciting and potentially useful results have come with the development of the concept and fabrication techniques of the photoconductive property sensor. Indeed, a system for the processing of pictorial data which utilizes one of these sensors was conceived and investigated during the latter stages of the program. This system uses the property sensor as a key component in transforming a gray scale photograph to black and white without any loss of pertinent pictorial detail for most pictures of interest. Furthermore, the transformed picture is amenable to many present day coding techniques, whereas the initial picture was not. A net reduction in bandwidth by a factor of between ten and twenty appears reasonable with the overall system.

SECTION V.

RECOMMENDATIONS

On the basis of the conclusions, it is recommended that a pictorial data transformation system utilizing a photoconductive property sensor be constructed. This system would be used to transform a large amount of representative pictorial data. The resulting pictures would be critically examined to determine their fidelity with reference to the various recognition tasks to be performed. Modifications in sensor configuration, sensitivity and threshold would then be made in an effort to produce pictures of high utility for a given task or series of tasks. Once the design of the transformation system was completed, the 7090 computer programs, already written for the task, should be used to construct an efficient code to be used in the transmission of the transformed data.

The critical component in the proposed system is the photoconductive property sensor. Although sensitive cells of the type needed have been produced in Armour's Microelectronics Laboratory, additional research aimed at improving cell sensitivity, frequency response, uniformity and stability should be carried out to improve overall system performance.

APPENDIX I

PHOTOCONDUCTIVE SENSOR CELLS FOR PATTERN PERCEPTION

Paper given by Eugene F. Uretz at 1963 BIONICS Conference

PHOTOCONDUCTIVE SENSOR CELLS FOR PATTERN PERCEPTION

INTRODUCTION

Recent biological research has demonstrated that the various peripheral sensory organs of animals often perform property discriminating functions, selecting and relaying to the brain that information important to the survival of the animal. This paper describes an optical sensing technique which utilizes present hardware capabilities to perform a similar data selection function.

Several sensor cells which perform sensing functions similar to those found in the frog's eye[1] have been described in a previous paper.[9] These property sensor cells utilize photoconductive films with special geometries. Research aimed at the development of faster and more sensitive films is presently being performed at Armour Research Foundation, and techniques which can be used in the synthesis of cells with special geometries are also being studied.

However, the primary emphasis in this paper will be on the utilization of such property sensitive sensor cells in information processing systems rather than on the cell synthesis procedures. In particular, this paper describes a property sensor with a special geometry which is used to abstract information for recognition of numerical characters. It also describes a vector model which allows this recognition to be performed over a large class of rotations and translations.

An electrolytic tank model of the photoconductive sensor was constructed and used in conjunction with distance measuring electronic circuitry. The experimental results obtained with this equipment are presented.

VECTOR MODEL

The photoconductive sensor cell with the configuration shown in Figure 35 is used as the information abstracting element of the system. It is evident that the values of the conductances, G_{P_i}, shown in this figure are functions of the configuration projected on the i photoconductive sensor cell. The seven conductances

$$G_{P_1}, \; G_{P_2}, \; G_{P_3}, \; G_{P_4}, \; G_{P_5}, \; G_{P_6}, \; G_{P_7}$$

may be considered seven features of an optical input configuration, P, and the seven can be interpreted as a vector:

$$G_P = \left(G_{P_1}, \ G_{P_2}, \ G_{P_3}, \ G_{P_4}, \ G_{P_5}, \ G_{P_6}, \ G_{P_7} \right).$$

The distance between any two vectors,

$$G_N = \left(G_{N_1}, \ G_{N_2}, \ G_{N_3}, \ G_{N_4}, \ G_{N_5}, \ G_{N_6}, \ G_{N_7} \right)$$

and $G_K = \left(G_{K_1}, \ G_{K_2}, \ G_{K_3}, \ G_{K_4}, \ G_{K_5}, \ G_{K_6}, \ G_{K_7} \right)$,

is defined in the usual Euclidean sense as

$$D = \left[\sum_{j=1}^{7} \left(G_{N_j} - G_{K_j} \right) \right]^{1/2} = D(G_N, \ G_K)$$

For this distance to be useful in the character recognition system, the following criterion must be satisfied:

> Relative to this distance, any character which is to be classified as an N, should have its corresponding vector closer to the vector G_N, than is the vector of any character which is not to be classified as an N.

That is, given the vectors G_I, G_J, and G_N corresponding to the characters I, J, and N, if J is to be classified as an N while I is not to be classified as an N then the inequality

$$D(G_J, \ G_N) < D(G_I, \ G_N)$$

should hold.

The normal character orientations, positions, and shapes shown in Figure 36 were assigned for each of the numerals 0, 1, 2, 3, 4, 5, 6, 7, 8, and 9. However, in classifying a non-normal input configuration; one must be rather careful. A character cannot be translated or rotated indefinitely without the vector distance from its associated normal vector becoming large. In fact, if a character edge crosses an electrode, the vector output is appreciably altered. Therefore, the translations and rotations illustrated in Figure 37 (using the number 3 as an example) were selected as extreme representatives of the class of configurations to be identified as identical with their normal counterpart. In addition experiments were performed to

determine the effect of altering character sizes and/or fonts. Although quantitative results are not included for these cases, it can be stated that character size and font were not at all critical in obtaining a correct identification.

ELECTROLYTIC TANK SIMULATION

Photoconductive cells with the necessary special geometries are presently under development at Armour Research Foundation. However, since such cells were not functional when the method was first proposed, an electrolytic tank model of the photoconductive sensor cell was used to test the feasibility criterion described earlier in the paper. The tank was used to simulate the electric field properties of the photoconductive film.

Figure 38 shows the impedance between 1/8 inch electrodes placed one inch apart in an electrolytic tank with tap water used as the electrolyte. Note that the impedance between electrodes is a non-linear function of electrolyte depth, and in fact even with a film of electrolyte, an impedance as low as 75 Kilohms was measured. Therefore, the experimental tank arrangement illustrated in Figure 39 was used. This simulated a dark to light impedance ratio of approximately 15 to 1 (a very nominal ratio when one considers the ratios obtainable with photoconductive films).

The circuit shown in Figure 40 was used to obtain data from which the conductances, G_{N_i}, could be computed. This circuit was placed across each of the seven [1] electrode pairs and seven independent readings were taken. A set of readings was obtained for each character normally placed and also for each character translated, rotated and followed by other characters. This data was reduced with the aid of Armour's UNIVAC 1105 computer, and the results are given graphically in Figures 41 through 44.

The graphs given in Figures 41 through 43 plot the distance of each non-normal character from its normal counterpart and also indicate which different character is closest to the normal character and what that closest distance is. Figure 44 plots the maximum distance of a character from its norm when followed by a second character and indicates which second character causes this maximum distance. The graphs shows that the criterion for the feasibility of the technique is satisfied with but two exceptions. (The character 9 rotated counter-clockwise is vectorially further

from a normal 9 than is the character 4 rotated clockwise, and the character 9 followed by a 4 is vectorially further from a normal 9 than is the character 4 rotated clockwise).

These two exceptions are not a serious deterrent to the overall feasibility of the system since an error can be eliminated simply by slightly increasing the threshold associated with the 9 (thereby reducing slightly the amount of rotation which a nine can undergo and still be identified).

In addition to obtaining ordinary vector distances as described above (square root of the sum of the squares), distances defined as

$$D = \sum_{j=1}^{7} \left| G_{N_j} - G_{K_j} \right| \tag{2}$$

$$D = \sum_{j=1}^{7} \left| G_{N_j} - G_{K_j} \right|^{3/2} \tag{3}$$

were used in a manner completely analogous to that described for the more conventional distance measures. The results with the distance measures of equation (2) and (3) were quite similar to those given in Figures 41 through 44 and will not be included here. They were computed to determine the feasibility of using various non-linear hardware techniques for computing distance (many of these techniques compute a "hybrid" distance similar to those given in equations (2) and (3)).

DISTANCE MEASURING HARDWARE

The initial hardware implementation of the vector distance measuring device is given in Figure 45. It used seven isolated current sources and seven bridge circuits. The output from the unbalanced bridge was rectified and fed to a differential amplifier. (A low output therefore corresponded to recognition.) However, it was found that the current flowing between a given pair of electrodes in the electrolytic tank was appreciably altered by induced currents generated by the voltage impressed across other electrodes. This difficulty can be corrected by using either frequency multiplexing or time switching circuitry, but both of these processes add appreciably to the overall complexity of the system.

Therefore, a modification of the vector model which allows simultaneous current measurement at a single frequency was tried and found to be satisfactory. A single current source is applied to the electrodes as shown in Figure 46 and the conductances G_A, G_B, G_C, G_D,..., G_H seen when looking into each of the eight electrodes is monitored. The conductances are then treated as the components of an eight dimensional vector.

$$G = (G_A, G_B, G_C, G_D, G_E, G_F, G_G, G_H).$$

The distance between vectors is then computed directly with the circuit of Figure 47. Although the vector model is altered, the interaction of currents between electrodes are now an integral part of the model and do not interfere with the successful operation of the circuit. The results when using this circuitry were quite similar to those already obtained using the computer calculation and will not be described again. It was found that all of the characters could be identified under the translations and rotations illustrated in Figure 37 provided the character rotations were limited to 25° in a few key instances.

SUMMARY

The character recognition method that has been described has several promising features. The method reduces the requirements on the necessary prenormalization equipment since character identification can be made over a large class of transformations. Also, by suitable selection of threshold, it is possible for the system to autonomously "recognize" the presence of a character thus eliminating any additional decision making operation. Present activity at Armour Research Foundation is directed toward the determination of the effect of change in character size and font, expansion of the methods to include alpha-numerics, and an investigation of the feasibility of using analagous procedures for encoding more general pictorial information.*
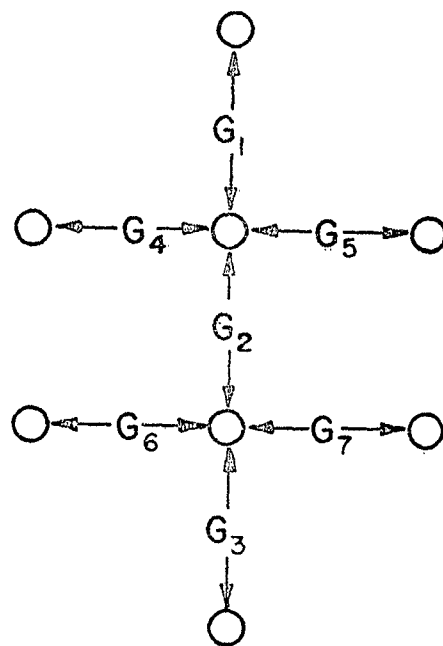
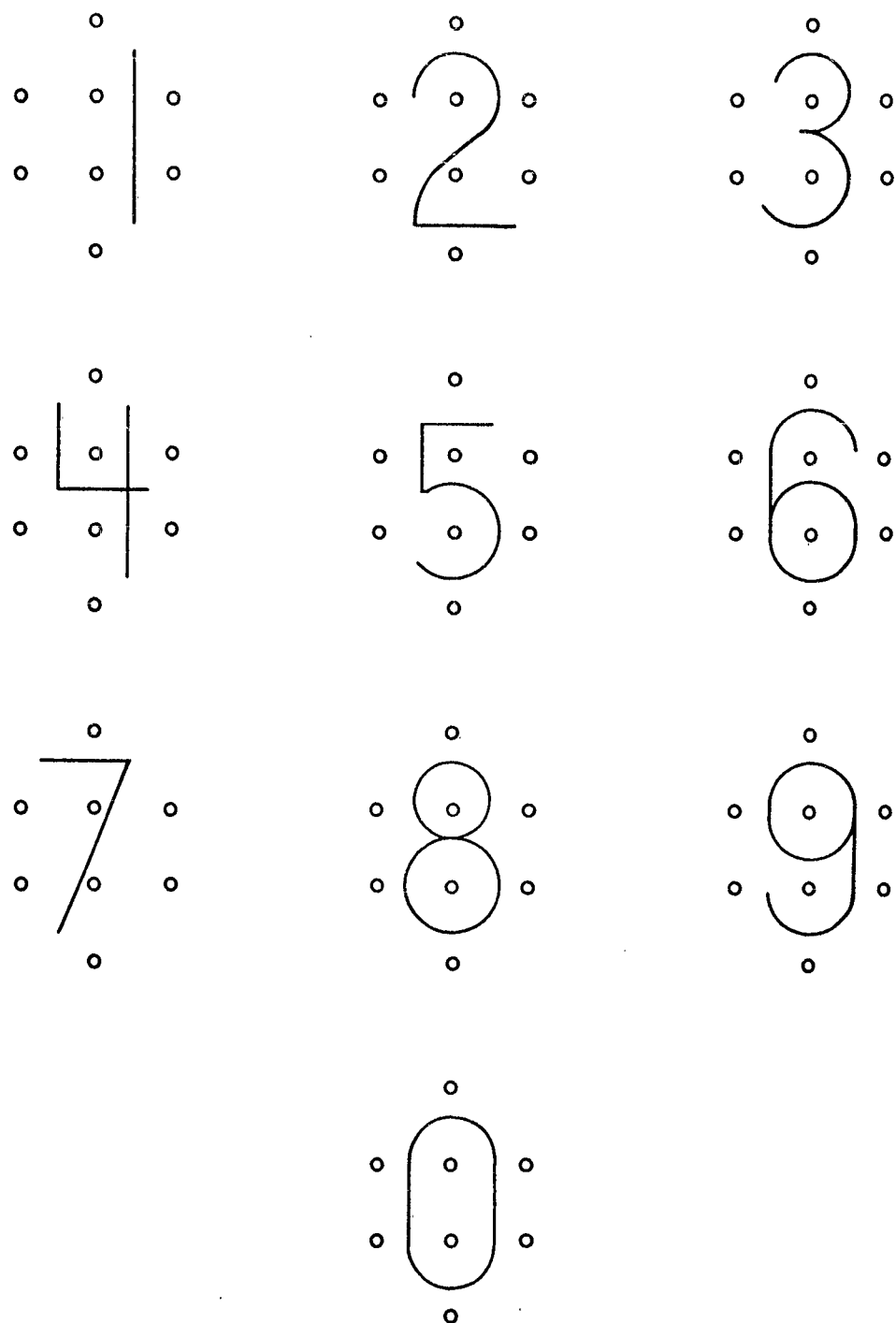FIG. 35   SENSOR CELL CONFIGURATION

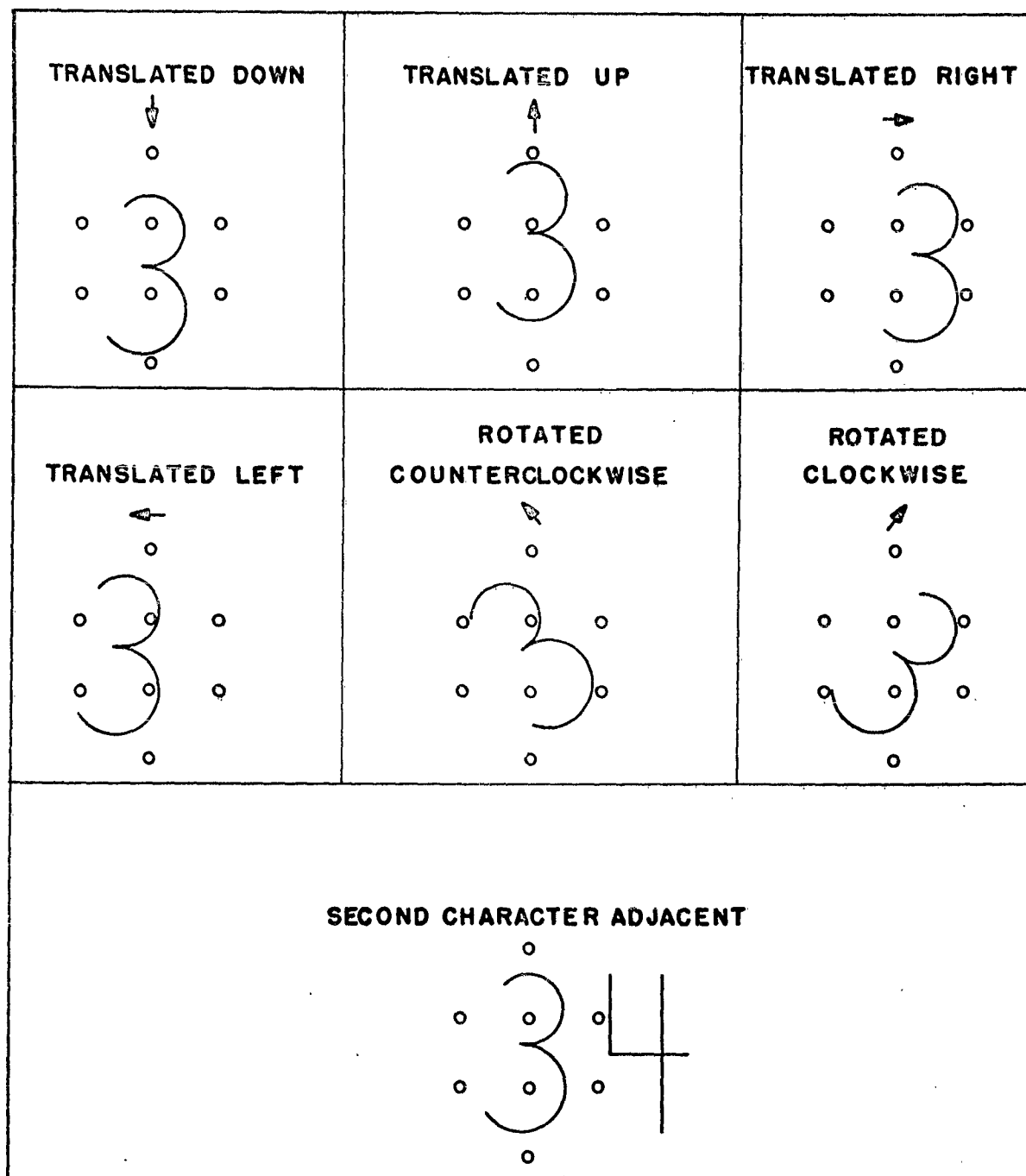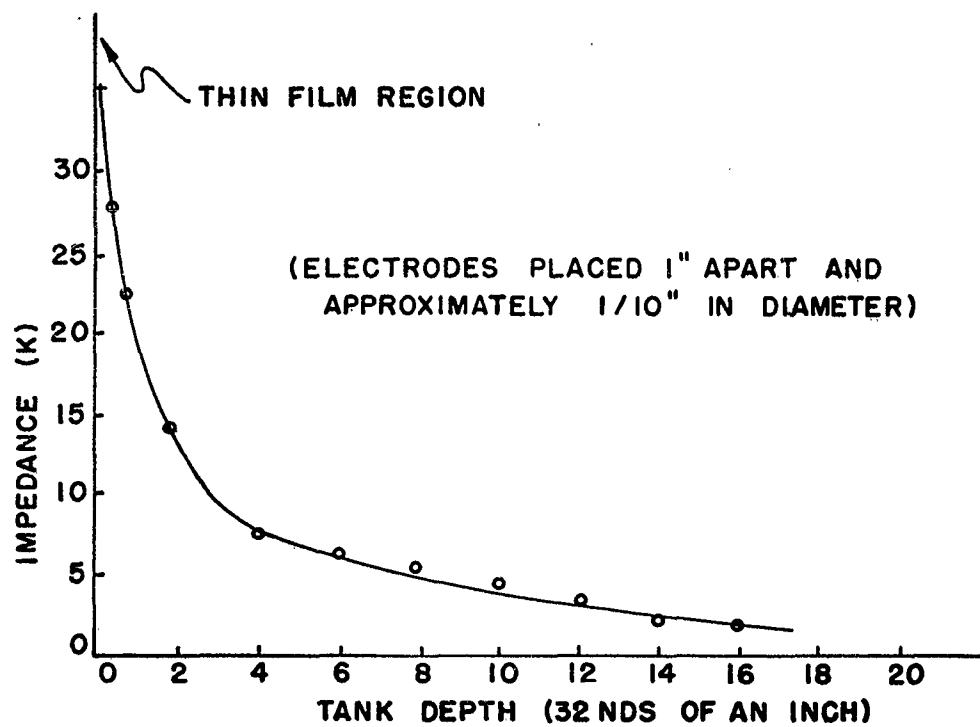FIG. 36 NORMAL CHARACTER ORIENTATION

FIG. 37 CHARACTER TRANSFORMATIONS

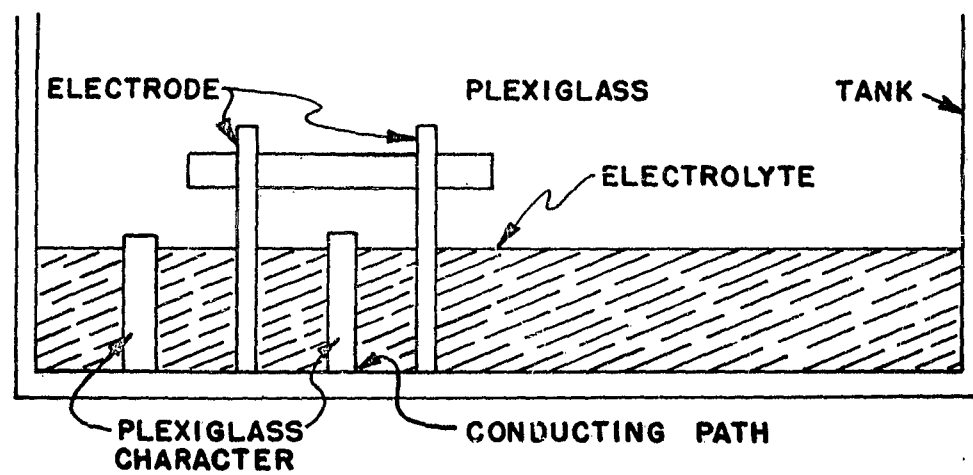FIG. 38   INTERELECTRODE IMPEDANCE VS TANK DEPTH
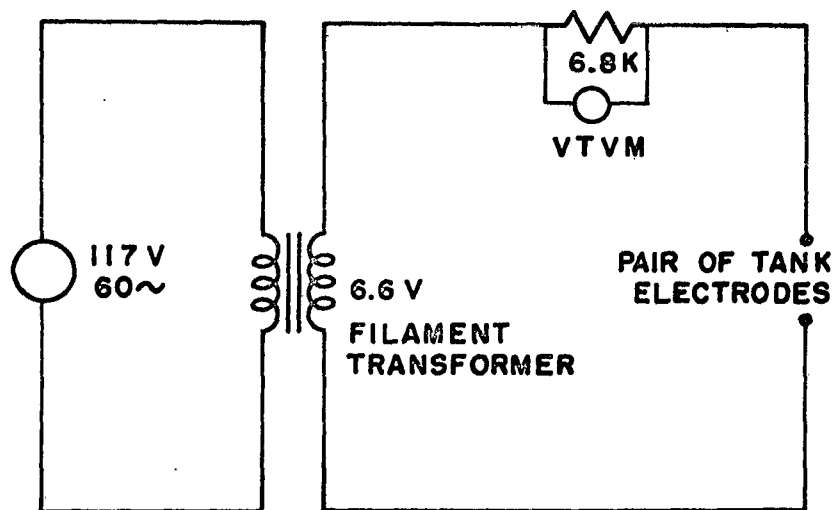
93

FIG. 39 ELECTROLYTIC TANK
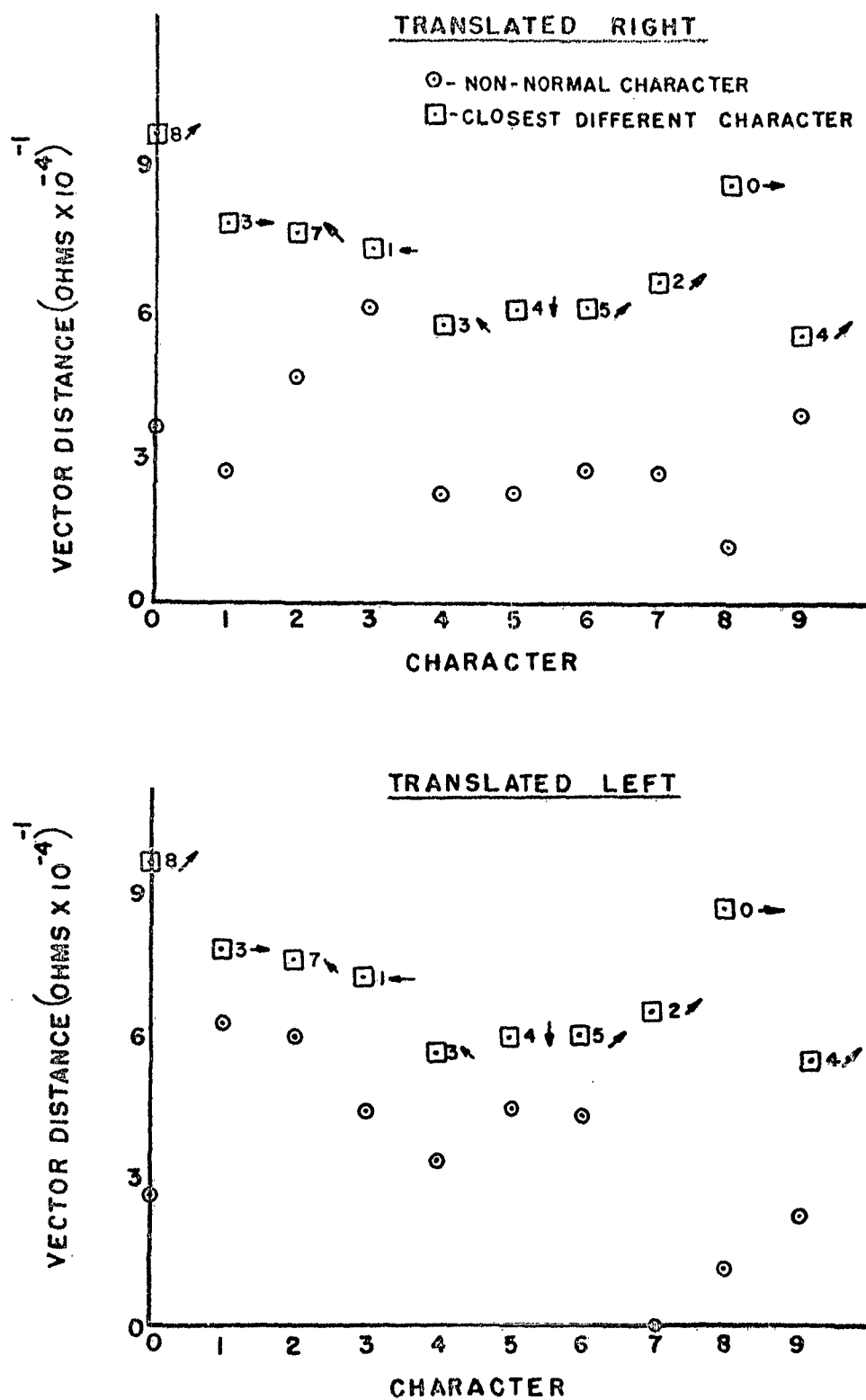
FIG. 40   IMPEDANCE DETERMINING CIRCUIT

95

FIG. 41   RESULTS FOR HORIZONTAL CHARACTER TRANSLATION

96
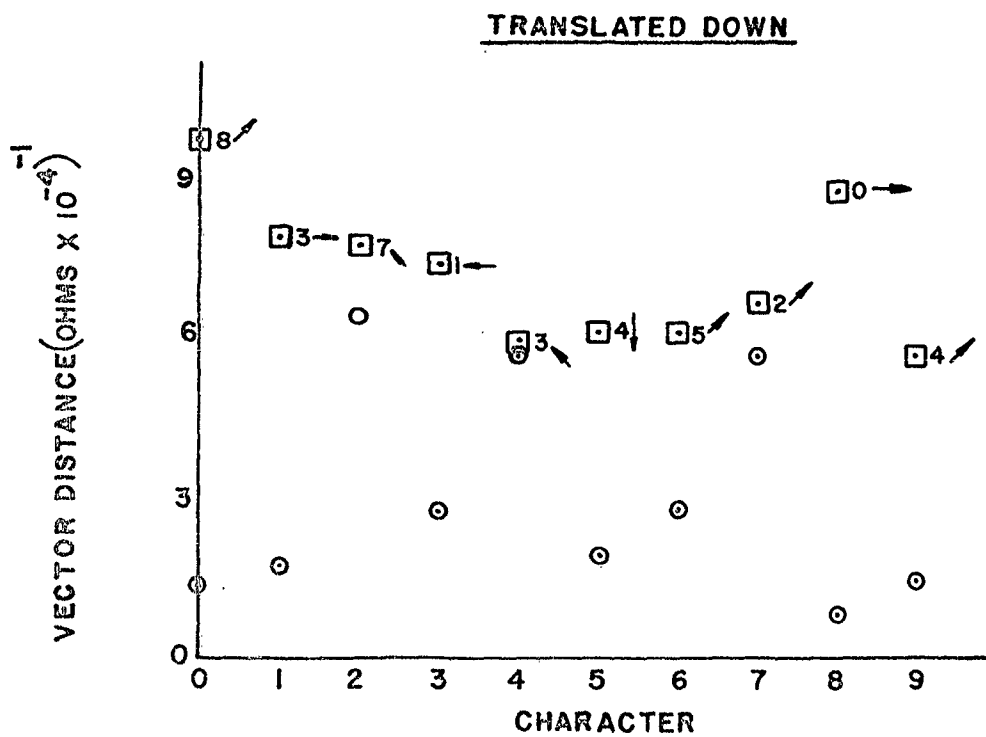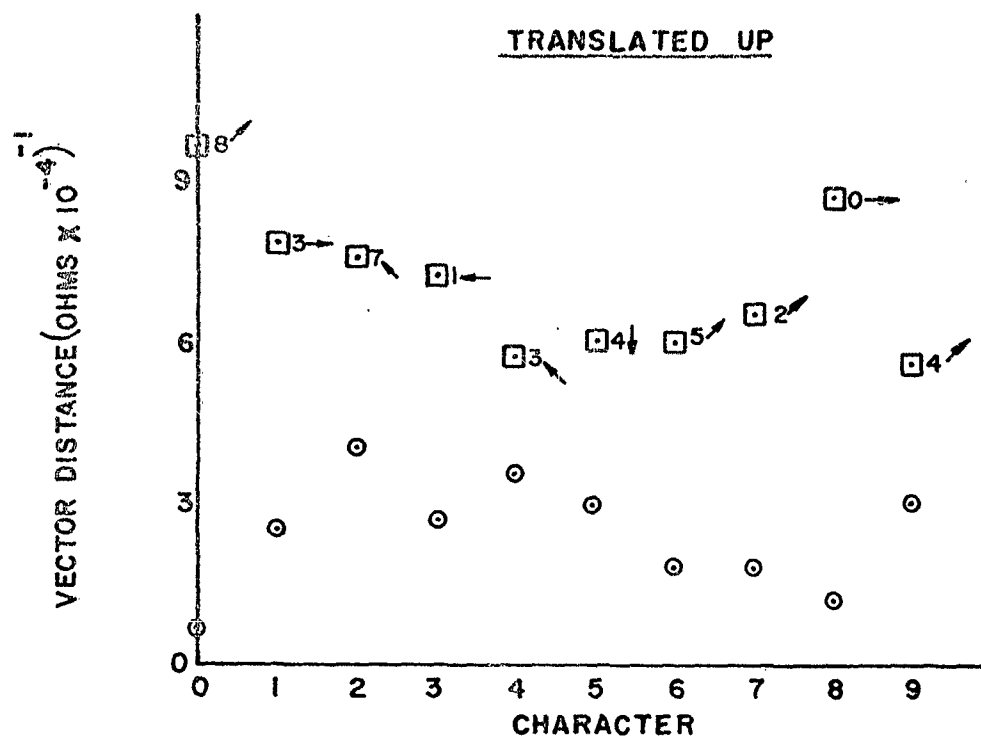
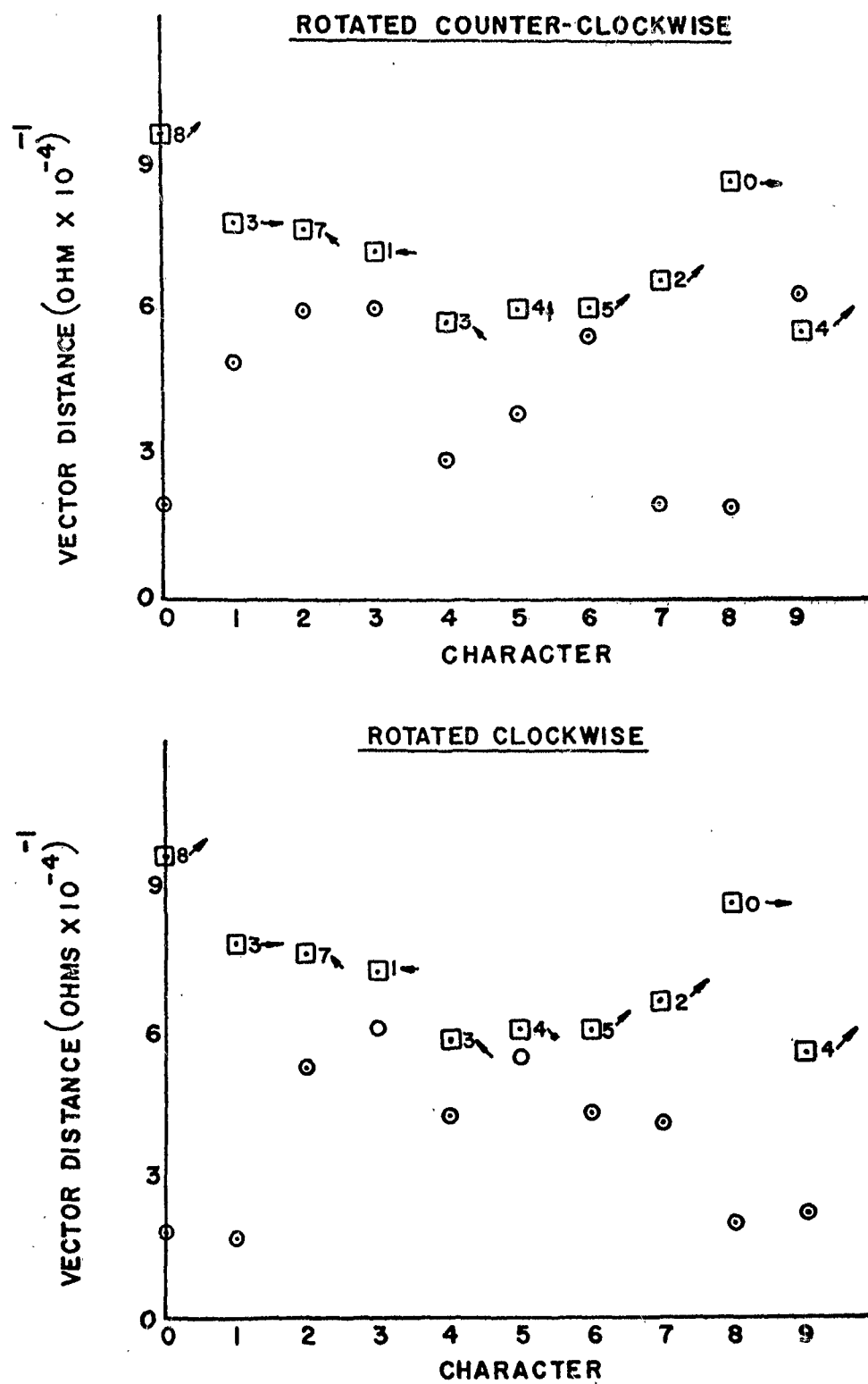FIG. 42   RESULTS FOR VERTICAL CHARACTER TRANSLATION
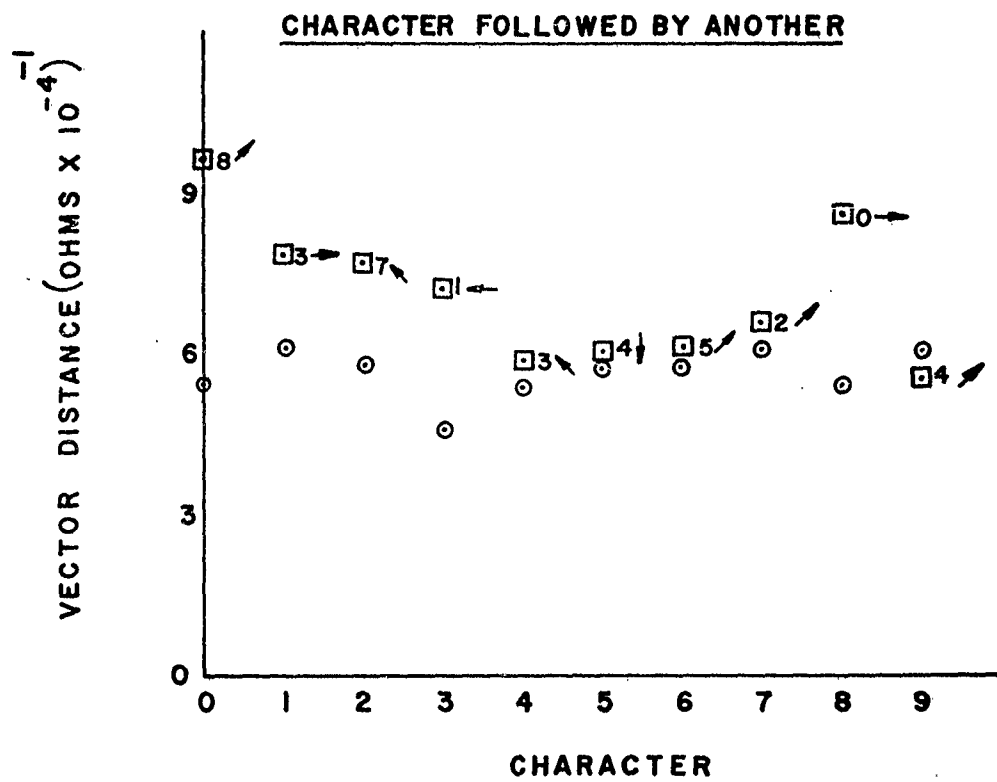
97

FIG. 43   RESULTS FOR CHARACTER ROTATION
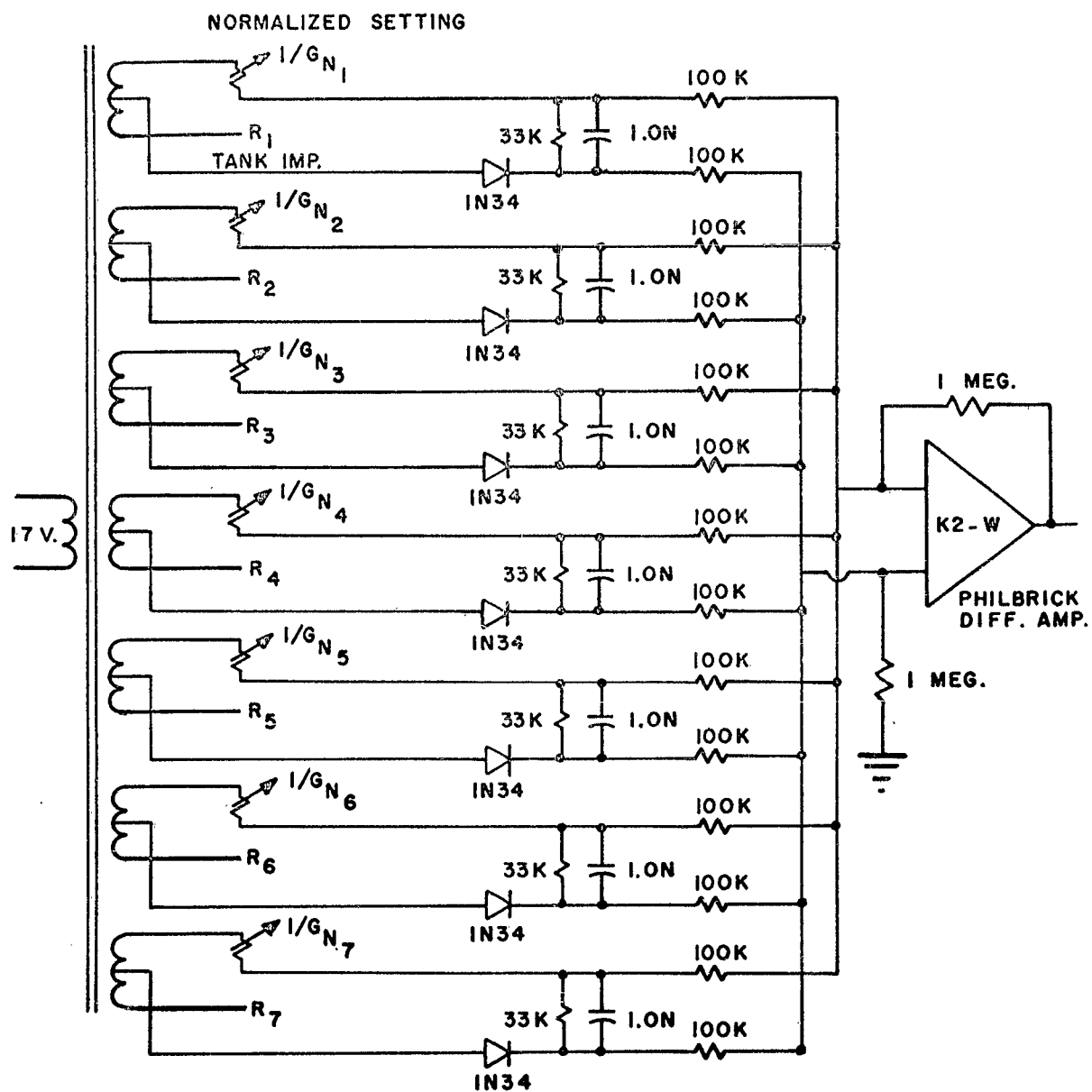
98

FIG. 44 RESULTS FOR ADJACENT CHARACTERS

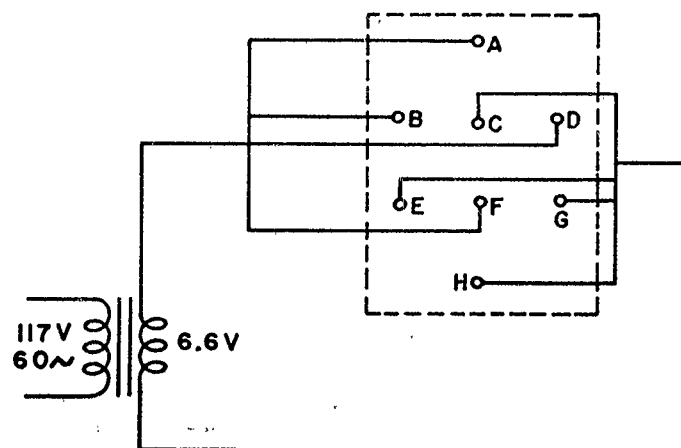FIG. 45 DISTANCE MEASURING CIRCUITRY

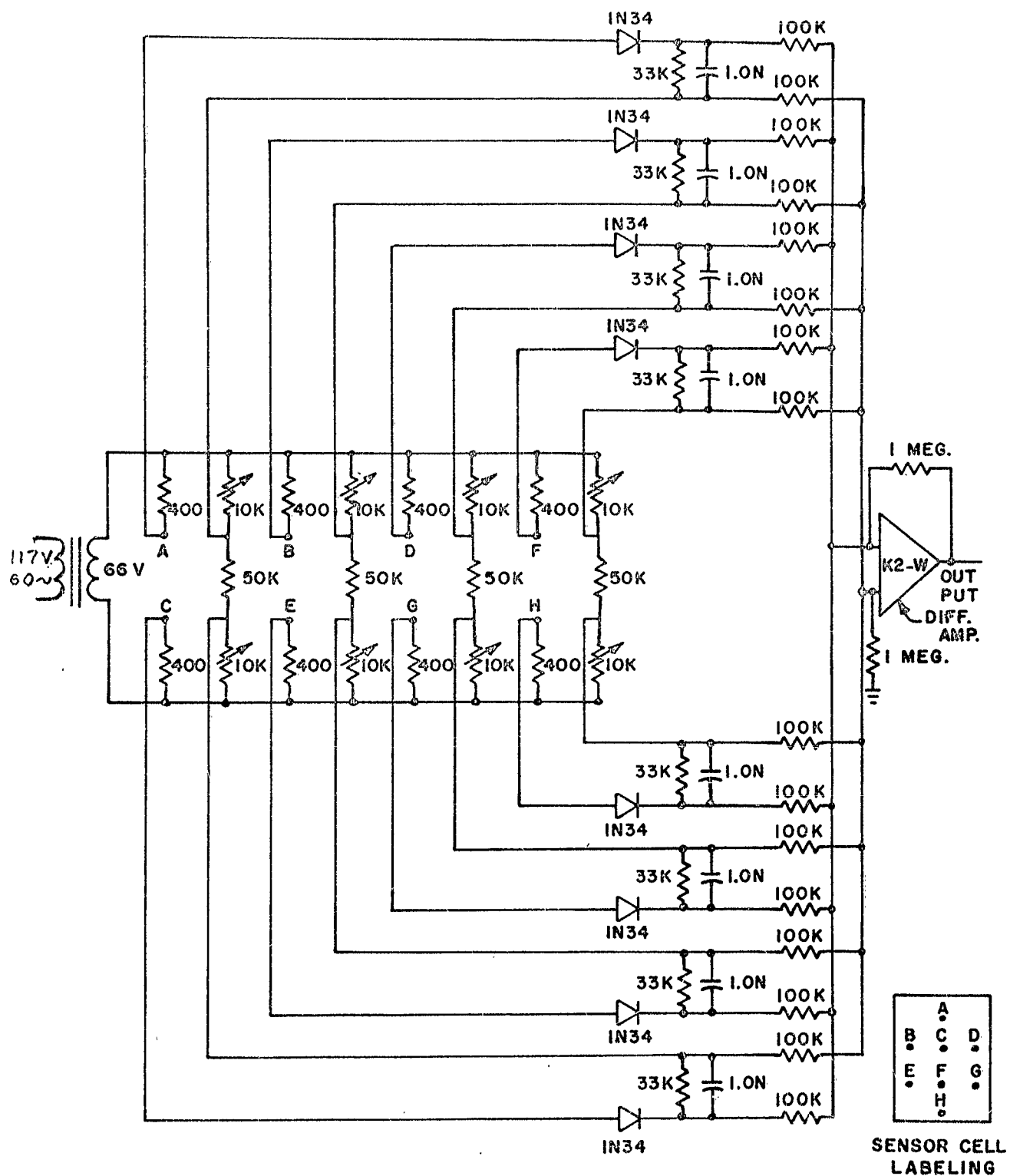FIG. 46   SINGLE SOURCE APPLIED TO ELECTRODES

101

FIG. 47 REVISED DISTANCE MEASURING CIRCUITRY

APPENDIX II

MECHANISM OF A CORRELATION THEORY OF HEARING

Paper by Henry B. Karplus given at 1963 BIONICS Conference

APPENDIX II

MECHANISM OF A CORRELATION THEORY OF HEARING

INTRODUCTION

To explain the excellent frequency analysis capabilities of the ear in the light of the known broad mechanical response of the basilar membrane it has been hitherto assumed that some form of neural interaction is capable of locating the point of maximum response with great precision. This hypothesis, however, fails completely when several tones are heard at the same time. The maximum displacement amplitude of the membrane may be exactly the same for different combinations of tones which are subjectively very easily distinguished. We talk of major chords, minor chords, discords, band limited noise all of which can be adjusted to produce identical maximum membrane excursions and yet sound subjectively quite different. However, although the maximum or the mean motion of the membrane is identical for all these different sounds the instantaneous displacement must still be different. This difference in phase of the motion at adjacent regions of the basilar membrane must carry the evident information.

OUTLINE OF THE MODEL

The basic clue to our hypothesis is Békésy's observation that a travelling wave displacement exists along the basilar membrane. The propagation velocity of this travelling wave varies with frequency at any point on the membrane. Békésy's[10] phase observations may be transformed to velocity by measuring the slope of the phase displacement as a function of position as shown in Figure 48 where the reciprocal of the phase velocity $(1/c)$ is plotted against position on the membrane. It is apparent from these curves that the propagation velocity of the travelling wave is a function of the position on the membrane at any one frequency, conversely at any given point on the membrane, this velocity is a function of the existing frequency.

We now postulate that several hair cell receptors $R_1 -- R_i -- R_n$ (Figure 49) are connected via delay lines $L_1 -- L_i -- L_n$ to a junction S, where their output is added. The delays of the lines $L_1 -- L_i -- L_n$ are an exact replica of the time retardation x/c for one particular frequency of the travelling

wave along the membrane. Other groups of receptors R_1'--R_i'--R_n' with different delays L_1'--L_i'--L_n' interspersed with the first set are shown in Figure 50.

The disturbance due to a signal of frequency f, will excite all the receptors R, R' in this region, however, the delays L_1--L_n correspond exactly to the delays of the wave along the membrane, whereas the delays L_i'--L_n' do not.. Consequently, all the signals from R_1--R_n arrive simultaneously at, S, and this junction or synapse fires the nerve coming from it. The delays L_1'--L_n' do not correspond so that signals arrive at S' at different times so that the signal does not go beyond S'. A signal with frequency f_2 close to, but slightly different from f_1, will excite all the same receptors R, R' but the corresponding membrane displacement wave will have a slightly different velocity so that now signals arrive simultaneously at S' but not at S. A further possibility suggests itself. The same receptors R_1--R_n may be connected through several sets of delay lines L_1--L_n, L_1'--L_n', L_n'' etc. to different synapses S, S', S''--- etc. so that each group of receptors may be used for several frequency components, (Figure 51). Branching is shown only at the output for clarity. Connection of several receptors to the same delay line is equally plausible.

DELAY LINES

The velocity of propagation of the travelling wave on the basilar membrane shown in Figure 48 as calculated from Békésy's data is of the order of 2 m/s at the point of maximum motion. This is of the same order as the velocity of signal propagation in unmyelinated nerve fibers (e. g. Grundfest[11]) so that nerve fibers running parallel to the basilar membrane could act as delay lines exactly in the manner described without an excessive amount of kinking or coiling. Such nerve fibers running in the required direction have been observed and described by de Lorente.[12]

The needed difference in delay between adjacent lines may utilize several possible mechanisms connected with the length of the line, velocity on the line, and latency at synaptic junctions themselves.

Delay line lengths could differ by virtue of changes in the relative distances between receptors and synapses or by nerve fibers varying by

different amounts from the shortest possible connection. The existence of several rows of hair cells might conceivably play a part here. Also, slight bends and twists in nerve fibers are known to exist.

Signal velocity along nerve fibers is a function of the myelin sheath. Slight variations of sheath thickness from fiber to fiber in the eighth nerve are possible, moreover the exact length of sheath is a function of the exact location of the cell body in the ganglion of Corti, there being no sheath or a much thinner one around the nerve fiber between the receptor on the membrane and the cell body in the ganglion. The existence of cell bodies without synaptic junctions has been a puzzle. A possible function for these is thus indicated.

Time delays across synaptic junctions have been observed in studies of lower animals with large, more accessible cell bodies. Variations of such latencies from junction to junction might also contribute to the exact "tuning" of the line delay.

The summation of the signals in the cochlear nucleus or higher centers rather than in the ear itself is not an essential feature of the theory. Evidence to support this view is found in the absence of synaptic junctions in the ganglion of Corti and the close resemblance of the activity of individual fibers of the eighth nerve to the amplitude function at any specific point on the basilar membrane when excited by different frequencies.[13]

Alternately it would be within the frame of this theory to postulate that several hair cells are innervated by the same nerve fiber and that a signal is conveyed only by correctly spaced triggers at the separate hair cells. As far as the basic theory is concerned, this possibility would be equally valid. For reasons stated in the preceding paragraph it is considered less likely.

DISCUSSION

The theory developed above will qualitatively explain the fine frequency resolving power of the ear and at the same time explain the ear's sensitivity to random noise and its ability to distinguish between different combinations of tones.

Furthermore, several hitherto incompletely explained observations are utilized and their function indicated. These include 1) the travelling wave

nature of the membrane vibration, 2) the placement of nerve fibers parallel to the membrane with their cell bodies further from the windows than their receptors, 3) the existence of junctions without synapses in the ganglion of Corti.

Quantitative estimates of resolution of the ear based on the operation outlined have not yet been undertaken. The task would be somewhat easier if the curves of Figure 49 were more uniform. These curves were rather crudely obtained using a protractor to measure the slope of the phase distance curve of a small picture in a journal. There also exists the possibility that these curves were slightly influenced by the hole which had to be cut into the wall of the cochlea to make the observations. Bekésy was careful to minimize the effect of the observation hole on the displacement distance function by making measurements for different size observation holes. It is not quite clear whether the effect on the velocity dispersion of the travelling wave is equally unaffected. The theory does not require uniform dispersion so long as the phase velocity of the travelling wave changes with frequency at any point on the membrane. This is undoubtedly the case.

To obtain quantitative estimates of the performance of the model we need to know the exact displacement-phase-frequency function of the membrane motion at every point. Furthermore, we need more data on the number of interconnections at synapses and their tolerance to slight departures from precise simultaneity. Conversely if some of these factors are known some conclusion may be obtained concerning the others by comparing results of different assumptions with subjective information on resolving power, critical bands, beats, beat tones, missing fundamentals, etc.

It is quite likely that some of these subjective phenomena may now be explained without resorting to an assumption of a non-linearity in the aural mechanism. This would be very desirable. More work is required in all these directions.

Several theories on the motion of the basilar membrane have been put forward ever since Bekésy described the motion. The most prominent of these theoretical investigators are J. Zwislocki; Peterson and Bogert; H. Fletcher; and Caldwell, Glaesser and Stewart.

1) The theory of Zwislocki[14] starts off with the measured compliance function of the cochlear duct (due to the stiffness of the basilar membrane) its mass, and the resistance and mass reactance of the perilymph in the scalae on each side of the duct. The mass of the cochlear duct is not a very important factor. It is assumed to be constant per unit length according to the observations that the area is approximately constant.

The theory yields a displacement function close to the observed one. The velocity of the wave propagating along the membrane is however entirely different. Apparent gross agreement cited by Zwislocki on closer examination is poorer than claimed; for Zwislocki compares the velocity of propagation predicted for a 1000 cps tone with the observed propagation of a pulse. He thus compares group velocity with phase velocity. Zwislocki's theory does not predict the very sharp change in velocity near the point of maximum displacement observed (and required by our new hypothesis for fine frequency discrimination). His formula could be adapted by changing some of the parameters in particular the resistance factor of the perilymph. If this is increase by an order of magnitude, velocity behavior can be made to conform qualitatively with observation.

2) The theory of Peterson and Bogert[15] also uses the observed stiffness function of the membrane and a cochlear duct of uniform mass per unit length in a cochlea with scalae of uniformly decreasing cross-section. The velocity of propagation of the membrane motion is predicted in this case to decrease precipitously near the resonant point in conformity with observation.

3) Fletcher[16] on the other hand assumes the mass per unit length of duct to be proportional to the square of its width. The stiffness function is fitted to observed data. The final results are obtained by a numerical iterative process and show fair agreement with observation.

4) The theoretical development by Caldwell,[17] Glaesser, and Stewart attempts a more precise estimate of the mass per unit length of cochlear duct. The loading effect of the fluid in the scalae is estimated from a measurement by Békésy. The membrane stiffness function is then adjusted so that the final model has the correct amplitude frequency-position function.

5) A totally different approach is due to Flanagan[18] who tries to match the observed amplitude-velocity-frequency-position functions with mathematical expressions. This very attractive approach must also be used with caution. Both Fletcher and Zwislocki find the frequency-displacement function to depart from a uniform logarithmic function near the low frequencies (in the vicinity of the helicotrema). Unfortunately it is only in this region, below 300 cps for which measurements have been possible.

The possibility of a correlation type of analysis by the ear has been suggested before by de Rose and Vallese.[19] However, the mechanical motion of the fluid within the cochlea assumed by them is at variance with the actual observation of von Békésy.

APPLICATION

All laboratory analyzers depend on the amplitude frequency function of some form of resonator. Resonators are either broad band (low Q) and have poor frequency resolution or they are sharply tuned and have a poor time resolution, ringing for an appreciable time after excitation. The ear achieves both good time resolution and sharp frequency resolution evidently with a highly damped mechanism. It seems very plausible that phase information discarded by laboratory equipment may be used by the ear to achieve the superior performance. It thus becomes possible in principle to design analyzers with an entirely different method of operation having desirable characteristics impossible to achieve with any technique now in use. Such a piece of hardware would consist of a dispersive element, delay lines and adding circuits. Conversion to a pulse code modulation as is known to exist in nerves may also be necessary for such devices. In practice such a system would be very elaborate.

CONCLUSION

The hypothesis of summation of delayed signals from several closely spaced points on the basilar membrane has been shown to elucidate some puzzling phenomena regarding the hearing mechanism. The concepts indicate entirely new avenues of approach for devices.
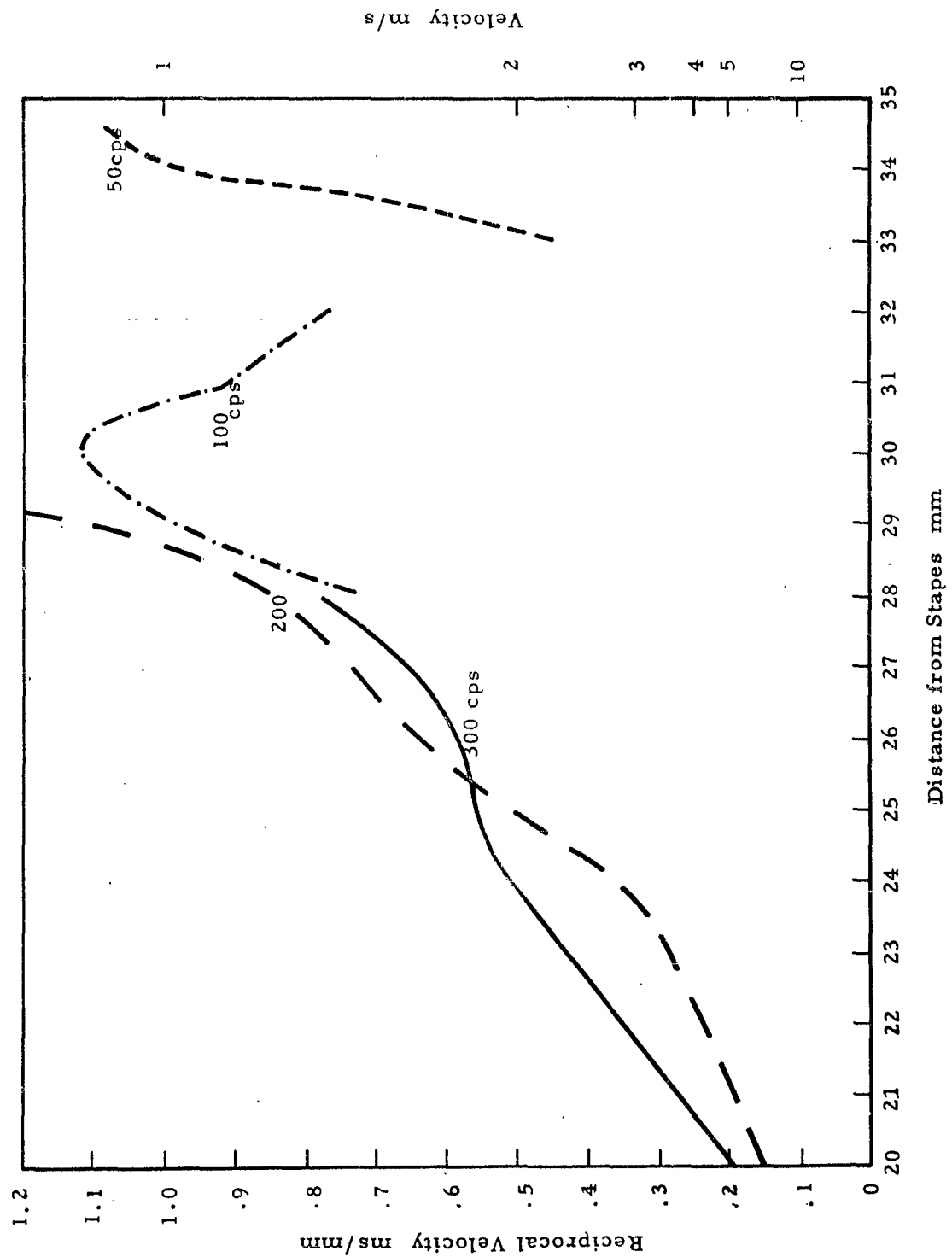
FIG. 48 RECIPROCAL PHASE VELOCITY OF MEMBRANE DISPLACEMENT

Displacement function
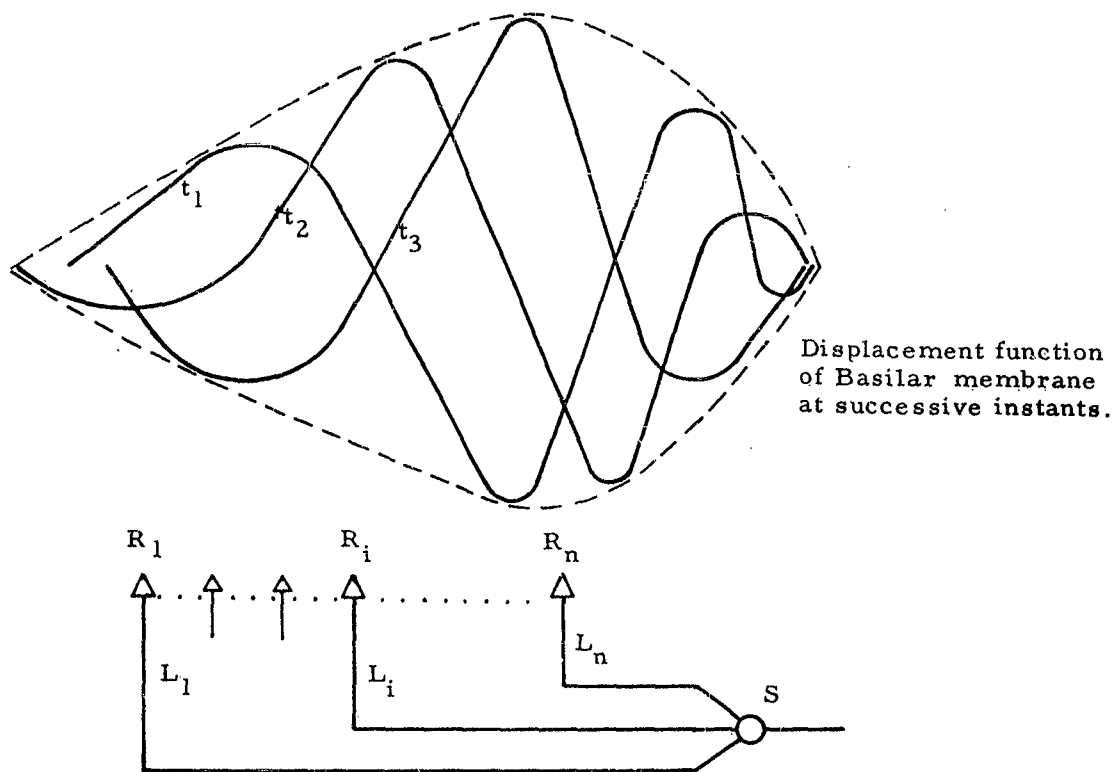of Basilar membrane
at successive instants.

FIG. 49   SUMMATION OF OUTPUT OF SEVERAL RECEPTORS R
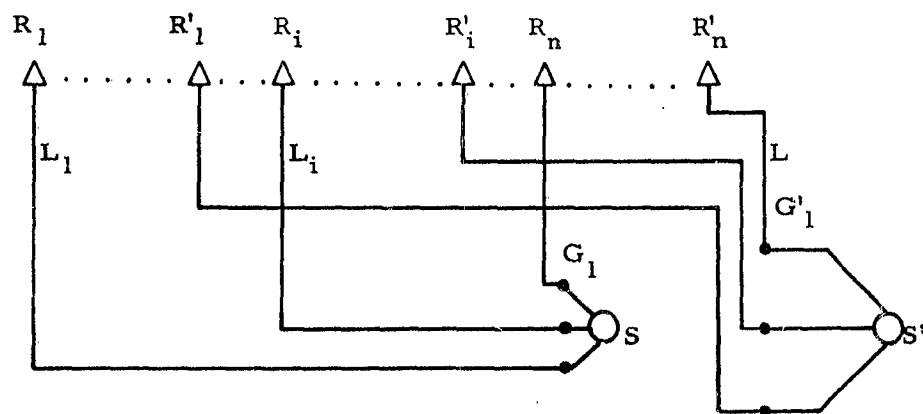VIA DELAY LINES L
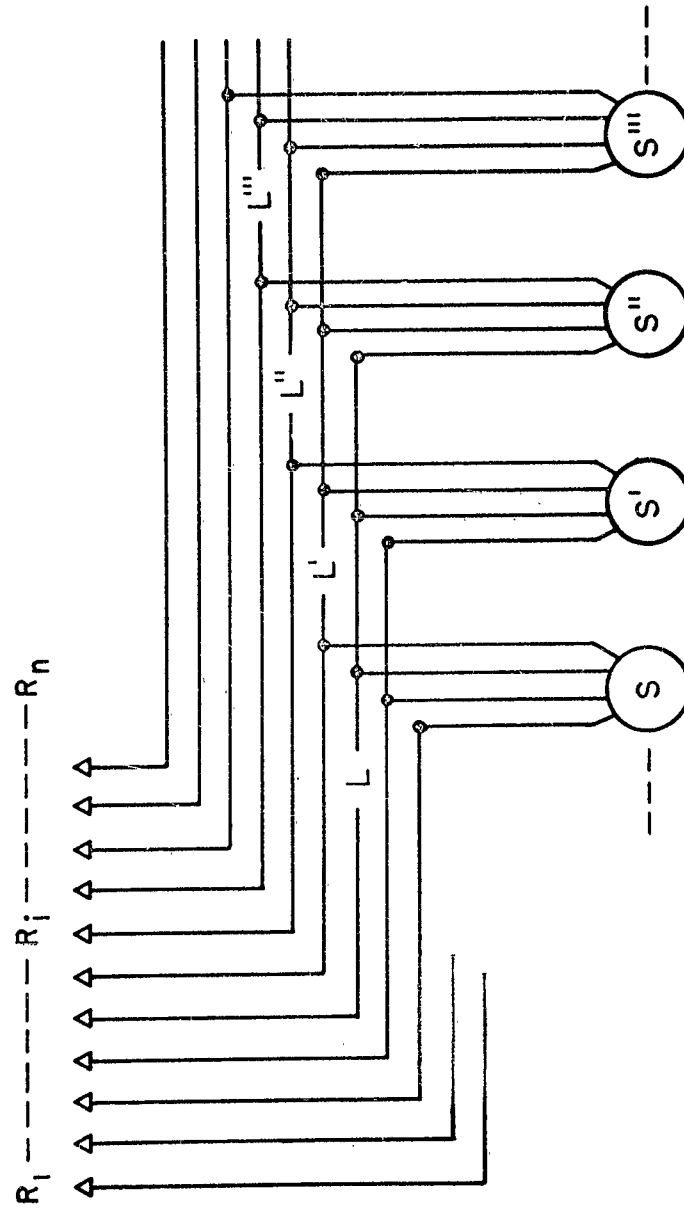

FIG. 50   RECEPTORS MAY BE INTERSPERSED AS SHOWN

FIG. 51 POSSIBLE INTERCONNECTION OF RECEPTORS R AND JUNCTION S, WITH BRANCHING DELAY LINES L, L', L'', L''' --- ETC.

APPENDIX III.

BIBLIOGRAPHY

115

APPENDIX III.

BIBLIOGRAPHY

1. Lettvin, J. Y. , Maturana, H. R. , McCulloch, W. A. and Pitts, W. H. , "What the Frog's Eye Tells the Frog's Brain, " Proc. IRE, Nov. 1959.

2. ASD Technical Report 60-620, "Creature Communications, " E. F. Uretz, Armour Research Foundation, December 1961.

3. Priest, J. , Caswell, H. L. , and Budo, Y. , "Stress Anisotropy in Silicon Oxide Films, " J. Appl. Physics, 34, No. 2, 347-51, Feb. 1963.

4. Robinson, R. J. , Private communication, Jan. 1963.

5. Arnold, W. and Maclay, H. T. , "Chloroplasts and Chloroplast Pigments as Semiconductors, " Brookhaven Symposia in Biology, 11, 1, June 1958.

6. Blasbalg, H. and Van Blerkom, R. , "Message Compression, " IRE Trans. on Space Electronics and Telemetry, SET-8, No. 3, 228, Sept. 1962.

7. Wholey, J. S. , "Coding of Pictorial Data, " IRE Trans. on Information Theory, IT-7, 99, April 1961.

8. Stevens, S. S. , "Honoring Fechner and Repealing His Law, " Science, 133, 80-83, Jan. 1961.

9. Uretz, E. F. and Weyer, J. R. , "Some Property Sensitive Photoconductive Configurations, " Proc. San Diego Symposium for Biomedical Engineering, 288-299, June 1962.

10. von Bekesy, G. , The Vibration of the Cochlear Partition in Anatomical Preparations and in Models of the Inner Ear, " J. Acoust. Soc. Am. , 21, 233, 1949.

11. Grundfest, H. , Bioelectric Potentials, " Ann. Rev. Physiol. , 2, 469, 1940.

12. de Lorente, N. R. , "Anatomy of the Eighth Nerve, " Laryngoscope, 43, 1, 1933.

13. Galambos, R. and Davis, H. , "The Response of Single Auditory Nerve Fibers to Acoustic Stimulation, " J. Neurophysiol. , 6, 39, 1943.

14. Zwislocki, J. , "Theorie de Schneckenmechaninik, " Acta Otolaryngologica, Supplement 72, 1948.

15. Peterson L. C. and Bogert, B. P. , "A Dynamical Theory of the Cochlea, " J. Acoust. Soc. Am. , 22, 369, 1950.

16. Fletcher, H., "On the Dynamics of the Cochlea," J. Acoust. Soc. Am., 23, 637, 1951.

17. Caldwell, W. F., Glaesser, E. and Stewart, J. L., Report On Contract AF 33(657)-8016.

18. Flanagan, J. L., "Models for Approximating Basilar Membrane Displacement," Bell Syst. Tech. Journ., 39, 1163, 1960.

19. de Rosa, L. A. and Vallese, L. M., "Nature's Contribution to Correlation Processes," Bionics Symposium, WADD Tech. Rpt. 60-600, 339, 1960.

Aeronautical Systems Division, Dir/
Avionics, Electromagnetic Warfare and
Communications Lab, Wright-Patterson
AFB, Ohio.
Rpt Nr ASD-TR-61-620, Pt II. STUDY OF
CREATURE COMMUNICATIONS. Final Rpt,
June 63, 118p. incl. illus., tables, 19 refs.
Unclassified Report

Work report has as its goal the develop-
ment of new communication components,
techniques and systems from the analysis
and/or use of biological phenomena. A
photoconductive sensor which acts as a
contrast detector was designed and fabri-
cated. Threshold operators serving as a
(over)

1. Bionics
2. Neural networks
3. Photoconductive
   sensors
I. AFSC Project 4335
   Task 433526
II. Contract AF 33(657)
    8807
III. Armour Research
     Foundation
IV. E. F. Uretz, et al
V. Not aval fr OTS
VI. In ASTIA collection

rough model of neural structure were
mathematically analyzed. Photoconductive
and photovoltaic sensors were made from
photosynthetic bacteria. A system for en-
coding multi-shade pictures was designed.
A contrast detecting sensor is used in the
system to convert the picture to a two-level
form. An analysis is presented which
determines the bandwidth saving which can
be attained by efficiently encoding the
transformed picture.